Chemical Functionalization of thiol-acrylate polyHIPEs

CAITLIN ROSE LANGFORD

Chemical Functionalization of Thiol-Acrylate polyHIPEs

A thesis submitted in fulfilment of the requirements for the degree of Master of Science.

Caitlin Rose Langford

2014

Abstract

The work described herein describes the synthesis and subsequent functionalization of thiol-acrylate emulsion templated porous polymers (polyHIPEs). Thiol-ene "click" chemistry has been employed in order to produce polyHIPEs from multifunctional thiol and acrylate monomers, and the level of residual thiol within the material determined. These residual thiols have then been used as "reactive handles" which allow for the functionalization of the thiol-acrylate polyHIPE post-polymerization. Both radical mediated thiol-ene "click" and amine catalysed Michael additions have been used in order to graft acrylates to the polymer surface, and the formation of disulphide bonds between the polymer surface and thiols has been explored.

The non-crosslinking monomer pentafluorophenyl acrylate (PFPA) has also been incorporated into thiol-acrylate polyHIPEs in order to provide a route to post-polymerization functionalization. The reaction between the PFPA within the polymer network and amines occurs under mild conditions and so this has been explored as a route to the incorporation of biomolecules in the polymer network.

Table of Contents

List of Figures

List of Reaction Schemes

List of Tables

Table 3.6 Percentage functionalization of PFPA-polyHIPE and PFPA-PEGMA-polyHIPE after post-polymerization functionalization with L-alanine and RGD as determined by elemental analysis.

List of Abbreviations

AIBN	Azobisisobutyronitrile
AM	Acrylamide
ASGPR	Asiaglycoprotein Receptor
ATDT	5-Amino-1,3,4-Thiadiazole-2-Thiol
ATRP	Atom-Transfer Radical-Polymerization
BET	Brunauer-Emmett-Teller
CuAAc	Copper (I)-Catalysed Azide-Alkyne Cycloaddition
CuBr	Copper Bromide
DCM	Dichloromethane
DMF	Dimethylformamide
DMSO	Dimethyl Sulfoxide
DPEHA	Dipentaerythritol Penta-/Hexa-Acrylate
DVB	Divinylbenzene
ECM	Extracellular Matrix
EGDMA	Ethyleneglycol Dimethacrylate
EHA	2-Ethylhexylacrylate
EHMA	2-Ethylhexylmethacrylate
EO	Ethylene Oxide
EVB	Ethylvinyl Benzene
FTIR	Fourier Transform Infrared

GGRGD	Glycylglycylarginylglycylaspartic Acid
GMA	Glycidyl Methacrylate
HA	Hydroxyapatite
HEMA	2-Hydroxyethyl Methacrylate
HFIPA	Hexafluoroisopropyl Acrylate
HIPE	High Internal Phase Emulsion
HLB	Hydrophile-Lipophile Balance
HPLC	High-Perfomance Liquid Chromatography
IBOA	Isobornyl Acrylate
LED	Light Emitting Diode
MALDI	Matrix-Assisted Laser Desorption/Ionization
MBAA	Methylene Bisacrylamide
MMA	Methyl Methacrylate
M_n	Number Averaged Molecular Weight
NaCl	Sodium Chloride
NASI	*N*-Acryloxysuccinimide
NMM	*N*-Methylmorpholine
NMR	Nuclear Magnetic Resonance
PB	1,2-polybutadiene
PCL	Poly(ε-Caprolactone)
PEG	Poly(Ethylene Glycol)
PEGMA	Poly(Ethylene Glycol) Methacrylate

PEO	Poly(Ethylene Oxide)
PFPA	Pentafluorophenyl Acrylate
PFPE	Perfluoropolyether Ammonium Carboxylate
PGA	Poly(Gluteraldehyde)
PLA	Poly(Lactic Acid)
PO	Propyleneoxide
PolyHIPE	Polymerized High Internal Phase Emulsion
PTFE	Poly(Tetrafluoroethylene)
PVAc	Poly(Vinyl Acetate)
PVC	Poly(Vinyl Chloride)
PyBOP	Benzotriazol-1-yl-oxytripyrrolidinophosphonium Hexafluorophosphate
RAFT	Reversible Addition-Fragmentation Chain Transfer
RGD	Arginylglycylaspartic Acid
ROMP	Ring Opening Metathesis Polymerization
$ScCO_2$	Super-Critical Carbon Dioxide
SEM	Scanning Electron Microscopy
ST	Styrene
TAEA	Tris(2-aminoethyl)amine
TFA	Trifluoroacetic Acid
THF	Tetrahydrofuran
TIPS	Triisopropyl Silane
TMEDA	Tetramethylethylenediamine

TMPTA	Trimethylolpropane Triacrylate
TMPTMP	Trimethylolpropane Tris(3-Mercaptopropionate)
TNB	5-Sulphido-2-Nitrobenzoate
TT	Pentaerythritoltetrakis 3-Mercaptopropionate
UV	Ultra Violet
VBC	4-Vinylbenzyl Chloride
VPBMP	4-Vinylphenyl 2-Bromo-2-Methyl-Propanoate
XPS	X-Ray Photoelectron Spectroscopy
µL	Micro-Stereolithography
2D	Two-Dimensional
3D	Three-Dimensional

Declaration

The work presented herein was carried out in the Department of Chemistry at Durham University between October 2012 and September 2013. Unless otherwise stated all work is my own and had not been submitted for a qualification at this or any other university

Statement of Copyright

Acknowledgements

Firstly, I would like to take the opportunity to thank my supervisor Neil Cameron for giving me the opportunity to undertake this Masters project. His guidance and support during this time has been greatly appreciated.

A big thank you to the past and present members of the NRC group, as well as those in office 235 for making this time so enjoyable, I couldn't have asked for a better group of people to work with. A special thank you to David Johnson for his help, support and endless patience, I will be forever grateful. Thanks to Didsy for teaching me how to make a polyHIPE, I never would have made it this far without you!

To the members of KA1 and KE2 (and Binky) thank you for all the good times, for providing a source of distraction, and for reminding me I can't make polymer without monomer...

To James for his unwavering support, encouragement and patience.

Finally, I would like to thank my parents for their advice and support during my studies.

1. Thiol-Ene "Click" Chemistry and the Production of Porous Polymer Materials

1.1 Thiol-Ene "Click" Chemistry and its Applications in Polymer and Materials Chemistry

1.1.1. "Click" Chemistry

Since its definition in 2001, "click" chemistry has received much attention in the fields of polymer and materials science[1, 2]. The need to synthesize polymers with defined molecular weights, narrow molecular weight distribution, and well controlled functional group distribution on the polymer backbone have been the main drivers of this interest in "click" chemistry. Advances in conventional polymer synthesis methods, as well as living polymerization and controlled radical polymerization techniques, have allowed for excellent control over both molecular weight and chemical composition of such macromolecules[3-9]. However, the limitations of these methods are exposed when the desired architectures have complex structures and chemical compositions. In order to overcome these limitations "click" chemistry has been used as a means of synthesizing and functionalizing complex macromolecules in a modular fashion.

In order for a reaction to be classed as a "click" reaction there are several criteria it must fulfil. These include: the reaction must proceed with a near quantitative yield; give stereospecific and regiospecific products; the starting materials must be readily available; any by-products produced must be inoffensive and easily removed; the reaction products must be simple to isolate; the reactions must be insensitive to oxygen and water; reactions should be carried out in the absence of solvent or using mild solvents[10].

There are several types of reactions which can be described as a "click" reaction. These reactions can be sorted into four categories:

1. Cycloaddition reactions[11-13]
2. Nucleophilic ring opening of strained heterocyclic electrophiles[14]
3. Non-aldol carbonyl chemistry
4. Additions across carbon-carbon multiple bonds[1, 15]

Of these reactions the most widely used in polymer chemistry is the copper catalysed Huisgen 1,3-dipolar cycloaddition (CuAAC)[16-22], the mechanism of which is shown in Scheme 1.1. Its use within polymer chemistry has mainly been in conjunction with controlled radical polymerization methods. In particular, CuAAC and ATRP are easily combined as the end groups of polymers synthesized by ATRP contain halogens, which are easily converted to azide groups via a variety of organic reactions[23, 24]. ATRP and CuAAC "click" reactions can also be carried out in a one-pot manner[25, 26].

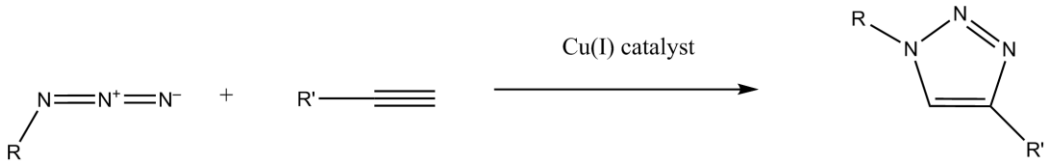

Scheme 1.1 Copper catalysed Huisgen 1,3-dipolar cycloaddition (CuAAC).

Despite the advantages of CuAAC in terms of its easy combination with other polymerization techniques the reaction has limited applications in the synthesis of biopolymers and biomaterials due to impurities from the copper catalyst. CuAAC is also not viable for internal alkynes. Other disadvantages of common click reactions include the low reactivity of reagents used in Diels-Alder chemistry, and homo-coupling of double bond containing molecules.

As a result, the thiol-ene and thiol-yne reactions were put forward as a "click" reaction suitable for the synthesis and functionalization polymers and materials for biological applications.

1.1.2. Thiol-Ene "Click" Chemistry

The reaction between molecules containing carbon-carbon double bonds (enes) and thiols was first described in 1905[27]. The reaction is known to proceed by two mechanisms: free-radical addition to both electron-deficient and electron-rich carbon-carbon double bonds; and amine or base catalysed Michael additions across electron-deficient carbon-carbon double bonds.

The free-radical addition proceeds via a combination of step-growth and chain growth mechanisms. While the presence of both step-growth and chain growth mechanisms would suggest that the thiol-ene reaction is not a "click" reaction, the ideal thiol-ene reaction occurs via a purely step-growth mechanism[28], leading many to describe the thiol-ene reaction as "click" chemistry[1]. This mechanism has three steps: initiation, propagation and termination. The initiation step (Scheme 1.2) involves the formation of a thiyl radical, this can occur either upon exposure to UV light[29] or via a thermal process using initiators such as azobisisobutyronitrile (AIBN)[30].

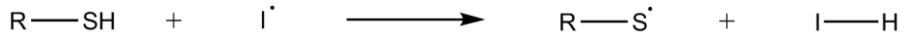

Scheme 1.2 Thiol-ene "click" initiation step.

The propagation step is the addition of the thiyl radical across the carbon-carbon double bond to give the anti-Markovnikov product, leaving a carbon centred radical. This carbon centred radical then under goes a chain transfer reaction in which a hydrogen radical is abstracted from a thiol group, generating a new thiyl radical[1], as shown in Scheme 1.3.

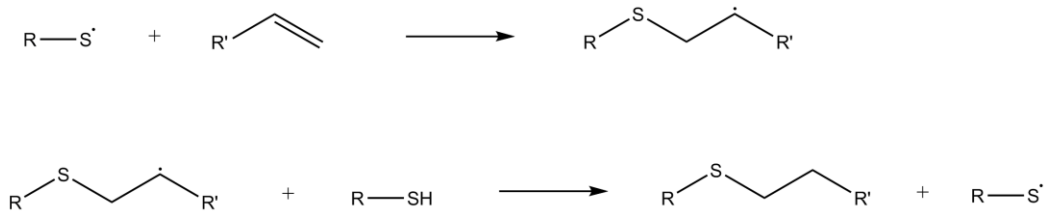

Scheme 1.3 Thiol-ene "click" propagation step.

Termination occurs via radical coupling mechanisms, including coupling and disproportionation reactions[1] as shown in Scheme 1.4.

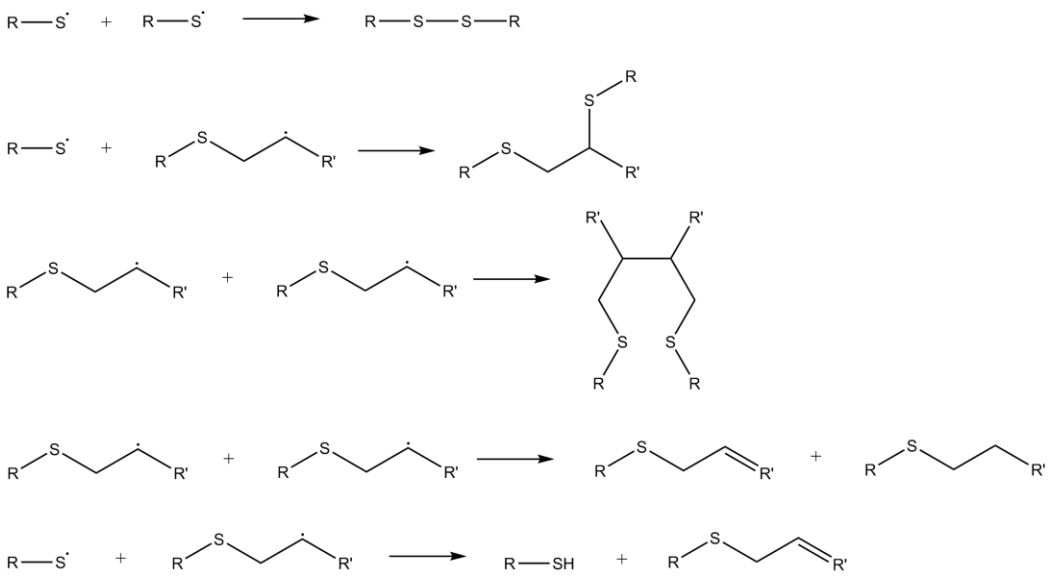

Scheme 1.4 Thiol-ene "click" termination step.

In non-ideal thiol-ene, homopolymerization of the "ene" monomer also occurs. This homopolymerization occurs via a chain-growth mechanism in which the carbon-centred radical reacts with another carbon-carbon double bond, resulting in the formation of a new carbon centred radical. The kinetics of the reaction, and the extent of "ene homopolymerization" observed, is determined by the structure of the ene monomer[31]. Double bonds with greater electron density, such as vinyl groups, are more likely to react with thiyl radicals than undergo homopolymerization. Less electron dense enes are, on the other hand, more likely to undergo a chain-growth reaction, forming a homopolymer[32, 33]. The step-growth thiol-ene reaction is a stoichiometric reaction and so any homopolymerization of the ene monomer results in an increased level of unreacted thiol groups upon completion of the reaction[34]. However, in a typical thiol-ene reaction the rate of the carbon-carbon step-growth reaction is much greater than the rate of "ene homopolymerization" reactions. The reaction mechanism for a non-ideal thiol-ene system is shown in Scheme 1.5.

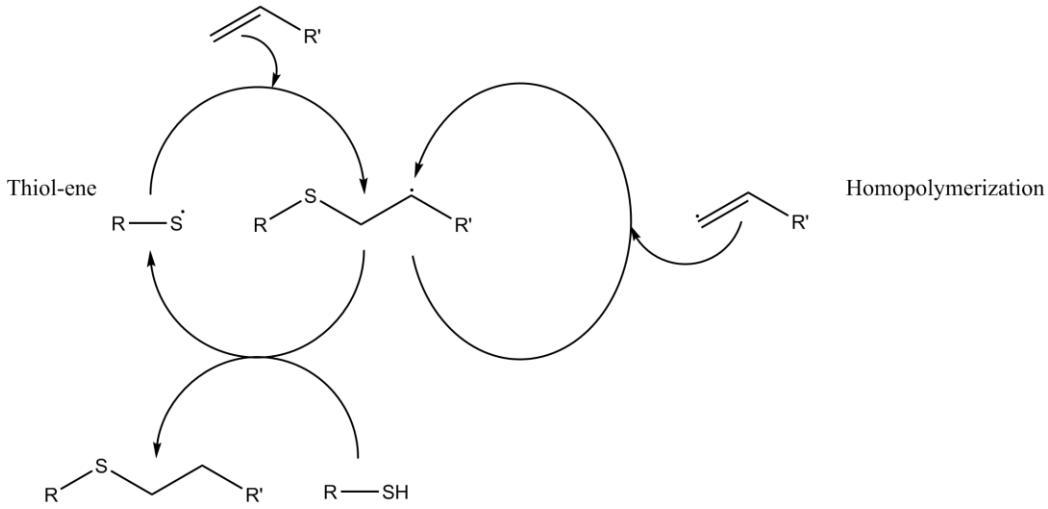

Scheme 1.5 Non-ideal thiol-ene "click" reaction.

Intramolecular reactions can also occur within thiol-ene polymerizations. These reactions include intramolecular chain transfer, converting carbon-centred radicals into thiyl radicals, and cyclization reactions. Cyclization reactions are a form of intramolecular propagation in which a thiyl or a carbon-centred radical attacks a double bond within the same molecule, leading to the formation of a ring structure[35].

While UV initiated thiol-ene reactions can occur without the use of a photoinitiator, provided an appropriate wavelength of light is selected and the monomers are sufficiently reactive[36-38], the addition of a photoinitiator can greatly reduce reaction times and increase the efficiency of such reactions. Type I photoinitiators have been found to be more effective at initiating thiol-ene reactions than Type II photoinitiators[39-41]. This is due to the mechanisms by which the photoinitiators form radicals. Type I photoinitiators undergo a unimolecular cleavage reaction upon exposure to UV light, yielding two radicals. Both of these radicals can initiate the thiol-ene reaction by abstracting hydrogen from a thiol group. The excited states of these radicals are also short-lived singlets; this short lifetime prevents quenching of the excited state by thiols. Type II photoinitiators, on the other hand, produce radicals by a bimolecular reaction in which interactions between the photoinitiator and a second co-initiator molecule leads to the formation of radicals. This reaction occurs at a much lower quantum yield

than the former process, resulting in less efficient initiation of the thiol-ene reaction. Examples of both Type I and Type II photoinitiators are shown in Figure 1.1.

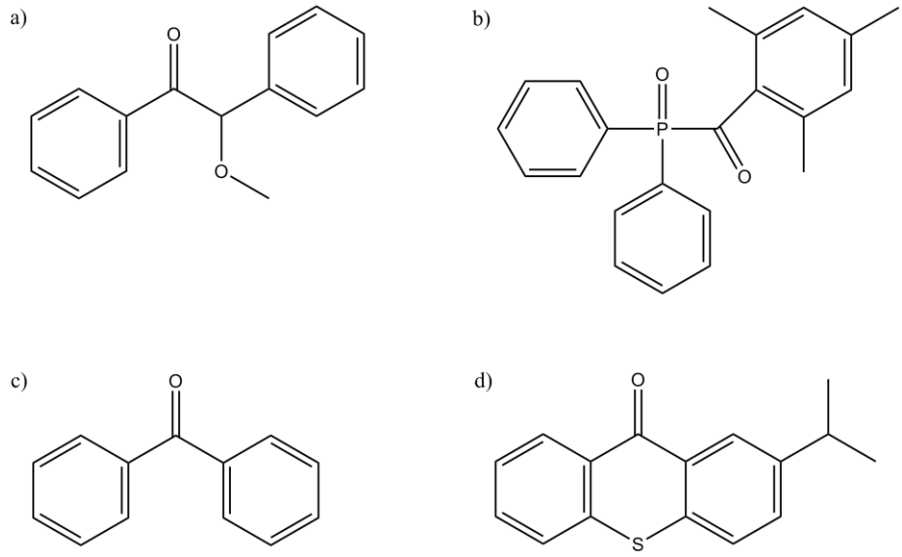

Figure 1.1 Examples of photoinitiators. a) benzoin methyl ether (type I). b) diphenyl(2,4,6-trimethylbenzoyl)phosphine oxide (type I). c) benzophenone (type II). d) thioxanthone (type II).

The radical mediated thiol-ene reaction is highly versatile, occurring between almost any carbon-carbon double bond and thiol; however, reaction rates can vary over several orders of magnitude. In general, the reactivity of enes in a typical radical mediated "click" reaction is as follows:

Norbornene > vinylether > propenyl > alkene ≈ vinylester > *N*-vinylamide > allylether ≈ allylisocyanurate > acrylate > *N*-substituted maleimide > acrylonitrile ≈ methacrylate > styrene > conjugated diene[1, 2]

As the electron density of the carbon-carbon double bond decreases, the reactivity of the "ene" decreases[29]. This is due to an increase in the stability of the carbon-centred radical, making a less reactive intermediate, decreasing the rate of propagation, and hence, the rate of the thiol-ene reaction as a whole. The reactivity of thiol monomers follows the trend:

Propionates > glycolates >> alkylthiols[1, 2]

The addition of a thiol group across a carbon-carbon double bond via a Michael addition can also be referred to as a thiol-ene "click" reaction. The reactions are generally catalysed by weak bases or strong nucleophiles and proceed via an anionic chain mechanism. The Michael addition reaction is open to fewer enes than the radical-mediated "click" reaction as the carbon-carbon double bond must be electron deficient for the reaction to occur. The first step of the weak base catalysed reaction (shown in Scheme 1.6) is the formation of a thiolate anion as the base removes the hydrogen from the thiol group[42].

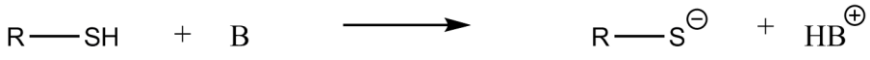

Scheme 1.6 Formation of the thiolate anion in the base catalysed thiol-ene Michael addition.

When catalysed by a strong nucleophile an intermediate enolate base is formed by nucleophilic attack on the carbon-carbon double bond of the ene, this base then attacks a thiol group, forming the thiolate anion[43] (Scheme 1.7).

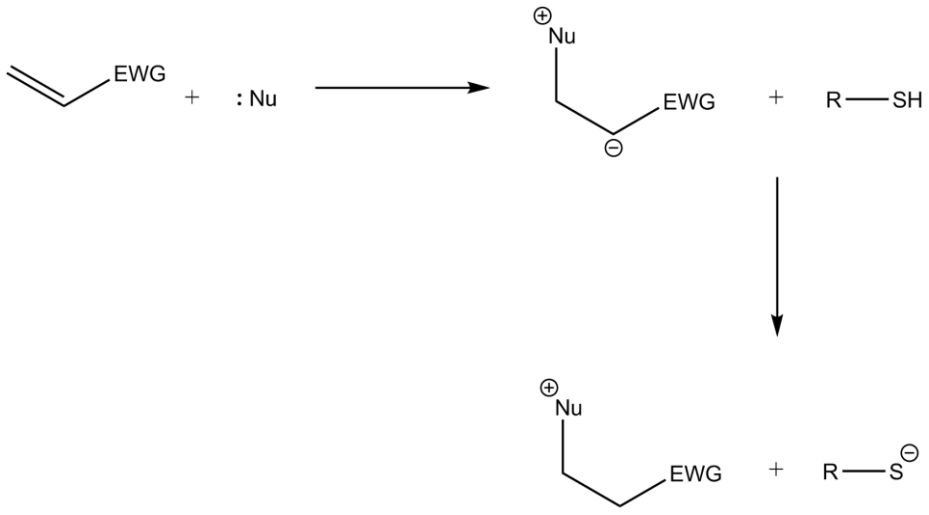

Scheme 1.7 Formation of the thiolate anion in the nucleophile catalysed thiol-ene Michael addition.

The thiolate ion then attacks the carbon-carbon double bond at the electrophilic β-carbon, yielding an enolate intermediate. This intermediate

then forms the thiol-ene product by abstracting hydrogen either from another thiol group or from the catalyst[42, 43] as shown in Scheme 1.8.

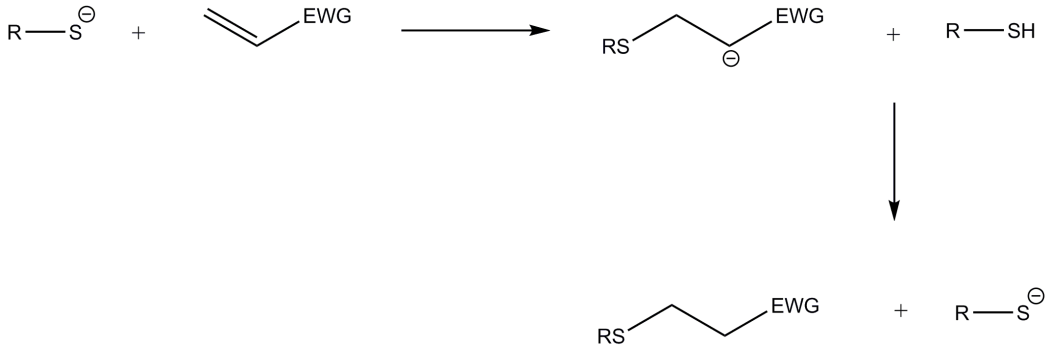

Scheme 1.8 Thiol-ene Michael addition.

Both the radical-mediated and Michael thiol-ene reactions are regiospecific, selectively yielding the anti-Markovnikov product and exhibiting the favourable features attributed to "click" chemistry. Both reactions are insensitive to oxygen and water and can occur in environmentally benign solvents such as alcohols. The reactions also proceed at a fast rate, and in near quantitative yields.

1.1.3. Applications of Thiol-Ene "Click" Chemistry

Although "click" chemistry was originally developed as a means of simplifying the synthesis of biomolecules, it is often used in the field of polymer chemistry. The regioselective nature and near quantitative conversions observed in "click" chemistry, particularly thiol-ene "click" chemistry, have been exploited in order to create many polymeric materials including cross-linked polymer networks[44], such as hydrogels[45]; dendrimers[46] and star polymers[47]; microfluidic devices[34]; and to functionalize polymers post-polymerization[48].

1.1.3.1. Polymer and Macromer Synthesis

A wide variety of different polymers have been synthesized and functionalized using the thiol-ene "click" reaction. One of the simplest examples of this is the functionalization of well-defined homopolymers of 1,2-polybutadiene (PB) and AB diblock copolymers of PB and poly(ethylene

oxide) (PEO) with a range of thiols[49]. The resulting polymer was found to be free form carbon-carbon double bonds but the reaction proceeds with less than quantitative conversions (generally between 70% and 80%)[50]. The lower conversion can be attributed to intramolecular cyclization reactions[50], as shown in Scheme 1.9. The occurrence of these undesirable side reactions and the large excess of thiol required (10 equivalents) means that this reaction cannot be described as a "click" reaction. However, the results show that polymers can be effectively functionalized post-polymerization by a thiol-ene reaction.

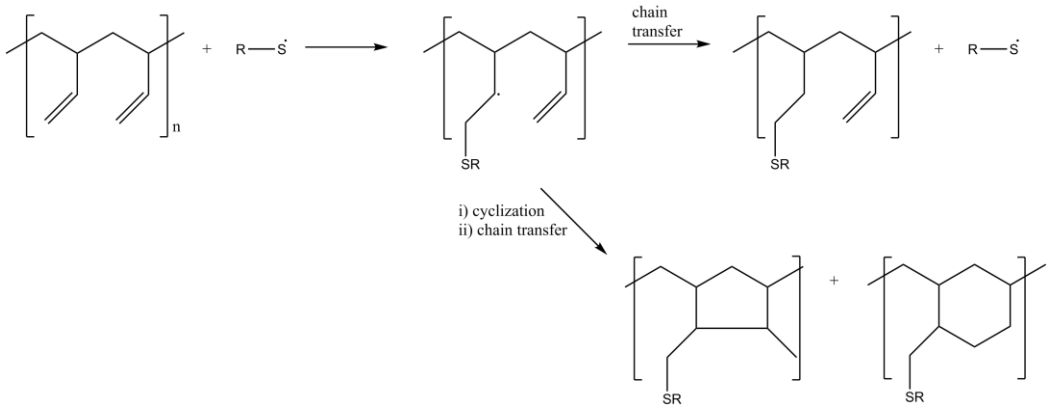

Scheme 1.9 Thiol functionalization of 1,2-polybutadiene, highlighting the competing intramolecular cyclisations.

The amount of thiol can be reduced to between 1.2-1.5 equivalents (to the number of ene groups), and the ene replaced with a macromer that cannot undergo homopolymerization or internal cyclization reactions, such as an oxazoline[51], as shown in Scheme 1.10. The method of initiation can include thermal radical (AIBN) and UV irradiation at room temperature[51, 52]. This enhanced reaction was found to proceed quantitatively, with no observed cyclization[53]. These observations led Diehl and Schlaad to describe this functionalization reaction as a "click" reaction[51]. A major advantage of this reaction is that the starting materials can include a range of materials, such as commodity polymers which can be purchased in bulk at low cost and then functionalized in order to synthesize materials that previously required complex, multistep, expensive chemistry[54]. Starting materials can also

include thiol or “ene” containing polymers which have been synthesized by conventional polymerization techniques[55-57].

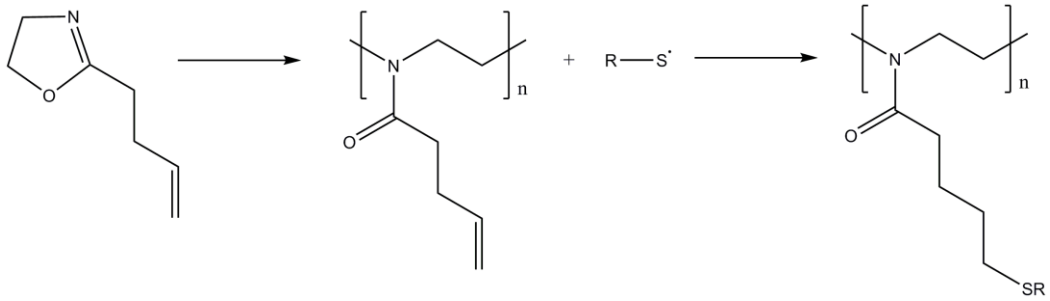

Scheme 1.10 Synthesis and thiol functionalization of polyoxazolines via thiol-ene “click” chemistry.

A combination of these polymerization techniques has been used in the synthesis of both star polymers and dendrimers. Poly(*N*, *N*-diethylacrylamide) homopolymers can be synthesized by RAFT polymerization of *N*, *N*-diethylacrylamide using 1-cyano-1-methylethyl dithiobenzonate as the RAFT agent (Scheme 1.11). The thiocarbonylthio groups at the chain ends can then be reduced to thiols with a primary amine. The resulting polymers can be conjugated to a triacrylate core via a phosphine catalysed thiol-ene “click” reaction to give a three-armed star polymer[58].

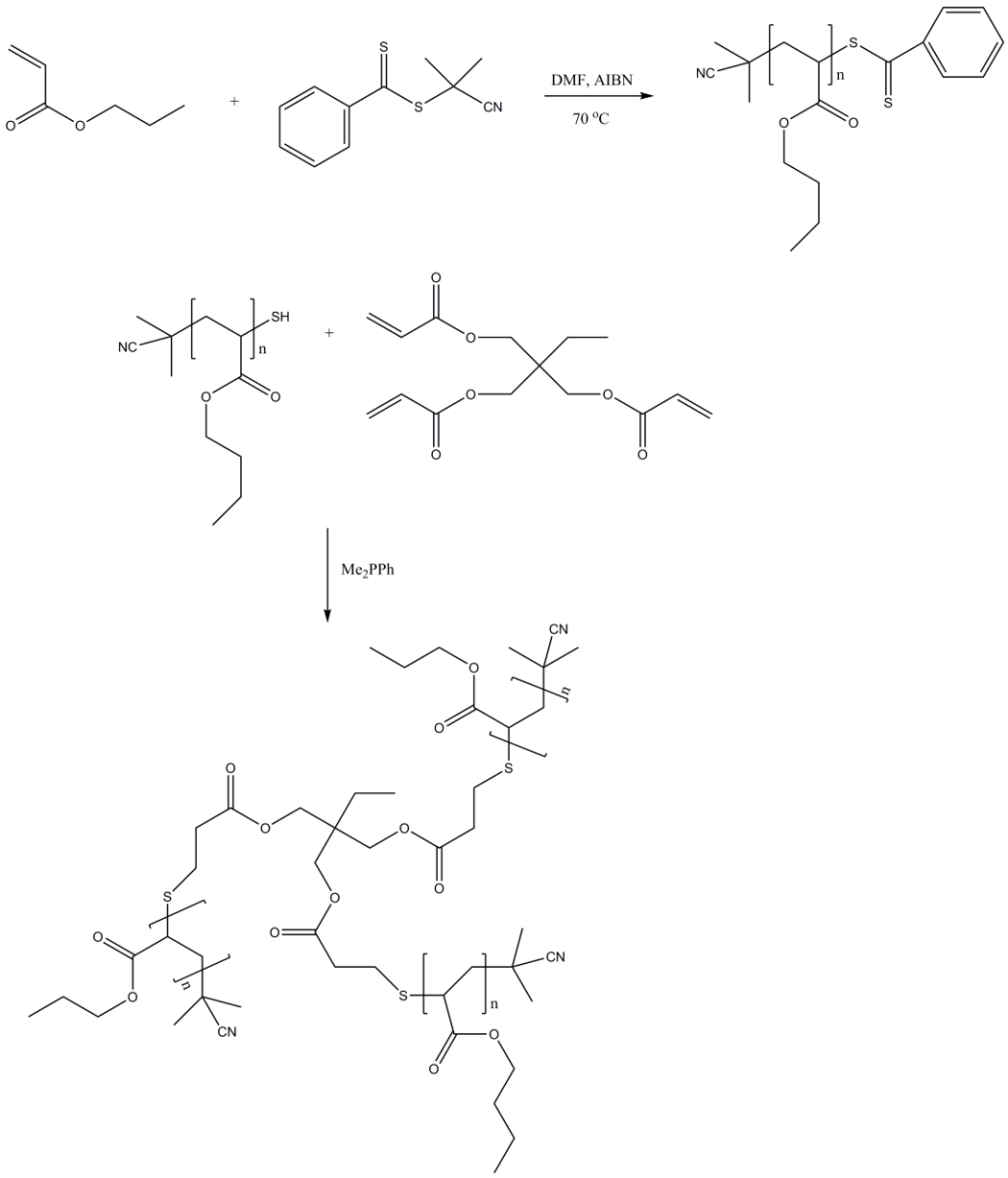

Scheme 1.11 RAFT polymerization of *N*, *N*-diethylacrylamide and subsequent conjugation a trimethylolpropane core by thiol-ene "click" chemistry, yielding the three-arm star polymer.

Killops et al. demonstrated that thiol-ene "click" chemistry can be used to create a dendrimer backbone, with the tris-alkene 2,4,6-triallyloxy-1,3,5-triazine as the core of the dendrimer, and then to functionalize the resulting chain ends[46]. The first generation dendrimer was formed via the reaction of 1.5 equivalents (to the number of ene bonds) of 1-thioglycerol with the dendrimer core under solventless conditions via a UV initiated reaction. The formation of the first-generation hexa-hydroxy dendrimer was then

confirmed by ^{1}H NMR spectroscopy. The first-generation dendrimer was then prepared for further thiol-ene reactions by esterification. The thiol-ene and the esterification reactions were then repeated in order to obtain the fourth-generation dendrimer. In keeping with the facile nature of "click" chemistry, the obtained dendrimers were purified by precipitation into diethyl ether at greater than 90% purity. Once obtained the hydroxyl chain ends on the fourth-generation dendrimer can then be converted to alkenes by the previously described methods and functionalized with monofunctional thiols, including biologically relevant molecules, such as cysteine, via another thiol-ene "click" reaction[46]. A simplified mechanism for the synthesis of the fourth-generation dendrimer is shown in Scheme 1.12.

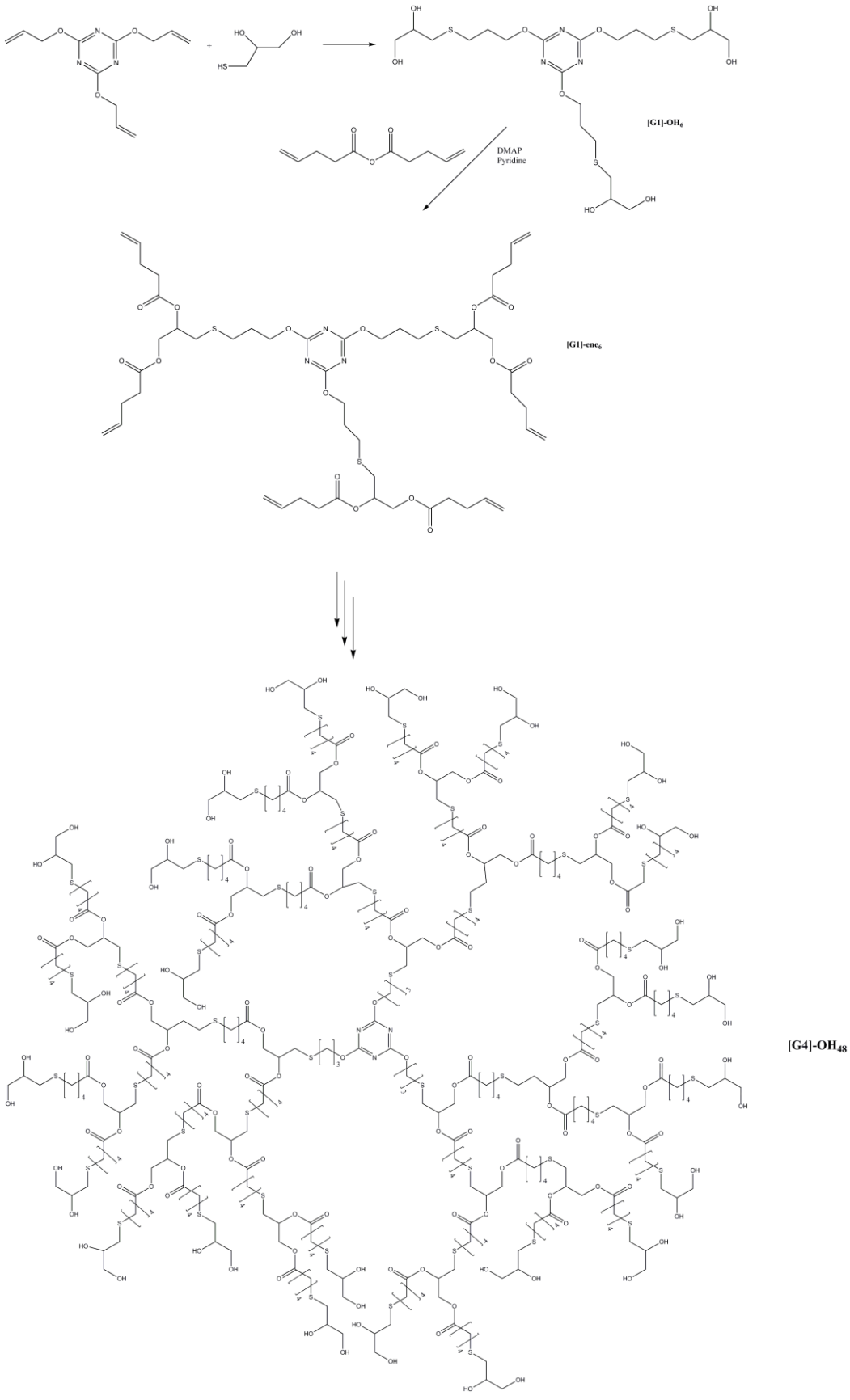

Scheme 1.12 Synthesis of 48-functional polyol dendrimer by sequential radical thiol-ene and esterification reactions.

Further exploration of the potential of "click" chemistry within dendrimer synthesis has led to the development of a synthetic strategy for sixth-generation dendrimers that can be synthesised in a single day[59]. While this synthetic strategy combines both CuAAC and thiol-ene "click" reactions, making it unsuitable for biological applications, the dendrimers can be synthesized on a multi-gram scale and are purified by simple purification techniques.

1.1.3.2. Polymeric Materials

The thiol-ene "click" reaction has found applications in the field of material chemistry where it has been used to synthesize a variety of crosslinked polymeric materials[44, 60, 61]. The reaction of multifunctional enes and multifunctional thiols leads to the formation of highly cross-linked networks. Of the "enes" available for this kind of reaction, acrylates and methacrylates are among the most commonly used. The thiol-ene reaction reduces the level of oxygen inhibition observed in acrylate and methacrylate polymerizations[62]. This allows for "ene" systems that would normally require nitrogen atmospheres and very high intensity UV radiation to be cured under much milder conditions. The introduction of thiols into the monomer system also helps to minimise the shrinkage and shrinkage stress experienced by the network by delaying the gel point[63]. This delayed gel point is a result of the step-growth nature of thiol-ene polymerizations[64]. While undergoing a step-growth reaction one thiol monomer is added across the carbon-carbon double bond, as opposed to the two monomer additions which would occur in chain growth reactions. Delaying the gel point also leads to the formation of more uniform networks[31]. These combined benefits make thiol-ene "click" chemistry ideal for the fabrication of polymeric materials such as microfluidic devices, hydrogels and porous polymer networks[65].

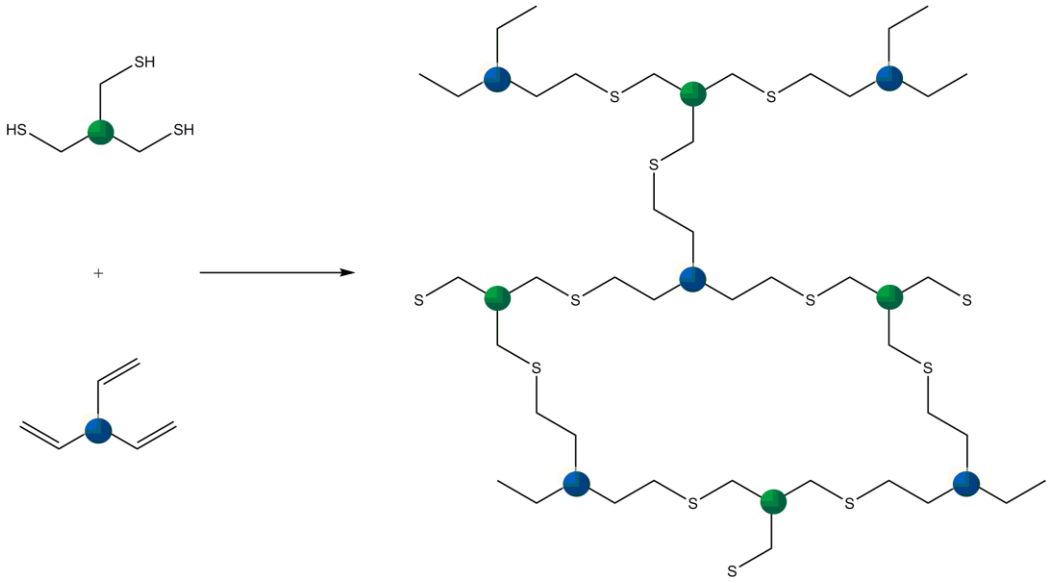

Figure 1.2 Formation of a crosslinked network via the ideal thiol-ene reaction.

In recent years, hydrogels have found several applications in the biomaterials field. These applications include scaffolds for tissue engineering[66, 67] and wound healing[68], and they have been explored as potential drug delivery vehicles. The hydrogels used for such biological applications are often synthesized from PEG macromers with double bond chain ends, including acrylates[45, 69, 70]and other enes such as norbornenes[71]. One of the main advantages of using hydrogels formed by thiol-ene "click" chemistry for biological applications is the degradability of these materials. In the case of PEG-norbornene-thiol hydrogels, the ester linkage formed between the ene chain end and the PEG backbone can undergo hydrolytic degradation[72]. The thioether-ester linkage in thiol-acrylate hydrogels can also degrade hydrolytically[69, 73]. Therefore, the rate of hydrolysis can be tuned by altering the number of functional groups each monomer possesses. This changes the crosslink density of the overall network, increasing or decreasing the number of bonds that need to be cleaved during degradation[74]. Photodegradable hydrogels can also be formed by careful selection of the monomers and photoinitiator used[75].

The step-growth nature of the photoinitiated thiol-ene reaction gives thiol-ene hydrogels an advantage over their chain-growth counterparts as the level of ene homopolymerization is reduced[71]. This reduction in

homopolymerization often results in a reduction in the chain length of the degradation products. Lower molecular weight degradation products are an advantage when developing materials for implant as they are more easily excreted by the body. Chain growth acrylate homopolymerization reactions require long gelation times as a result of oxygen inhibition, whereas thiol-ene reactions are not affected by the presence of oxygen[1], leading to faster gelation times[76]. While step-growth gels can be formed by both photoinitiated "click" thiol-ene reactions and Michael addition thiol-ene reactions, the photoinitiated reaction offers crosslinked networks with lower levels of network defects, and hence improved mechanical properties[71]. These improved mechanical properties are the result of several features of the radical-mediated thiol-ene reaction. The first of these features is the high reactivity of the radical species. The increased level of reactivity can be observed as a reduction in gelation time. The gelation of PEG-norbornene-thiol gels formed by a photoinitated thiol-ene "click" reaction was found to be approximately 230 times faster than the equivalent hydrogel formed by a Michael addition reaction[72]. The photoinitiated reaction also leads to a decrease in the number of disulphide bonds formed between thiol monomers as these bonds are weak and so are easily cleaved by the radical species present in the reaction mix[71, 77]. Both of these features of the radical-mediated thiol-ene "click" reaction lead to an increase in the network crosslink density without the need to change the functionality of the monomers used. Hydrogels formed by a photo-reaction are found to have higher shear moduli and lower mass swelling ratios than their Michael addition counterparts[76].

There are three important variables which need to be considered when synthesizing thiol-ene hydrogels with defined mechanical properties. These variables are: the functional groups used to form the crosslinked network; the molar mass of the monomers/macromers used, for example, the length of PEG chain used in PEG-norbornene-thiol hydrogels; and the choice of solvent and the concentrations used[72]. The choice of functional group is important when trying to define the mechanical and degradation properties

of a hydrogel. The reactivities of the functional groups will determine the rate of gelation and the number of network defects observed. “Ene” monomers/macromers can be susceptible to homopolymerization and internal cyclization reactions, which reduce the crosslink density of the network, decreasing the tensile strength of the hydrogel[78]. The molar mass of the monomers and macromers used also affects the degree of crosslinking observed. Gels containing longer polymer chains require longer gelation times due to the high mobility of the polymer chains, and the lower number of functional groups per unit mass of polymer, reducing the likelihood of the thiol groups reacting with the “ene” groups, leading to less densely crosslinked hydrogels[78]. Finally, the choice and concentration of solvent also impacts the likelihood of the reaction between thiol and “ene” chains ends. Using a solvent that will disperse the monomer solution well will yield a hydrogel with a higher tensile strength than a gel formed using a poor solvent[78]. This increase in tensile strength is due to a better dispersion of the functional groups required for network crosslinking. The concentration of functional groups in the reaction mixture can also be controlled by changing the concentration of solvent within the mixture. Reducing the volume of solvent decreases the distance between functional groups, this reduced distance increases the probability of a reaction, leading to a more densely crosslinked gel.

The ease with which the mechanical and degradation properties of thiol-ene hydrogels can be tuned has made them an attractive option for the synthesis of scaffolds for tissue engineering. Hydrogels with consistent mechanical properties can be produced from nontoxic, hydrophilic polymers, and biomolecules which help support cell proliferation, migration and differentiation can be easily incorporated into the gels. Control of the swelling of hydrogels can be achieved by controlling the crosslink density of the network. This allows for better control of mass transfer through the gel, which is important in ensuring nutrients can be transported to and waste products away from the cells[79-81].

The thiol-ene reaction has been exploited in the formation and post-polymerization functionalization of porous polymer networks[44]. The emulsion templating method is a facile way of producing porous polymers with well-defined morphologies and porosities. Emulsion templating involves the formation of an emulsion with the monomers as the continuous phase and a porogen as the non-continuous droplet phase. The continuous phase is then polymerized and the porogen removed, leaving behind a polymer foam[82]. The photo-initiated thiol-ene reaction allows for the polymerization of emulsions that would otherwise collapse before the polymerization reaction goes to completion. These biodegradable porous polymers have also been used in tissue engineering and 3D cell culture applications[83]. Porous polymer monoliths have also been used as the stationary phase for detection, separation and chromatography purposes[84, 85]. The surface chemistry of these polymer networks is of great importance when designing material for chromatography. The surface of the polymer must be either resistant to or have a specific interaction with the targeted chemical. Functionalizing the polymer network post-polymerization allows for specific chemistries to be found at the polymer surface without the need to reoptimize the polymerization conditions. The thiol or ene groups on the polymer surface can be included either during polymerization of the polymer network or via a post-polymerization functionalization step. Once on the polymer surface they can then be used to impart a particular chemical functionality onto the polymer surface. For example, the usually hydrophobic poly(glycidyl methacrylate-co-ethylene dimethacrylate) porous monoliths can be made hydrophilic and have been used to separate both alkyl benzenes and peptides depending on the nature of the polymer surface[84]. Thiol functionality is added to the polymer surface in a post-polymerization grafting reaction using cystamine, followed by cleavage of the disulphide bond using tris(2-carboxyethyl)phosphine. Hydrophilicity is then imparted on the polymer surface by clicking [2-(methacroyloxy)ethyl]-diemthyl-(3-sulfopropyl)ammonium betaine to the surface. While the efficiency of this porous monolith as a separation column was not as high as

its silica based counterparts, these monoliths can be hypercrosslinked in order to improve the efficiency[84].

1.2. Porous Polymers

Porous polymers have found applications in a wide range of areas. These applications include: as membranes for separation[86], filtration[87] and chromatography[88]; scaffolds for tissue engineering[89]; supports for catalysts[90] and reagents used in synthesis; to encapsulate and facilitate the controlled release of drugs[87]; as a support for sensors[91]; as gas storage devices[92-94]; and as masks for lithography[95], as well as many other uses. The type of application suitable for a porous polymer is determined by a number of factors, including the size and morphology of the pores, as well as the chemical properties of the polymers used. Porous polymers have a number of advantages over other commonly used porous materials, such as zeolites, activated carbons and porous silicas. The wide range of polymerization reactions that can be used to form porous polymers, and hence the wide range of monomers available, allow for the production of polymers with different chemical functionalities[96-98]. As a result of the different monomers that can be utilized, a wide range of chemical functionalities can be imparted onto the pore surface using various grafting techniques[99-101]. Solvent-based processing techniques can also be employed for processing porous polymers[102]. Due to the lightweight elements used in their production, porous polymers are generally more lightweight than other porous materials[103, 104].

Polymer structures with either single or multiple pores can be described as porous polymers. Pore sizes can be over a large range from nanometres to hundreds of microns. According to IUPAC recommendations[105], porous polymers can be placed in three categories based on pore size:

1. Microporous polymers – pore diameter less than 2 nm
2. Mesoporous polymers – pore diameter in the range 2 – 50 nm
3. Macroporous polymers – pore diameter larger than 50 nm

The pore size is related to the Brunauer-Emmett-Teller surface area of the polymer. Generally, polymers with smaller pore sizes, such as microporous polymers, have larger surface areas than mesoporous or macroporous polymers. The surface area, and hence the pore size, of a polymer often impacts the applications for which a particular porous polymer can be used. Other characteristics that dictate the suitable applications for a porous polymer include: the pore geometry, which can range from individual spherical pores, to a hierarchical network of fully interconnected pores; the chemical functionality of the pore surface; and the nature of the polymer's topology with pores being found in ordered or disordered arrays.

As a result of the impact that the overall network properties of a porous polymer has on its usefulness in certain applications, several synthetic procedures have been developed aiming at designing polymers with well-defined pore sizes and structures. These synthetic routes often allow the polymers to be imparted with the desired chemical functionality either during polymer synthesis or via post-polymerization modification techniques. These synthetic methodologies include:

1. Direct templating
2. Self-assembly of block copolymers
3. Direct Synthesis
4. Breath Figure
5. Emulsion templating

For the purpose of this work the emulsion templating method will be discussed in detail. Detailed discussions of other synthetic routes to porous polymers mentioned above can be found in the literature[98].

1.2.1. Synthesis of Emulsion Templated Porous Polymers

Emulsions are formed when at least two immiscible liquids are blended to give a heterogeneous suspension of droplets of one liquid inside a continuous phase of the other. If this continuous phase is polymerized, a porous polymer is formed. Emulsions can be described as either oil-in-water

(o/w) or water-in-oil (w/o), where the droplet phase is oil or water respectively.

1.2.1.1 High Internal Phase Emulsions

In order to produce highly porous materials a certain class of emulsion, known as a high internal phase emulsion, or HIPE, is used. HIPEs are defined as having an internal, or droplet, volume phase ratio, ϕ, of 0.74 or greater[82]. A volume fraction of 0.74 represents the maximum volume ratio at which the droplet phase will pack as uniform non-deformable spheres. Values of ϕ up to 0.99 can be observed, indicating that the droplet phase in a HIPE is either non-uniform or that the droplets are deformed into polyhedra[82].

The most commonly used method of forming HIPEs is by the slow addition of a porogen (non-continuous phase) to the continuous phase with mixing[83, 106, 107], as demonstrated in Figure 1.3, although other methods can be used[108]. The continuous phase generally consists of a mixture of monomer, comonomer and a suitable surfactant; a solvent may also be included in order to reduce the viscosity of the continuous phase. Mixing is generally at a high shear rate and is an important stage in HIPE formation as it breaks up any larger droplets into smaller ones. Other methods of HIPE formation include the multiple emulsification method and the spontaneous formation method. HIPEs can be both oil-in-water (o/w) and water-in-oil emulsions (w/o). In w/o emulsions the continuous phase is the oil phase and the porogen is water, in o/w emulsions it is the reverse. The type of emulsion formed is dependent on the ratio of each phase and the type of surfactant used.

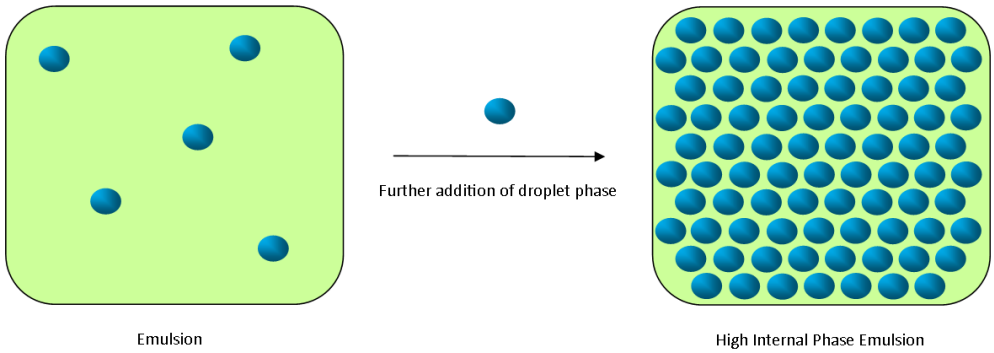

Figure 1.3 Formation of a high internal phase emulsion (HIPE)

HIPEs are thermodynamically unstable, but exhibit varying degrees of kinetic stability. The stability of the HIPE is strongly dependent on the internal phase volume ratio, as well as the hydrophilic properties of the monomers, and the type and volume of surfactant used. Increasing the internal phase volume ratio increases the likelihood of droplet coalescence, where droplets merge in order to form larger droplets, and Ostwald ripening[109], a phenomenon which causes larger droplets to grow at the expense of smaller ones as a result of the high surface energy associated with smaller droplets. The combination of droplet coalescence and Ostwald ripening results in collapse of the HIPE as the size of the droplets become too large for the continuous phase to support them.

One of the main applications of HIPEs is as a template in the formation of highly porous polymers, known as polyHIPEs.

1.2.1.2 High Internal Phase Emulsion Templated Porous Polymers

Polymerization, or curing, the continuous phase of a HIPE gives a porous polymeric material known as a polyHIPE[110, 111], as shown in Figure 1.4. The continuous phase of the emulsion must contain a cross-linker in addition to the monomer and surfactant. The cross-linker is needed in order to form the polymer network that makes up the polyHIPE structure. Once cured, the porogen is removed and the porous material is washed by Soxhlet extraction and dried.

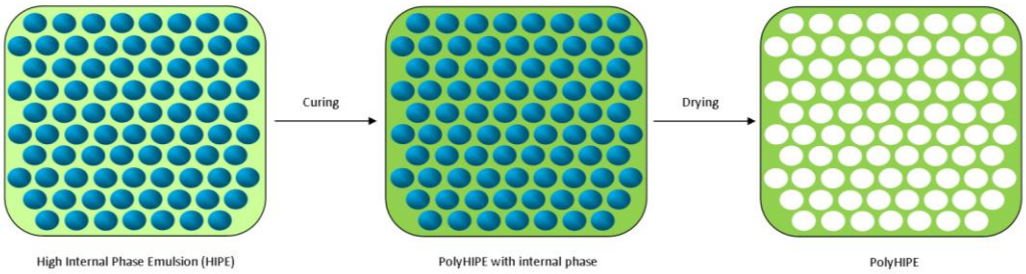

Figure 1.4 Formation of a polyHIPE.

The obtained polymer is a highly porous and permeable material, with a complex pore morphology. An SEM image of typical a polyHIPE is shown in Figure 1.5. The spherical cavities shown are referred to as voids, while the smaller interconnecting spheres between voids are known as windows. The much smaller structures within the walls of the polyHIPE are referred to as pores[82].

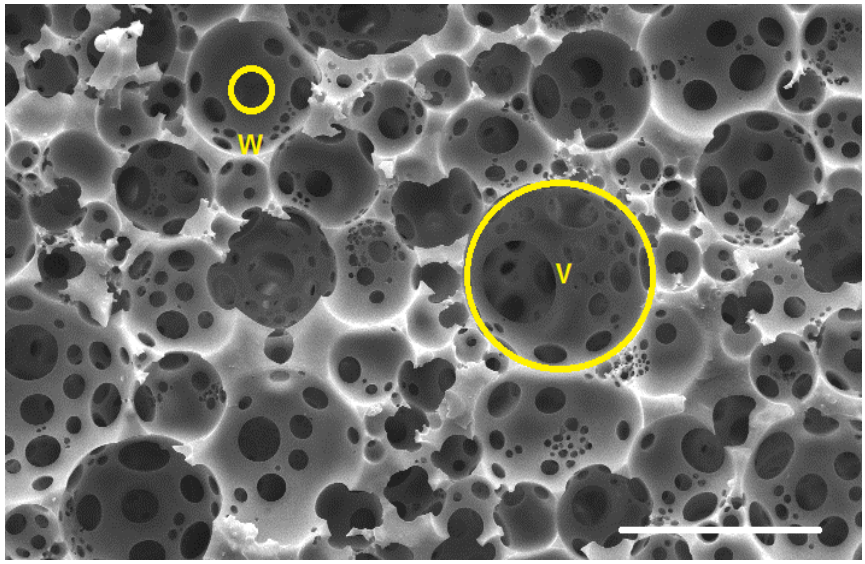

Figure 1.5 SEM of a typical polyHIPE polymer where V indicates a void and W indicates a window. Scale bar = 100 µm.

The polyHIPE void diameter can be varied from 1 µm to diameters greater than 100 µm by controlling the diameter of the droplets in the HIPE[112]. The 3D structure of a polyHIPE is of great importance when the material is intended for a particular application, and the ability to tune the structure by varying the properties of the HIPE precursor is particularly attractive. The ability to tune the void diameters in a polyHIPE material is generally

allowed for by control over the stability or instability of the HIPE[112-114], although, the rate of shear upon HIPE formation can also have an impact. There are two major factors that affect HIPE stability: Ostwald ripening and droplet coalescence. Ostwald ripening occurs as a direct result of the differences in surface tension and chemical potential between large and small droplets. Smaller droplets experience a higher solubility in the continuous phase as a result of the Kelvin effect[115]. The Kelvin effect describes the relationship between the curvature of a liquid's surface and the vapour pressure associated with the liquid. Curved surfaces exhibit a higher vapour pressure than flat surfaces and so smaller droplets have much higher vapour pressures than their larger counterparts. As a result, smaller droplets have a much higher tendency to dissolve and diffuse through the interfacial layer, finally being re-deposited into larger droplets. Droplet coalescence occurs as a result of the thinning and subsequent rupture of the interfacial layer[116].

By far the most studied polyHIPE system is that of styrene (ST) with a divinylbenzene (DVB) crosslinker[107, 117-119]. The factors that affect the 3D structure of this polyHIPE system have been studied in great detail. It has been shown that the nature and concentration of the surfactant used has an impact on the appearance and size of the interconnecting windows[113]. The interconnecting windows are believed to form by contraction of the continuous phase upon curing. The addition of surfactant causes the monomer film separating each individual droplet to thin. Since the film is at its thinnest at the point of nearest contact between each droplet, any contraction in the continuous phase would lead to the formation of holes at this point. In order to study this more closely ST/DVB polyHIPEs were prepared using varying concentrations of the surfactant Span 80. Closed-cell materials with no interconnecting windows were obtained at surfactant concentrations between 3% and 5% (w/w). As the surfactant concentration was increased to between 7% and 10% an open-cell morphology was observed. Increasing the surfactant concentration further resulted in an increase in the interconnecting window diameter, up to 80% (w/w)

surfactant. A visual representation of the formation of interconnecting windows can also be obtained using cryo-SEM[117]. Images of frozen HIPE samples at different curing times indicate that the windows are produced by shrinkage during polymerization. The formation of the interconnecting windows appears to coincide with the gel point of the polymer, further supporting the hypothesis that the windows are produced by shrinkage of the continuous phase upon polymerization.

Increasing the temperature of the aqueous phase has an impact on both the void diameter and the diameter of the interconnecting windows. This increase in temperature leads to a decrease in the stability of the HIPE precursor. This decrease in stability is due to two main factors: increased mobility of the droplets and increase solubility of the surfactant in the aqueous phase. Both factors increase the likelihood of droplet coalescence, leading to an increase in void diameter[107].

A further factor that impacts the 3D structure of a polyHIPE polymer is the inclusion of additives into the emulsion. Small organic molecules, such as acetone, methanol, and THF, can have a destabilising effect on a HIPE when added as a co-solvent. The emulsion destabilization is as a result of the solubility of the co-solvent in both the organic and aqueous phases. This solubility increases the likelihood of both droplet coalescence and Ostwald ripening by diluting the interfacial layer and increasing the solubility of the surfactant in the aqueous phase. The relative solubility of the co-solvent in each phase determines the extent of the effect on the polyHIPE morphology and the mechanism by which emulsion destabilization occurs. PolyHIPEs prepared with THF as the co-solvent show a much wider range of void diameters than those with methanol as the co-solvent as well as a higher average void diameter. This is believed to be due to the increased solubility of THF in the organic phase compared to methanol. As the concentration of the co-solvent is increased, materials with a narrow distribution of void diameters and a higher degree of interconnection are obtained. Other additives, including salts, have also been shown to have an effect on the morphology of polyHIPE polymers[107].

Due to their high porosity and relatively large void sizes, polyHIPE materials are found to have low surface areas, typically between 3 $m^2 g^{-1}$ and 20 $m^2 g^{-1}$ by BET analysis[118]. This can be increased to up to 350 $m^2 g^{-1}$ by increasing the crosslinker concentration and by the addition of a non-polymerizing organic solvent[118]. The addition of a non-polymerizable organic solvent increases the surface area of polyHIPE polymers by introducing a secondary pore structure into the material. This secondary pore structure is as a result of phase separation occurring in the continuous phase of the HIPE during polymerization. The increase in surface area can be controlled by selecting a solvent with a solubility parameter close to that of the growing polymer chain, delaying the onset of phase separation, producing smaller pores, and hence, a higher surface area.

The morphology of a polyHIPE material can also be controlled by the moulding process[82]. Before curing the HIPE is poured into a mould, where it remains during the curing process and the final polyHIPE polymer retains the shape of the mould. A wide variety of different moulds with different sizes and shapes are available, however, typically plastic bottles are used. The mould substrate used during curing has been found to influence the morphology of the polyHIPE surface. This has, again, been investigated for the ST/DVB polyHIPE system. Glass moulds were found to be unsuitable for ST/DVB polyHIPEs due to bonding between the surface and the polymer. This bonding leads to the surface of the polyHIPE having a different morphology to that of the polyHIPE interior, whereas, plastic substrates such as PVC were found to leach plasticizer, destabilizing the emulsion. Other plastic substrates investigated included polypropylene and PTFE. PolyHIPEs cured in polypropylene moulds were found to have a closed cell morphology in areas that were in contact with the mould. This is believed to be caused by preferential wetting of the monomer phase, resulting in a thin film that then forms a polymer skin upon curing. PTFE, on the other hand, was found to have no impact on the polyHIPE morphology, giving open cell surfaces. The dimensions of the mould can also be controlled in order to produce large polyHIPE monoliths or porous membranes[82].

1.2.2. Functional Porous Polymer by High Internal Phase Emulsion Templating

As mentioned previously, the ST/DVB polyHIPE system is the most widely studied, however, a much wider range of monomers can be used in order to produce polyHIPE materials a wide range of mechanical, chemical and degradation properties.

The mechanical properties of ST/DVB polyHIPEs can be tuned by the simple addition of other hydrophobic monomers into the continuous phase of the emulsion. Monomers including 2-ethylhexylacrylate (EHA) and methacrylate (EHMA) have been shown to cause a decrease in the glass transition temperature of ST/DVB polyHIPEs, leading to a more elastomeric polymer network[120]. Isobornyl acrylate (IBOA) has been shown to have the opposite effect, and its inclusion in a HIPE leads to the formation of a network with increased rigidity[121].

Chemical functionality can be imparted on ST/DVB polyHIPEs in one of two ways. The first of these is by the post-polymerization modification of the ST phenyl rings by electrophilic aromatic substitution (Scheme 1.13) to yield bromo-, nitro- and sulfonic acid substituted polyHIPE polymers[122]. The relatively low hydrophobicity of the electrophilic reagents compared with the ST/DVB polymer resulted in materials with a higher degree of substitution at the surface than in the centre. In order to overcome this, reagents with a higher level of hydrophobicity, such as lauroyl sulphate in cyclohexane were used. The use of reagents with higher hydrophobicity produced materials with more even levels of functionalization throughout their entirety[122, 123].

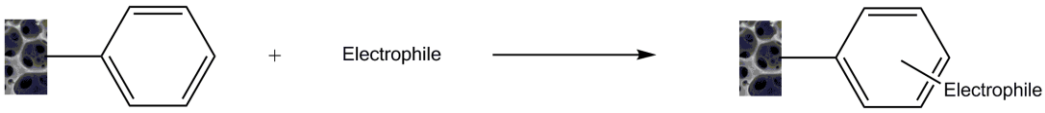

Scheme 1.13 Electrophilic aromatic substitution of phenyl rings of ST/DVB polyHIPE.

The second method of chemical functionalization is to replace the ST monomer with 4-vinylbenzyl chloride (VBC)[124]. The inclusion of VBC in the

emulsion does not have any effect on the morphology of the resulting polyHIPE and the benzyl chloride groups function as "reactive handles", allowing for the polyHIPE material to be modified post-polymerization with nucleophilic amines, such as morpholine and tris(2-aminoethyl)amine (TAEA)[125, 126], as shown in Scheme 1.14. In a similar manner VBC/DVB polyHIPEs have been used to immobilize Wang linkers, commonly used in solid phase peptide synthesis with loadings up to 3.1 mmol g^{-1} observed[127].

Scheme 1.14 Amine functionalization of ST/VBC polyHIPEs.

Materials with reactive pendant vinyl groups can be produced in a similar manner to the production of VBC/DVB polyHIPEs. The thermal free radical polymerization of a HIPE with continuous phase consisting DVB and ethylvinyl benzene (EVB) results in a material which the authors describe as a (vinyl)polystyrene polyHIPE[128]. The pendant vinyl groups can undergo both bromination and thiol addition via so-called batch and flow methods, resulting in a dimethylene spacer between the polymer network and newly introduced functionality[128, 129], as shown in Scheme 1.15.

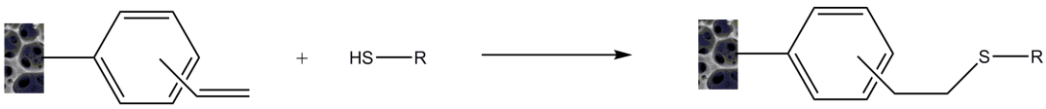

Scheme 1.15 Thiol functionalization of (vinyl)polystyrene polyHIPEs.

The copolymerization of the DVB crosslinker with the brominated styrenic monomer 4-vinylphenyl 2-bromo-2-methyl-propanoate (VPBMP) has been shown to result in a bromoester functionalized polystyrene polyHIPE. This bromoester functionality was then used to initiate the polymerization of monomers including methyl methacrylate (MMA) and glycidyl methacrylate (GMA) via a CuBr catalysed ATRP reaction, as shown in Scheme 1.16. The surface bound poly(MMA) and poly(GMA) were not found to have any adverse effects on the morphology of the polyHIPE, and hence the permeability of the materials was retained. As a result, a proposed

application for these polyHIPE materials is as monolithic scavengers for use in organic synthesis[130].

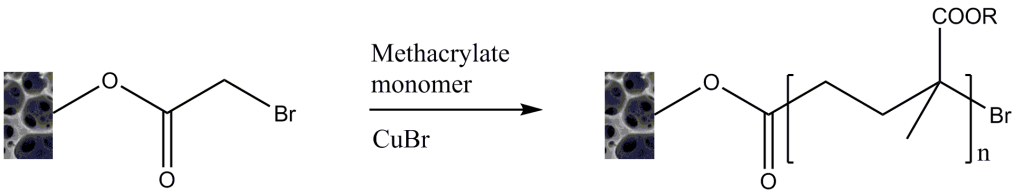

Scheme 1.16 ATRP from the surface of a bromoester functionalized polyHIPE.

As the relative hydrophilicity of the monomers is increased, the stability of the result HIPE decreases. The use of surfactant with low hydrophile-lipophile balance (HLB) numbers, allows for the stabilization of these HIPEs. HLB numbers for non-ionic surfactants are determined from Equation 1.1, based on Davies' method[131],

$$HLB = \sum H_i - n(0.475) + 7 \qquad (1.1)$$

where H_i represents the group number of hydrophilic group *i*, and *n* is the number of methylene groups, each of which is assigned a value of 0.475. Generally, HLB values range between 0 (very lipophilic) and 20 (very hydrophilic). Using a low HLB number polyglycerol ester surfactant, HIPEs with a continuous phase of up to 80% GMA were polymerized with a DVB crosslinker via a thermally initiated free-radical reaction[132]. GMA based polyHIPEs have also been prepared with ethyleneglycol dimethacrylate (EGDMA) crosslinker with the use of other low HLB number surfactants[133], including triblock copolymers of ethylene oxide (EO) and propyleneoxide (PO)[134]. The GMA is an attractive monomer for use in polyHIPEs due its reactive epoxy groups which react readily with nucleophiles[90, 135] by the mechanism shown in Scheme 1.17. While hydrolysis of the epoxy groups is observed, GMA polyHIPEs have been successfully used to immobilise proteins and enzymes[90].

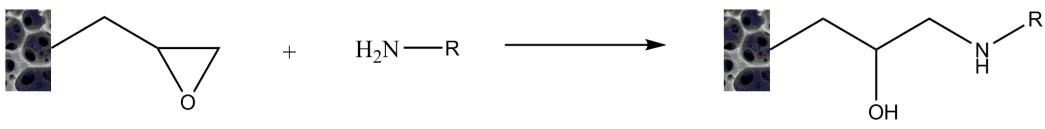

Scheme 1.17 Amine functionalization of GMA polyHIPE.

Biodegradable polyHIPEs can be synthesized by the thermal free radical polymerization of acrylated poly(ε-caprolactone)[106] or poly(lactic acid)[136]. The polymer networks, which have been investigated as scaffolds for tissue engineering, have been shown to degrade completely in a sodium hydroxide solution over a period of 10 weeks.

PolyHIPE polymers have also been produced by the ring opening metathesis polymerization (ROMP) of norbornene derivatives[96, 137]. A water tolerant ruthenium Grubb's catalyst was used in this case, and the resulting HIPE was stable enough to undergo thermal curing. Delueze et al., described the polymerization as having a living character, such that the metal carbene chain end is expected to remain active[96], allowing for further modification of the polyHIPE post-polymerization.

1.2.2.1. Emulsion Templating of Hydrophilic Monomers

Polymerizing the continuous phase of an o/w HIPE yields a hydrophilic porous polymer. Hydrophilic polyHIPEs may have great potential in the field of biotechnology, and several examples of hydrophilic polyHIPE polymers designed for use as biomaterials have already been described[138-140]. Biocompatible polyHIPE materials have been produced from the polymerization of emulsions containing the monomer 2-hydroxyethyl methacrylate (HEMA). Both w/o and o/w HIPEs can be produced for the HEMA monomer with EGDMA[141] and methylene bisacrylamide (MBAA)[138] crosslinkers. Upon thermal polymerization of the emulsion, hydrophilic porous polymers are produced. The wettability of these polyHIPEs has been shown to increase as the concentration of MBAA crosslinker is increased.

Another route to biocompatible, hydrophilic polyHIPE materials is through the use of methacrylated gelatin and dextran[139, 142-144]. Thermally initiated radical polymerization of the vinyl terminated gelatin resulted in materials with porosities of up to 95%, which, upon the addition of additives including NaCl and DMSO, had void diameters within range suitable for tissue engineering.

Despite their advantage in the formation of porous polymers for use a biomaterials, there are relatively few examples of o/w HIPEs. Perhaps the main reason for this is the large volumes of organic solvents required to produce the HIPEs[145]. These organic solvents are often difficult to completely remove from the polymer network, causing issues with biocompatibility. One route to the formation of HIPEs from hydrophilic monomers is to replace the continuous organic phase with super-critical CO_2 ($scCO_2$)[146]. $ScCO_2$ has many advantages when compared to organic solvents due to it being non-flammable, clean and inexpensive[147]. $ScCO_2$ is easy to completely remove from the polyHIPE material as the CO_2 returns to the gaseous state once depressurized[148]. One of the first examples of the use of $scCO_2$ in polyHIPE synthesis is the preparation and subsequent polymerization of a CO_2 in water (c/w) HIPE with a continuous phase consisting of and aqueous solution of acrylamide (AM) and MBAA, resulting in a highly porous polyacrylamide material[146]. The hydrocarbon surfactants required in the formation of o/w HIPEs display limited effectiveness in c/w systems and so have been replaced with fluorinated surfactants, including perfluoropolyether ammonium carboxylate (PFPE), which exhibit a higher solubility in the CO_2 phase[146].

Dextran polyHIPEs have been synthesized from c/w HIPEs using the fluorinated surfactant PFPE. The polyHIPEs obtained upon the thermal curing of the aqueous continuous phase were found to have a fully interconnected open-cell morphology and the degree of interconnectivity increased with increasing ϕ. As a result of the highly interconnected morphology, it is believed that these materials may be suitable for biomedical applications[140].

A major drawback of the use of c/w HIPEs in the synthesis of hydrophilic porous polymers is the use of fluorinated surfactants. These surfactants are expensive and are not biodegradable. In order to remove these surfactants there has been some investigation into the use of more inexpensive hydrocarbon surfactants[135, 136]. Polyacrylamide polyHIPEs, similar to those described previously, were prepared from c/w HIPEs using a variety of low

cost, commercially available, biodegradable hydrocarbon surfactants. The inclusion of the redox co-initiator tetremethylethylenediamine (TMEDA) allowed for a reduction in the temperature required to polymerize these materials from 60 ^{o}C to 20 ^{o}C[149]. The AM monomer has been found to be toxic and so hydrophilic polyHIPEs have been prepared from monomers such as HEA and HEMA with the intention of using these polymers as biomaterials[149]. Other surfactants that have been explored for use in c/w emulsions include di- and tri-block copolymers of poly(vinyl acetate) (PVAc) and poly(ethylene glycol) (PEG), which have allowed for the formation of AM/MBAA polyHIPEs under the same milder conditions as described previously[150], as well as fluorinated sugar based surfactants[151, 152].

While the use of $scCO_2$ offers several advantages for the synthesis of hydrophilic emulsion templated porous polymers, the requirement for specialized equipment and the need to at work at high pressures remain the limiting factors of this technique.

1.2.2.2. Photopolymerization

Photoinitiated polymerizations offer an attractive route to the synthesis of porous polymers due to the rapid rates of polymerizations. Photoinitiation can reduce the length of time required to cure the polyHIPEs from several hours to a matter of seconds. This rapid rate of curing offers an advantage when curing highly unstable emulsions. There have been several examples of the use of photo-, usually UV, initiation in polyHIPE synthesis. The earliest example of this in the literature is the photopolymerization of the acrylate monomers EHA and IBOA with a trimethylolpropane triacrylate (TMPTA) crosslinker and an organic soluble photoinitiator[153]. Prior to this the use of photopolymerizations had been described in two patents[154, 155]. Once conditions were optimized, *N*-acryloxysuccinimide (NASI) was incorporated into the HIPE in order to produce a polyHIPE with “reactive handles”. ATRP initiators can also be incorporated into the EHA/IBOA HIPE prior to curing, resulting in porous polymers which can undergo surface functionalization via polymer grafting[156]. Other acrylates, including GMA and EGDMA, have

been cured in this way, forming polyHIPEs that can be further functionalized[90, 157, 158].

Until recently most photoinitiated HIPE polymerizations involved the use of a UV bulb and the resulting materials were in the monolithic form. However, the rapid cure times associated with UV initiation make acrylate based HIPEs suitable candidates for UV laser curing, resulting in macrostructured polyHIPE materials. Emulsions with continuous phase consisting EHA, IBOA, TMPTA, photoinitiator and a surfactant were produced. The nominal porosities of the material was varied between 75%, 80% and 90% porous and the emulsions were cured using both scanning and projection micro-stereolithography (μL) techniques. The resulting polyHIPE materials were found to have the 3D macroscopic structure defined by the laser writing as well as the porosity exhibited by bulk cured polyHIPEs[159], as shown in Figure 1.6. The ability for fine control over both the macroscopic structure and porosity material may find an important role in the design of scaffolds for tissue engineering. μL techniques have already found applications in the synthesis of microstructured 3D PCL[160], PLA[161] and PEG-diacrylate[162] scaffolds and biomaterials.

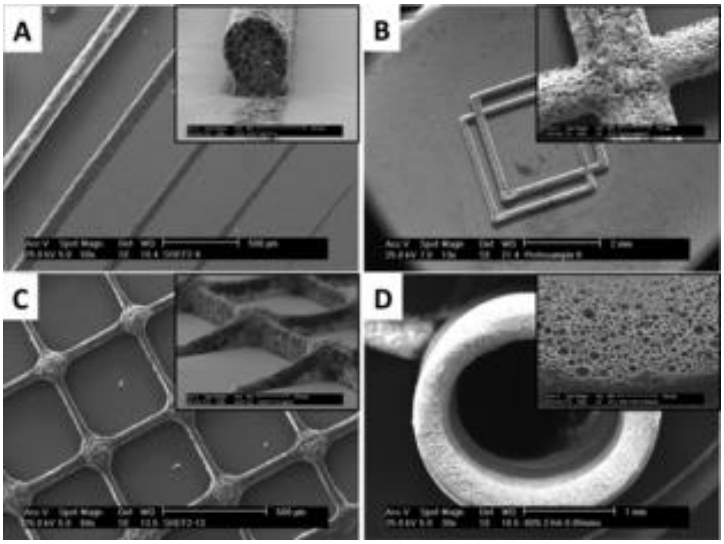

Figure 1.6 SEM images of polyHIPE materials produced by μL[159]. A) Printed lines at write speeds of 1-5 mm s^{-1} from left to right, scale bar 500 μm. B) Two overlapping printed squares, scale bar 2 mm. C) Printed grid structure, scale bar 500 μm. D) Tube produced by photopolymerization of HIPE while translating in the z-direction, scale bar 1 mm. All insets have scale bar 100 μm. Figure reproduced with permission of John Wiley and Sons.

As previously discussed, there are many reasons why thiol-ene chemistry is attractive to the fields of materials and polymer science. The combination of thiol-ene and thiol-yne chemistries with the rapid cure times associated with photopolymerizations have led to a new class of thiol-ene polyHIPEs which have been shown to have morphologies suitable for tissue engineering and the added benefit of biodegradability[83]. Thiol-ene polyHIPEs were first prepared from an emulsion with continuous phase consisting TMPTA, trimethylolpropane tris(3-mercaptopropionate) (TMPTMP), a surfactant and photoinitiator, with nominal porosities of up to 80%. The HIPEs were cured in a simple mould consisting a 50 x 50 x 5 mm PTFE square frame secured between two glass slides[44]. The thiol-yne HIPE was prepared in a similar manner, replacing the acrylate monomer with the alkyne octadiyne[44]. While photoinitiated polymerizations are the most commonly used in the preparation of thiol-ene polyHIPEs, examples of thermally initiated curing have been described[163].

μL techniques have also been applied to the curing of thiol-ene HIPEs. TMPTA and pentaerythritoltetrakis 3-mercaptopropionate (TT) w/o HIPEs

have been successfully cured in a layer-by-layer manner using a high power LED as the light source. The resulting polyHIPEs were found to exhibit porosity on two scales: the micron scale, as formed during the emulsion-templating process; and the millimetre scale as dictated by the curing pattern[164].

1.2.3. Applications of Emulsion Templated Porous Polymers

As a result of their morphologies and the ease with which chemical functionality can be imparted, emulsion templated porous polymers have found applications in a wide range of areas. These areas include: the immobilization of enzymes[90, 153], catalysts[123] and other reagents used in organic synthesis[126]; as scaffolds for tissue engineering[136] and 3D cell culture[89]; as materials for gas storage[165]; and as materials for water purification[166] and other separation processes[167].

1.2.3.1. Enzyme Immobilization

Enzymes immobilized on solid supports have found a wide variety of applications ranging from catalysts for chemical synthesis[168] to biosensors[169]. The high permeability and ease with which the polymer surface can be chemically functionalized has led to the use of polyHIPE polymers as solid supports for enzyme immobilization[153, 170, 171].

Lipase enzymes are widely used as a cheap and versatile catalyst in the food, pharmaceutical[172] and energy industries for the hydrolysis of lipids[173]. One major application of these enzymes is the synthesis of biodiesel from vegetable oils as an alternative fuel source by the transesterification of triglycerides with short chain alcohols[174]. Immobilizing these enzymes on a solid support ensures their reusability, and it has been shown that the hydrophobicity of the support has a large impact on the activity of the enzyme[175]. ST/DVB HIPEs copolymerized with polyglutaraldehyde (PGA) result in highly hydrophobic polymer networks suitable for the immobilization of the lipase enzyme from *Thermomyces lanuginosus* via covalent binding of the enzyme to the polymer surface[176-178]. In addition to its high hydrophobicity, the polyHIPE support was found to offer a number

of other advantages over other support materials. These advantages include the ease with which the polymer can be produced in large quantities, the presence of glutaraldehyde groups on the polymer surface allows for both covalent binding of the enzyme to the polymer surface as well as adsorption of the enzyme, resulting in loadings of up to 11.4 mg enzyme per 1 g polyHIPE. At these loadings biodiesel production from canola oil was found to proceed with a conversion of 97%[177]. The immobilized lipase was found to retain its high levels activity across 10 repeat reactions[176]. Lipase enzymes, obtained from *Candida antartica*, have been successfully immobilized on photopolymerized acrylate-based polyHIPEs bearing the *N*-succinimide ester moiety at high loadings, and with stable levels of enzyme activity[153].

Proteases are another group of enzymes being used as catalysts in chemical synthesis[179]. Protease-catalysed peptide synthesis allows for reactions to occur with greater selectivity and under milder reaction conditions than solid phase peptide synthesis[180]. Protease K, obtained from *Tritirachium album,* has been successfully immobilized onto photopolymerized GMA-polyHIPEs via amine functionalization of surface bound epoxy groups[90]. The activity of the surface bound enzyme, assessed by monitoring the hydrolysis of N-acetyl-L-tyrosine ethyl ester monohydrate, was found to be low, but increased upon inclusion of a PEG spacer between the enzyme and polymer surface[90].

1.2.3.2. Hydrogen Storage

Fossil fuels are currently the most relied on source of energy, however, due to depleting reserves and the effects of greenhouse gases, such as CO_2, on the environment there is a need to investigate other, cleaner and more sustainable sources of energy. Hydrogen gas is an attractive energy source due to its high energy density by mass (143.0 MJ kg^{-1})[181], however, its use has been limited so far due to two main factors:

1. Its low energy density by volume (0.0108 MJ l^{-1})[181]
2. Hydrogen gas is highly explosive in air

As a result, hydrogen storage tanks must be highly reinforced in order to prevent explosions, and able to store large volumes. Motorized vehicles are a major source of greenhouse gas pollution, and the need for large, heavily reinforced fuel storage tanks makes the use of hydrogen as a clean energy source less viable. In order to overcome this alternative hydrogen storage methods must be considered.

While the most common methods of storing hydrogen still remain the storage of the compressed gas in high-pressure tanks, storage of cryogenically cooled liquid hydrogen, or a combination of the two[181-183], there has been research into alternative hydrogen storage methods. Physisorption of hydrogen onto porous scaffolds and the storage of chemical hydrides are two such methods currently being considered[184].

A high surface area is required if a material is to be considered suitable for the storage of H_2 by physisorption[185]. While most polyHIPE materials are found to have very low surface areas, typically ranging from 3 $m^2 g^{-1}$ and 20 $m^2 g^{-1}$, the use of inert porogenic solvents and hypercrosslinking reactions can lead to dramatic increases in this value[82]. In the 1970s a class of hypercrosslinked polymers with surface areas up to 2000 $m^2 g^{-1}$ [186] were developed by Davankov et al[187]. Hypercrosslinking is achieved by the Friedel-Crafts condensation of polystyrene with bishalide monomers after swelling of the polymer in a good solvent. ST/VBC/DVB polyHIPEs can be hypercrosslinked using the Davankov method to yield monolithic porous polymers that retain the open pore network typical of a polyHIPE polymer but with surface areas up to 1200 $m^2 g^{-1}$. The high surface area is as a result of the formation of a network of micropores on the surface of the polymer network[188]. This microporosity imparts the material with a gravimetric hydrogen storage capacity of 2.02 wt%[189], a value which is much lower than the target set by the United States Department of Energy (DOE). The iron catalysts used in Friedel-Crafts alkylations creates difficulty in purifying the polyHIPE polymers after hypercrosslinking, therefore, the ability to introduce microporosity at the polymer surface without the need for a Friedel-Crafts catalyst would ease the purification process. ST/DVB

polyHIPEs reswollen in a suitable solvent have been hypercrosslinked via radical polymerization, initiated by the peroxy initiator di-tert-butyl peroxide. Surface areas of up to 355 m^2 g^{-1} were obtained using this method[119], with the lower values being attributed to the hypercrosslinking reaction being a continuation of the polymerization reaction which formed the initial polyHIPEs. As a result, any vinyl groups that remained unreacted due to lack of a reaction partner would experience the same issue during the hypercrosslinking reaction.

A second approach to the storage of hydrogen in polyHIPE polymers takes advantage of the hydrogen storage potential of clathrate hydrates[190]. The use of clathrate hydrates offers an environmental advantage as a high proportion of their mass is water. One of the major drawbacks of using clathrates lies in the kinetics of clathrate formation in the bulk[191]. The rate of formation can be increased by increasing the surface-to-volume ratio of the clathrate. This can be achieved in several ways, but perhaps the most appropriate for applications such as the onboard storage of H_2 is to disperse the clathrate on a solid support[192, 193]. The large pore volumes and high interconnectivity found in polyHIPE materials allow for the support of large volumes of clathrate on small masses of polymer. PolyHIPEs comprised of DVB and ethylstyrene (ES) have been trialled as clathrate supports[165]. The addition of a THF stabiliser prior to clathrate formation reduced the pressure required during clathrate formation[194] and helped to overcome the hydrophobicity of the ES/DVB polyHIPEs. An H_2 storage capacity of 0.18 wt% was obtained, once again much lower than DOE targets[165].

Despite both the hypercrosslinked polyHIPEs and polyHIPE supported clathrate hydrate storage methods investigated giving lower than required storage capacities, the low density, and ease with which the materials can be produced in bulk make polyHIPEs attractive materials for the storage of hydrogen as an alternative fuel source.

1.2.3.3. Tissue Engineering and 3D Cell Culture

At present there is significant interest in the fields of tissue engineering and 3D cell culture[195-197]. In the event of severe injury, or failure, of a tissue an effective treatment method must be employed in order to repair or replace the tissue. Tissue grafting and organ transplantation are, at present, the most commonly used treatment methods[197, 198], however, there are several drawbacks[198, 199]. The number of donors restricts allografting (the transplantation tissue from a donor to a recipient of the same species) with demand often greatly outstripping the supply of donated organs and tissues, and the risk of rejection results in patients requiring immunosuppressant drugs for life[199, 200]. Autografting (the transplantation of tissue from one part of the body to another) is limited by the size and location of injury, as well as the tissue type affected[200]. The procedure is also painful and can also result in severe scarring. Xenografting (the cross-species transplantation of tissues) was considered as an alternative treatment method, however, the other species used generally have shorter lifespans than humans, and hence their tissues age quicker. Xenografted tissues can also be a source of disease transmission[201], rejection[202], and introduced a wide range of ethical issues surrounding the permanent alteration of an animal's genetic code[203]. As a result of these drawbacks, the ability to regrow tissues or organs from a patient's own cells in order to transplant them back into the body is becoming increasingly attractive.

In order to culture cells in a 3D environment a scaffold is required to support the cells and provide the biological cues found in the cells' native environment. There are several features a material must possess before it can be considered for use as a biomaterial. These features include: biocompatibility; a surface that allows sufficient cell attachment; a morphology that allows for cell infiltration and the transport of nutrients to and waste products away from the cells; mechanical properties that resemble the mechanical properties of the native tissue; and, if the scaffold is to be implanted, biodegradability[198]. There is a wide range of biomaterials that feature the attributes required for tissue engineering and 3D cell

culture, including hydrogels[204, 205] and electrospun fibres[206], and the scaffolds have been fabricated from a wide range of materials, including natural[207] and synthetic polymers[208].

The highly interconnected, porous morphology of a polyHIPE and the ease with which the void sizes, elasticity, and chemical functionality of the surface can be tuned makes polyHIPE polymers suitable materials for 3D cell culture and tissue engineering applications. Early work focussed on the development of materials for 3D cell culture, fabricated from the non-biodegradable STV/DVB polyHIPEs[209, 210]. A wide variety of cells lines have been successfully cultured on ST/DVB polyHIPEs, including hepatocytes[211], osteoblasts[210] and neural cells[212]. Cells grown in 2D behave differently to cells grown in the body, and it is believed that cells cultured in 3D will exhibit behaviour closer to those *in vivo*. The morphology of hepatocytes cultured on a thin membrane of ST/DVB polyHIPE were found to more closely resemble that of typical liver cells and had significantly more microvilli than the same cells cultured in 2D[213, 214]. The cells grown in 3D were also found to synthesize higher concentrations of albumin, a protein found in the liver which plays a critical role in several liver functions including scavenging free radicals and the binding and transport of drugs. Albumin concentration is commonly used as a marker of hepatocyte metabolic activity[215], and so the higher concentration of albumin observed in 3D culture of hepatocytes indicates that growing cells in 3D leads to enhanced cell function[214]. Hepatic cell function can be further explored by monitoring cell sensitivity to drugs metabolised in the liver. Methotrexate is one such drug which is commonly used in the treatment of solid cancer tumours, such as breast cancer, and leukaemia[216]. Hepatocytes cultured in 2D were found to be sensitive to methotrexate, and the cells' metabolic function was impaired in a dose-dependent manner. As the concentration of methotrexate was increased, a reduction in the number of microvilli was observed and the cells were seen to become flat and eventually disintegrate. When cultured in the 3D environment provided by the ST/DVB scaffold, the

cells showed greater viability when exposed to higher concentrations of the drug and responded to the drug in a manner more similar to the liver[214].

The surface of an ST/DVB polyHIPE is relatively inert and the polymer is highly hydrophobic. The ability to introduce biofunctionality at the polymer surface, either via chemical functionalization or by adsorption of biomolecules onto the surface, can be used to provide the biological cues cells would normally receive from the extracellular matrix *in vivo*. There are several routes to the preparation of chemically functionalized polyHIPEs, the most commonly used during the preparation of polyHIPEs for 3D cell culture applications is the copolymerization of a monomer that can be further functionalized post-polymerization. Two recent examples are the incorporation of acrylic acid into the aqueous phase of a ST/DVB/EHA HIPE[217], and the incorporation and subsequent modification of PFPA into the continuous phase of the same HIPE[211]. The hydrophilic nature of the acrylic acid monomer resulted in an increase in the wettability of the scaffold without having a negative impact on hepatocyte adhesion. As a result of these observations, it has been suggested that the acrylic acid can be used as a route to further functionalization of ST/DVB polyHIPEs[217]. The use of active esters, such as PFPA, as a route to the post-polymerization modification of polyHIPE polymers was first explored in a thiol-ene polyHIPE system[99]. Subsequently, its inclusion in a ST/DVB/EHA polyHIPE was investigated as a route to galactose functionalized polyHIPEs[211]. Hepatocyte cells are known to possess a cell-surface asiaglycoprotein receptor[218] (ASGPR) which binds specifically to galactose[219]. This interaction can be targeted in order to improve cell-scaffold binding and cell function. As with previous studies, albumin production was monitored as an indication of the metabolic function of the hepatocyte cells, and was found to be increased in cells cultured on galactose functionalized polyHIPEs. This enhanced albumin production diminished with longer culture times. This decrease is believed to be due to non-specific binding of serum proteins to the polyHIPE surface, and needs to be addressed if galactose-functionalized polyHIPEs are to find widespread application in hepatocyte culture[211].

ST/DVB scaffolds can be enhanced for 3D cell culture applications by the adsorption of biologically relevant molecules onto the polymer surface[210]. The mineral hydroxyapatite (HA) is found in bone and teeth[220], and many implants, such as hip replacements, are coated in HA to promote integration between living bone and the implant[221]. Osteoblast cells cultured on ST/DVB scaffolds exhibited mineralization upon culture for 28 and 35 days and the genes associated with osteoblast differentiation were observed. When cultured upon HA modified polyHIPEs, there was an increase in the number of cells penetrating into the polyHIPE polymer, and an increase in mineralization was observed, indicating that coating the polyHIPE with HA improves the osteoconductivity of the polyHIPE[210].

There is a desire to prepare scaffolds for tissue engineering that are biodegradable. These scaffolds can be implanted into the body in order to support the growing tissue, degrading over time, until the tissue has been fully repaired, and the scaffold replaced with ECM. Degradable scaffolds are particularly attractive as it removes the need for a second surgery to remove the scaffold. As previously discussed, biodegradable polyHIPE have been prepared from vinyl-terminated PLA and PCL, as well as by thiol-ene chemistry[136, 222]. Human fibroblasts cultured on PCL-polyHIPEs for 2.5 days were shown to exhibit the spindle morphology typical of fibroblasts, indicating cell proliferation and tissue growth. Human keratinocytes were also successfully cultured on scaffolds prepared using thiol-ene chemistry, indicating that these scaffolds are biocompatible[83], however further investigation into biodegradable scaffolds prepared by both thiol-ene chemistry and from biopolymers is needed.

1.3. Aims and Objectives

The aim of this project is to explore the use of thiol-ene “click” chemistry in the synthesis and subsequent functionalization of emulsion templated porous polymers.

PolyHIPEs materials have been prepared using multi-functional thiol and acrylate monomers, and the presence of residual, unreacted thiols within

these materials has been investigated. Two routes to the chemical functionalization of the polymers using these unreacted thiol groups are explored, using a range of acrylate and thiol monomers.

Thiol-acrylate polyHIPEs incorporating an active ester monomer were also prepared and investigated as a route to the preparation of polyHIPEs featuring biologically relevant molecules at the polymer surface.

2. Experimental

2.1. PolyHIPE Synthesis

2.1.1. Materials

The monomers trimethylolpropane tris(3-mercaptopropionate) and trimethylolpropane triacrylate were obtained from Sigma Aldrich and used without any further purification. The photoinitiator, diphenyl (2, 4, 6-trimethyl benzoyl) – phosphine oxide/ 2-hydroxy-2-methylpropiophenone, and solvent, 1,2-dichloroethane, were also obtained from Sigma Aldrich and used as supplied. The surfactant, a polyhydroxystearic acid and polyethylene glycol copolymer (Hypermer B246), was obtained from Croda and used as supplied.

2.1.2. PolyHIPE Preparation

The oil phase, consisting of trimethylolpropane tris(3-mercaptopropionate), trimethylolpropane triacrylate, 1,2-dichloroethane, surfactant and photoinitiator, was added to a 250 ml two-necked round bottom flask with continuous stirring at 350 rpm from an overhead stirrer. The water phase was added dropwise, until an emulsion formed. This was then stirred for a further minute in order to ensure the emulsion was homogenous.

The emulsion was then poured into a mould, consisting of a 80 mm x 80 mm x 3 mm PTFE square between two glass slides, and photocured. The photocuring was conducted using a Fusion Systems Inc. Light Hammer 6 variable power system fitted with an H-bulb. UV radiation is emitted over a broad spectrum, with most emission between 200-450 nm. The cured polyHIPE was then then washed in acetone, and then washed further by Soxhlet extraction with dichloromethane at 50 °C overnight. The polyHIPE was then left to dry under high vacuum for several hours.

2.1.3. PFPA-PolyHIPE Preparation

The oil phase, consisting of trimethylolpropane tris(3-mercaptopropionate), dipentaerythritol penta-/hexa-acrylate, pentafluorophenyl acrylate, 1,2-dichloroethane, surfactant and photoinitiator, was added to a 250 ml two-necked round bottom flask with continuous stirring at 350 rpm from an overhead stirrer. The water phase was added dropwise, until an emulsion was formed. This is then stirred for a further minute in order to ensure the emulsion is homogenous. The emulsion is then moulded and photocured as described previously.

2.1.4. UV Curing

All UV curing was carried out using a Fusion UV Systems, Inc. Light Hammer 6 variable power UV curing system with bench-top conveyer. The operating wavelength of the H-bulb is 200-450 nm.

2.2. PolyHIPE Functionalization – Residual Thiol

2.2.1. Materials

All chemicals were obtained from Sigma Aldrich and used without further purification with the exception of the initiator azobisisobutyronitrile, AIBN, which was obtained from BDH Chemicals and was used without further purification.

2.2.2. UV Initiated Post-Polymerization Functionalization of PolyHIPEs by Clicking to Residual Thiols

100 mg polyHIPE was frozen in liquid nitrogen and then ground to a powder with a mortar and pestle. This powder was then transferred to a glass vial and 10 ml chloroform added. The polyHIPE was left to swell in the chloroform for 10 minutes. Two molar equivalents of the desired acrylate (mass given in Table 2.1, structure in Figure 2.1) and 0.5 equivalents AIBN were added to the polyHIPE and the resulting solution was exposed to UV radiation. The polyHIPE was then washed with chloroform and dried under reduced pressure. The quantities of acrylates used are shown in Table 2.1.

2.2.3. Thermally Initiated Post-Polymerization Functionalization of PolyHIPEs by Clicking to Residual Thiols

100 mg polyHIPE was frozen in liquid nitrogen and then ground to a powder with a mortar and pestle. This powder was then transferred to a glass vial and 10 ml toluene added. The polyHIPE was left to swell in the toluene for 10 minutes. Two molar equivalents of the desired acrylate (mass given in Table 2.1, structure in Figure 2.1) and 0.5 equivalents AIBN were added to the polyHIPE and the resulting solution was left in an oven at 60 ^{o}C overnight. The polyHIPE was then washed with toluene and dried under reduced pressure. The quantities of acrylates used are shown in Table 2.1.

2.2.4. Post-Polymerization Functionalization of PolyHIPEs by Amine Catalysed Michael Addition

100 mg polyHIPE was swollen in 10 ml methanol for 10 minutes. Two molar equivalents of the desired acrylate (mass given Table 2.1, structure in Figure 2.1) and 5 µl triethylamine were added to the polyHIPE and the resulting solution was left at room temperature for 48 hours. The polyHIPE was then washed with methanol and dried under reduced pressure.

Table 2.1. Quantities of acrylates used to functionalize thiol-acrylate polyHIPEs

Acrylate	Mass of Acrylate (g)	No. Moles Acrylate (mmol)
Hexafluoroisopropyl Acrylate	0.070	0.3
Fluorescein O-Acrylate	0.120	0.3
Poly(ethylene glycol) methacrylate methyl ether	0.154	0.3

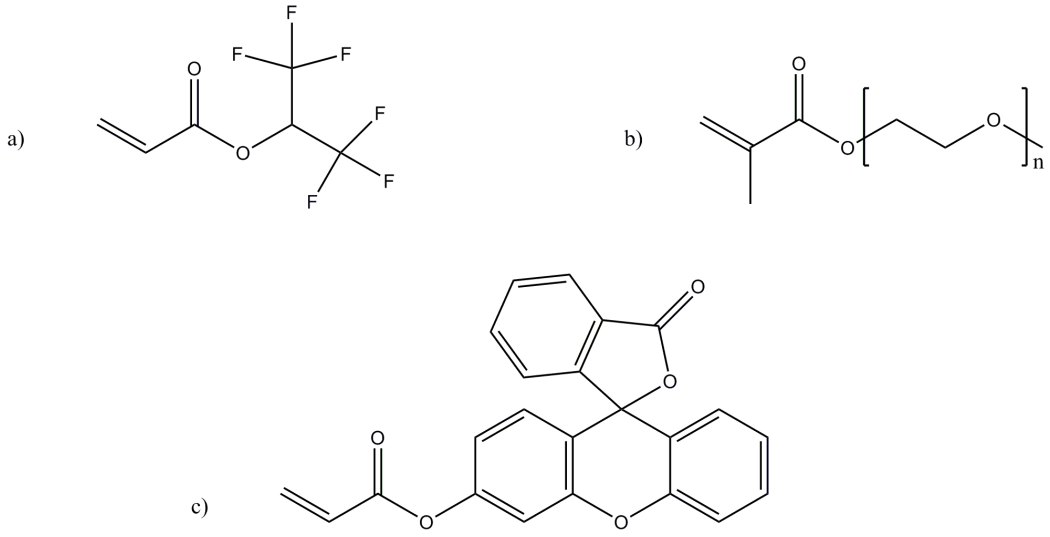

Figure 2.1 Chemical structure of acrylates used to functionalize thiol-acrylate polyHIPEs via thiol-ene "click" chemistry and Michael addition. a) hexafluoroisopropyl acrylate (HFIPA), b) poly(ethylene glycol) methacrylate methyl ether (PEGMA), c) fluorescein O-acrylate.

2.2.5. Post-Polymerization Formation of Disulphide Bonds by Disulphide Exchange

200 mg polyHIPE was swollen in THF for 10 minutes. Two molar equivalents of Ellman's reagent and diisopropylethylamine (15 µl) were dissolved in methanol (7 ml), and the solution added to the polyHIPE. The reaction was then left to proceed for 1 hour at room temperature after which the polyHIPE was washed in methanol and dried under reduced pressure.

2.2.6. Post-Polymerization Formation of Disulphide Bonds via a Sulfenylthiosulphate Intermediate

200 mg polyHIPE was swollen in methanol for 10 minutes. 100 mg sodium tetrathionate was added to the polyHIPE and left to react for 1 hour. Any salt impurity was removed by Soxhlet extraction in methanol. The polyHIPE was then swollen in a solution of ATDT (42 mg) in methanol (15 ml). The reaction was left to proceed for 2 hours at room temperature. The polyHIPE was then washed in methanol and dried under reduced pressure.

2.3. PolyHIPE Functionalization – PFPA

2.3.1. Materials

All chemicals were obtained from Sigma Aldrich and used without further purification.

2.3.2. PFPA Synthesis

4.00 g pentafluorophenol and 2.64 g triethylamine were dissolved in dry diethyl ether in a two-neck round bottom flask. 2.36 g acryloyl chloride was added dropwise under cooling with an ice bath. The ice bath was then removed and the mixture was stirred for two hours at room temperature. The precipitate salt was removed by filtration. After evaporation of the solvent the residue was filtered again and purified by column chromatography (silica gel, petroleum ether).

The mass of PFPA obtained was 3.20 g, giving a yield of 80%.

^{1}H NMR ($CDCl_3$): δ/ppm: 6.70 (d, 1H), 6.35 (dd, 1H), 6.16 (d, 1H).

2.3.3. Post-Polymerization Functionalization of PFPA-PolyHIPEs – Tris(2-Aminoethyl) Amine

0.5 g polyHIPE was left to swell in methanol for 10 minutes. A solution of tris(2-aminoethyl) amine (0.027 g) and triethylamine (0.025 g) in 2 ml methanol was prepared and added to the polyHIPE. The polyHIPE solution was then left for 48 hours at room temperature. The polyHIPE was then removed from the methanol solution and washed by Soxhlet extraction in methanol for 12 hours. The polyHIPE was then dried under reduced pressure.

2.3.4. Post-Polymerization Functionalization of PFPA-PolyHIPEs – L-Alanine

0.25 g polyHIPE was swelled in methanol for 10 minutes. A solution of *L*-alanine (0.01 g, chemical structure shown in Figure 2.2) and triethylamine (0.013 g) in 20 ml methanol was prepared and then brought to pH 10 using

sodium hydroxide. The swollen polyHIPE was then transferred to the amino acid solution and left at room temperature for 48 hours. The polyHIPE was then washed by Soxhlet extraction for 12 hours and then dried under reduced pressure.

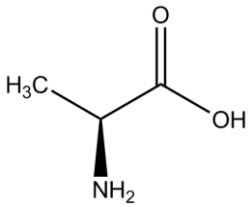

Figure 2.2 Chemical Structure of *L*-alanine.

2.3.5. Post-Polymerization Functionalization of PFPA-PolyHIPEs – RGD

0.25 g polyHIPE was swelled in methanol for 10 minutes. A solution of arginylglycylaspartic acid (RGD) (23 mg) and triethylamine (0.013 g) in 20 ml methanol was prepared and then brought to pH 10 using sodium hydroxide. The swollen polyHIPE was then transferred to the amino acid solution and left at room temperature for 48 hours. The polyHIPE was then washed by Soxhlet extraction for 12 hours and then dried under reduced pressure.

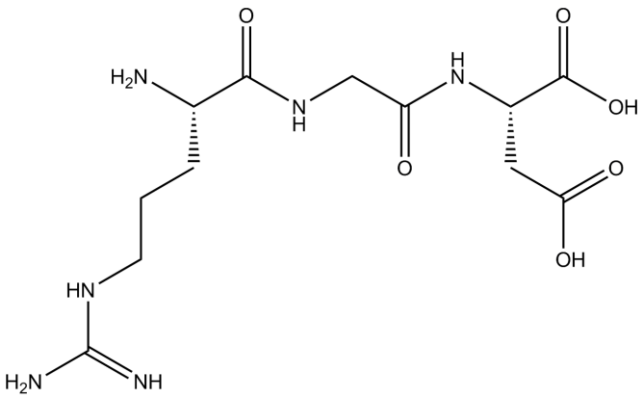

Figure 2.3 Chemical structure of RGD.

2.4. Peptide Synthesis

2.4.1. Materials

Rink amide resin and amino acids were obtained from Novabiochem and used as received.

PyBOP was obtained from Apollo Scientific and used without further purification.

All other chemicals were obtained from Sigma Aldrich and used as received.

2.4.2. Peptide (GGRGD) Synthesis

1 g rink amide resin (loading 1.1 mmol g^{-1}) was swollen in a mix of 2.5 ml dimethylformamide (DMF) and 2.5 ml DCM for 1 hour. The DCM was then washed off with DMF. The resin was then deprotected for 5 minutes in 5 ml of a solution of 20% piperidine in DMF. The piperidine was then washed off and the deprotection repeated for 10 minutes. The resin was then washed thoroughly with DMF.

A solution of 0.796 g of PyBOP, 0.19 ml *N*-methylmorpholine (NMM) and 0.641 g aspartic acid in 5 ml DMF was prepared and left for 10 minutes in order to activate the c-terminus of the amino acid. This solution was then added to the deprotected resin, which was then shaken for 2 hours at 320 rpm. The resin was then washed with DMF and the procedure was repeated. The amino acid was then deprotected using the same procedure used for resin deprotection and the next amino acid then coupled by the same method as described above.

Once all amino acids were coupled, the peptide was then cleaved from the resin and any acid sensitive protecting groups removed from the amino acid side chains. This was done by adding a 38:1:1 mixture of trifluoroacetic acid (TFA), water and triisopropyl silane (TIPS, 3 ml in total) to the resin. The resin was then left for 3 hours with occasional stirring. The resin was then removed from the peptide solution by filtration and the peptide was then

precipitated into cold diethyl ether. The ether was then removed with a pipette and the peptide was then freeze dried in a minimum of water.

The chemical structure of the GGRGD peptide is shown in Figure 2.4.

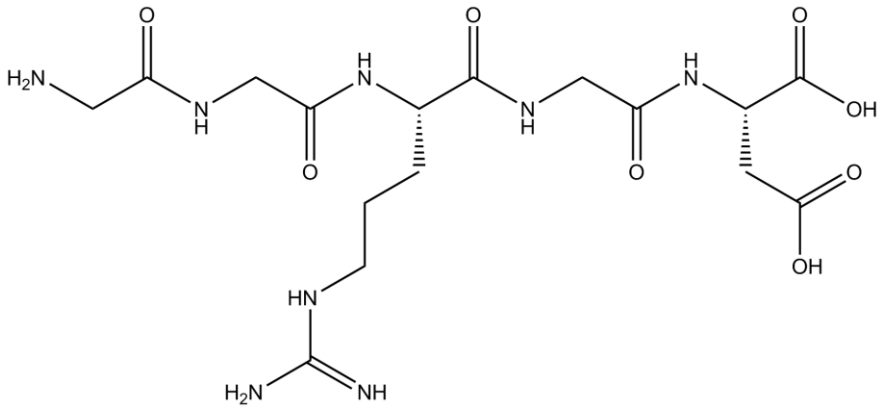

Figure 2.4 Chemical Structure of GGRGD.

2.5. PolyHIPE Characterization

2.5.1. Raman

All Raman spectroscopy data was recorded using a HORIBA Jobin Yvon LabRAM HR 800 with a built in 633 nm He:Ne laser. All spectra are referenced to Si band (ν = 520.07 cm^{-1}).

2.5.2. Solid State NMR Spectroscopy

Solid-state ^{19}F NMR spectra were obtained using a Varian VNMRS 400 spectrometer using a direct polarisation experiment at a frequency of 282.087 MHz.

Solid-state ^{13}C NMR spectra were obtained using a VNMRS 400 spectrometer using a direct polarisation excitation experiment at a frequency of 100.56 MHz.

All solid state NMR spectra were obtained using the on board Varian NMR software and spectral referencing is the respect to external, neat tetramethylsilane. All polyHIPE samples were ground to a powder prior to obtained solid state NMR spectra.

2.5.3. XPS

X-ray photoelectron spectra were carried out by Dr. Naoko Sano at the National EPSRC User's Service (NEXUS) at Newcastle University, an EPSRC Mid-Range Facility.

2.5.4. FT-IR

All IR spectra were obtained using a Perkin Elmer 1600 series FTIR spectrometer equipped with a Golden Gate ATR element.

2.5.5. Elemental Analysis

Elemental microanalyses were carried out by Mr. Stephen Boyer at the Microanalysis Service, London Metropolitan University.

2.5.6. Scanning Electron Microscopy

PolyHIPE morphology was investigated using a Philips/FEI XL30 ESEM operating at 20 kV. Fractured polyHIPE pieces were sputter-coated with gold to enhance conductivity and mounted on carbon fibre pads adhered to aluminium stubs. The void diameters were obtained using Image J Version 1.44p. One hundred voids were measured in a random walk of voids across the obtained micrograph. During fracturing, voids are unlikely to be exactly bisected, and so the voids obtained by this method are an underestimation. In order to account for this a statistical correction factor is applied[107].

2.5.7. Determination of Thiol Loading Using Ellman's Reagent

5-10 mg polyHIPE was frozen in liquid nitrogen and then ground to a powder with a mortar and pestle. This powder was then transferred to a 5 ml volumetric flask and 1 ml THF was added. The polyHIPE was left to swell for 10 minutes. During this time a 1 ml solution of Ellman's reagent (5 μmol) in ethanol was prepared. This solution was then added to the polyHIPE along with 5 μl diisopropylethylamine. The flask was then shaken for 30 minutes and then diluted to 5 ml with ethanol. This solution was then filtered and diluted to a concentration between 5 μmol and 5mmol in a 96 well plate and the absorbance measured at 412 nm.

3. Results and Discussion

3.1. Trithiol-Triacrylate PolyHIPEs

3.1.1. Trithiol-Triacrylate PolyHIPE Synthesis

The preparation of thiol-ene polyHIPEs from trimethylolpropane tris-mercaptopropionate (TMPTMP) and trimethylolpropane triacrylate (TMPTA) has been described previously[44] (Scheme 3.1). Briefly: water was added dropwise to an oil phase consisting of TMPTMP, TMPTA, 1,2-dichloroethane, surfactant and a photoinitiator. Once the emulsion was formed it was then poured into a mould and cured by passing under UV radiation. The solid polyHIPE was then washed in acetone to remove the aqueous droplet phase and dried under reduced pressure to yield the final polyHIPE polymer.

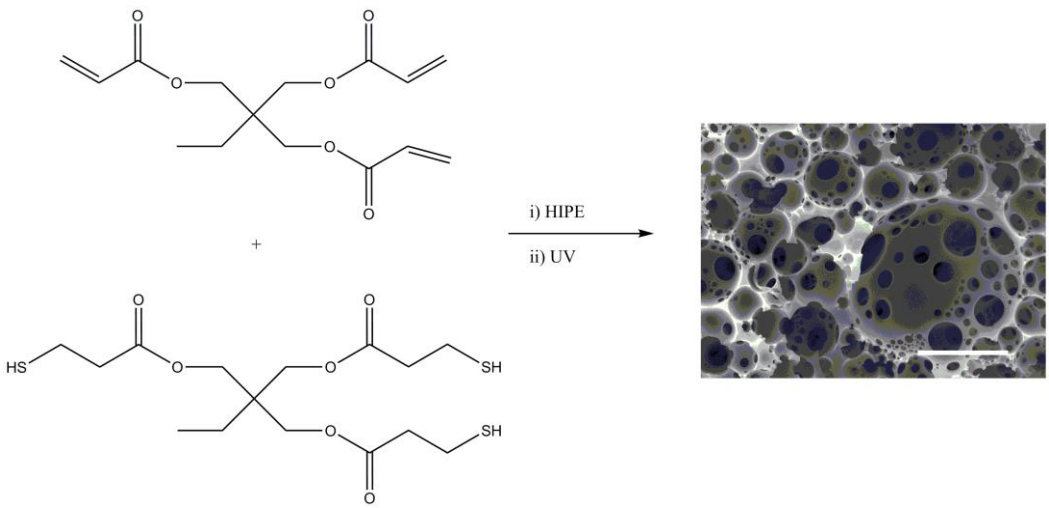

Scheme 3.1 Preparation of thiol-acrylate polyHIPEs from TMPTMP and TMPTA. Scale bar = 50 µm.

The morphology of the obtained polyHIPEs was investigated using scanning electron microscopy (SEM). The polyHIPE samples were found to be highly porous and a fully interconnected, open cell morphology was observed (Figure 3.1).

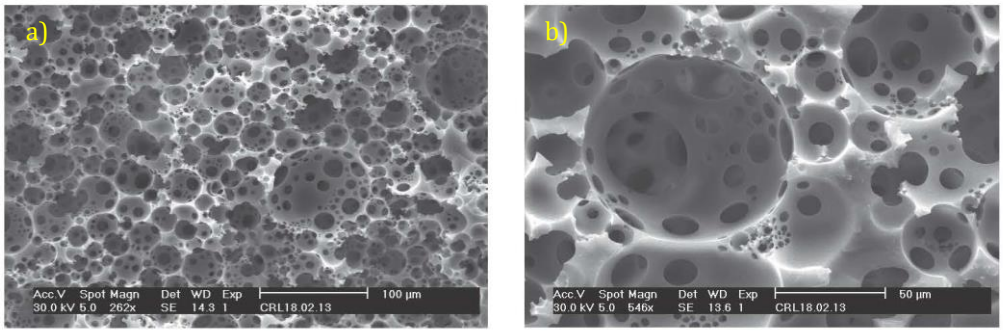

Figure 3.1 Morphology of 50:50 TMPTMP/TMPTA polyHIPE as obtained by SEM polyHIPE at two different magnifications.

The measured void diameters are found to range from 10 – 100 µm, as shown in Figure 3.2.

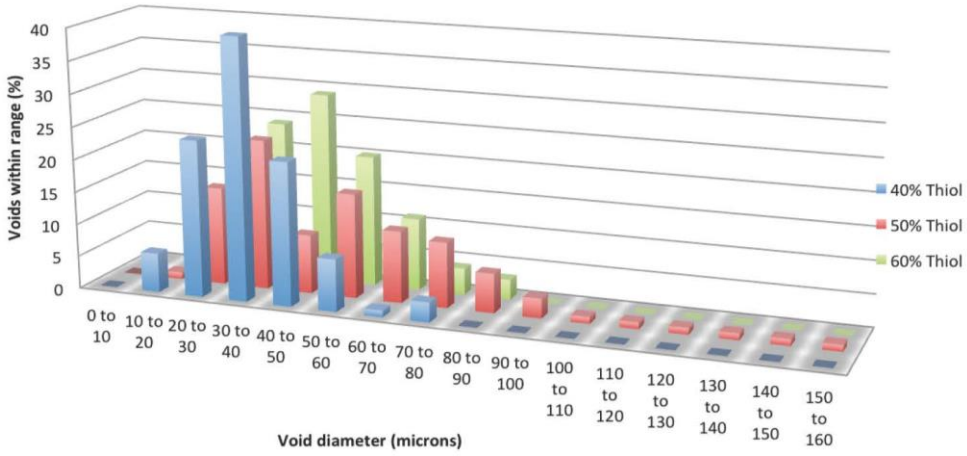

Figure 3.2 Void diameter range observed for (front to back) 40%, 50% and 60% TMPTMP polyHIPEs.

A major advantage of using thiol-ene "click" chemistry is the resilience of any unreacted carbon-carbon double bonds and thiols within the polymer network to reaction upon storage compared to reactive monomers, such as pentafluorophenyl acrylate (PFPA), which may undergo hydrolysis. The presence of residual vinyl groups in (vinyl)polystyrene polyHIPEs has previously been used as a route to the functionalization of these polymers post-polymerization. Thiol-bearing molecules were added across these double bonds via both batch and cross-flow methods, and the reactions were monitored using analytical techniques such as fourier transform

infrared (FT-IR spectrscopy) and elemental microanalysis. This project aims to show that residual thiols found within thiol-acrylate polyHIPEs can be used to functionalize the polymer surface with acrylate-containing molecules and can also be used in the formation of disulphide bonds.

Raman spectroscopy (Figure 3.3) was used in order to show the presence of unreacted thiol groups within the thiol-acrylate polyHIPEs.

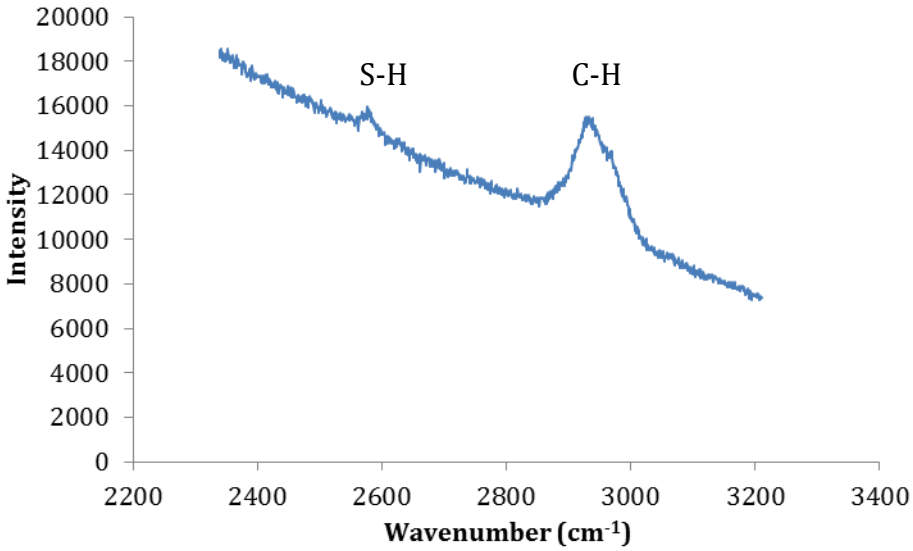

Figure 3.3 Raman spectrum of 60 % thiol trithiol-triacrylate polyHIPE.

The small peak at ~2500 cm^{-1} indicates the presence of thiol groups within the polyHIPE, while the larger peak at ~2900 cm^{-1} represents the aliphatic C-H bonds.

The theoretical level of unreacted thiol within the 60% thiol polyHIPE can be calculated using Equation 3.1[223]

$$ThiolLoading = \frac{(n_{initial\,thiol\,groups} - n_{initial\,\pi\,bonds})}{Total\,mass\,of\,reagents} \quad (3.1)$$

where $n_{initial\ thiol\ groups}$ is the number of thiol groups in the HIPE prior to curing and $n_{initial\ \pi\ bonds}$ is the number of carbon-carbon double bonds in the HIPE prior to curing. The theoretical level of thiol loading was found to be 1.7 mmol g^{-1}; however, possible acrylate homopolymerization during the

formation of the polyHIPE leads to unreacted thiol groups in polyHIPEs containing 50% of the trithiol monomer and 40% of the trithiol monomer, which the above equation cannot account for. In order to quantify the amount of unreacted thiol within these polyHIPEs a colorimetric assay using Ellman's reagent was used[224]. The mechanism for the formation of the chromophore is shown in Scheme 3.2 and the number of moles of thiol detected using the assay is shown in Figure 3.4.

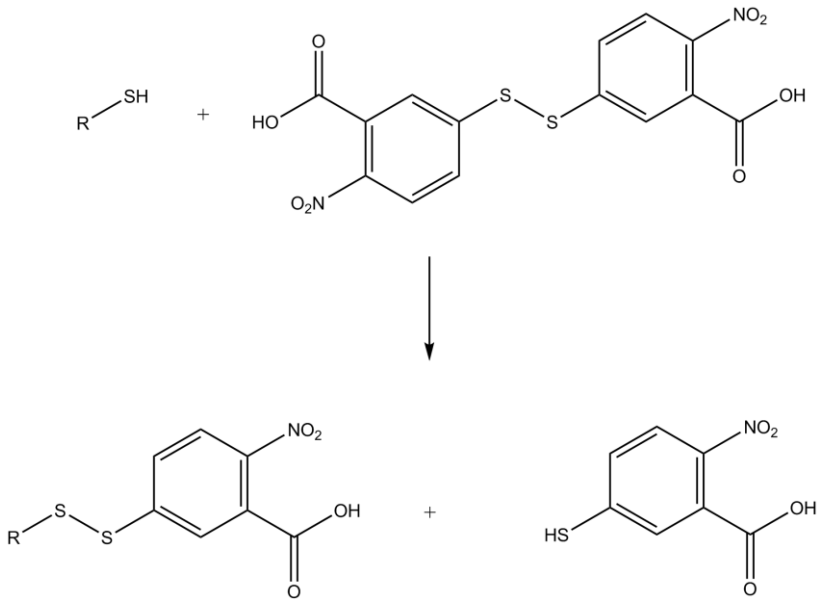

Scheme 3.2 Formation of the chromophore during colorimetric assay using Ellman's reagent.

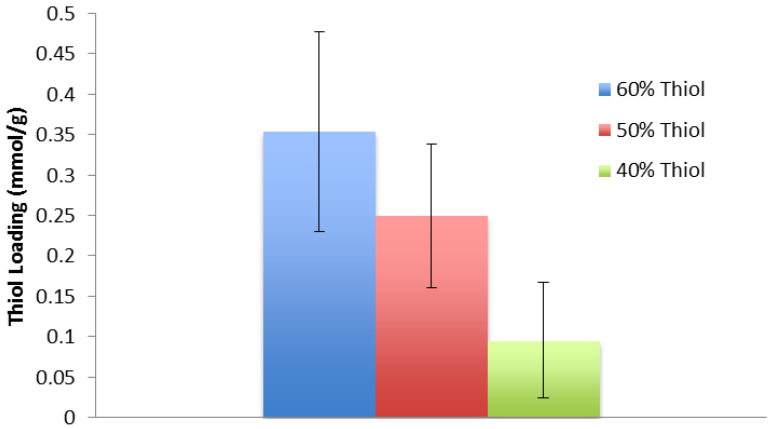

Figure 3.4 Number of moles of unreacted thiol groups in trithiol-triacrylate polyHIPEs.

As expected, the highest level of unreacted thiol is seen in the 60% thiol polyHIPE, with the next highest being found in the 50% thiol polyHIPE and the lowest level in the 40% thiol material.

3.1.2. Radical-Mediated Thiol-Ene "Click" and Michael Addition Reactions to Residual Thiols in Triacrylate-Trithiol PolyHIPEs

The unreacted thiol within the thiol-ene polyHIPEs was utilized in order to functionalize the polyHIPEs post-polymerization. Both radical-mediated thiol-ene "click" reactions and Michael additions were explored for this purpose, the mechanism for which are shown in Scheme 3.3. Both thermally initiated and photoinitiated "click" reactions were carried out. The acrylates chosen to be added to the polyHIPE surface included hexafluoroisopropyl acrylate (HFIPA), fluorescein-O-acrylate and PEG-methacrylate (PEGMA). These were chosen due to the ease with which they could be detected using common analytical techniques such as NMR spectroscopy and x-ray photoelectron spectroscopy (XPS) or due to change in surface properties. Functionalization reactions were originally carried out on powdered polyHIPE samples as intended characterization, including solid state NMR and colorimetric assays, require powdered samples. Further characterization techniques, including XPS, require monolithic samples and so the methodology was changed and functionalization was carried out on solid polyHIPE samples which were then ground to a powder post-functionalization when required.

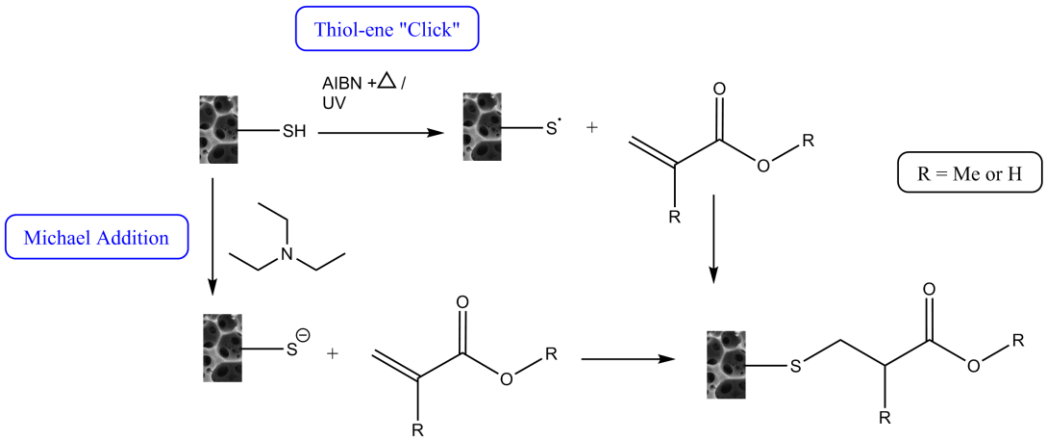

Scheme 3.3 Functionalization of thiol-acrylate polyHIPEs by radical mediated "click" and Michael addition reactions.

The addition of HFIPA to the polyHIPE surface was monitored by solid state ^{19}F NMR spectroscopy (Figure 3.5). In all three cases (photoinitiated "click", thermally initiated "click", and Michael addition), a peak at ~73 ppm was observed, indicating the presence of HFIPA in the polyHIPEs. The ^{19}F NMR spectrum of an unfunctionalized polyHIPE sample did not show any peaks.

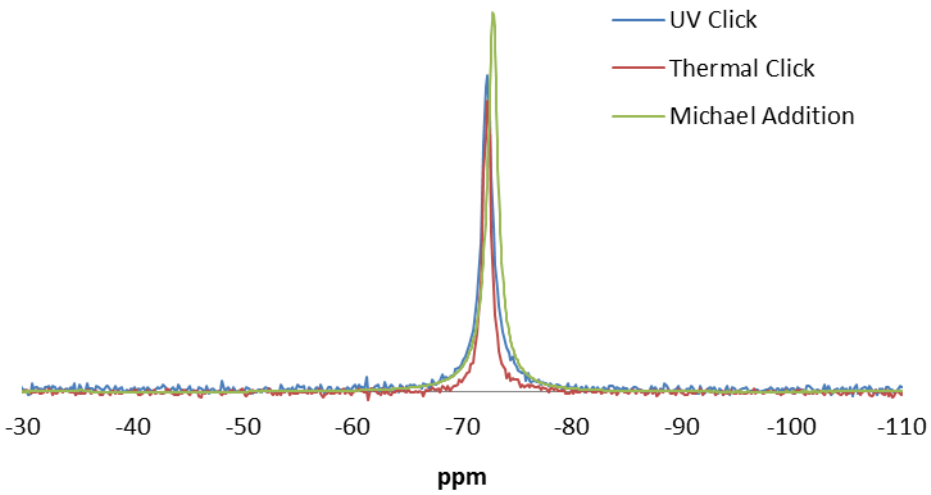

Figure 3.5 Solid state ^{19}F NMR spectrum of 50% TMPTMP thiol-acrylate polyHIPE functionalized post-polymerization with HFIPA via thermal and photo-initiated "click" reactions and by a Michael addition.

X-ray photoelectron spectroscopy (XPS) can also be used to monitor the surface functionalization of the thiol-acrylate polyHIPEs. Both survey and

high-resolution spectra were obtained for each sample, and are shown in Figure 3.6.

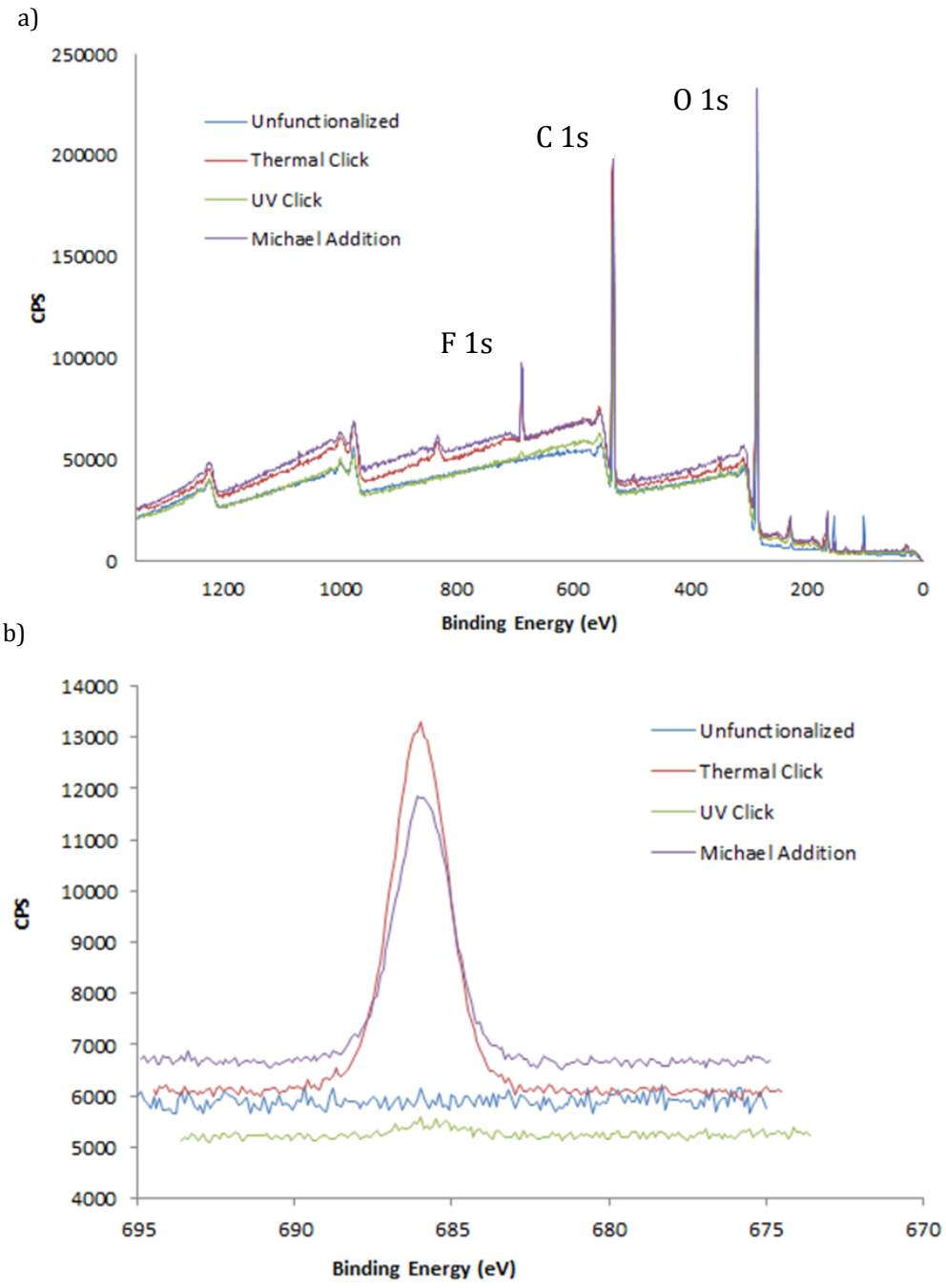

Figure 3.6 XPS of 40% TMPTMP polyHIPEs surface functionalized with HFIPA. a) Survey scan, b) high-resolution F 1s spectrum.

The fluorine 1s electron can be observed at 686 eV in both the survey and high-resolution spectra, with the peaks at 534 eV and 284 eV representing the 1s electrons in the carbon atoms of carbonyl groups and oxygen 1s

electrons respectively. The difference in peak heights indicates a higher level of functionalization has been achieved for the thermally initiated "click" and Michael addition methods than for the photoinitiated "click" functionalization. In order to investigate this further, the Ellman's reagent colorimetric assay was repeated on the functionalized polyHIPEs, and the results are summarized in Table 3.1.

Table 3.1 Percentage Functionalization of thiol-acrylate polyHIPEs surface functionalized with HFIPA as determined using Ellman's reagent.

PolyHIPE	Unfunctionalized	Thermal Click		UV Click		Michael Addition	
	Thiol Concentration (mmol)	Thiol Concentration (mmol)	% Functionalization	Thiol Concentration (mmol)	% Functionalization	Thiol Concentration (mmol)	% Functionalization
40% Thiol	0.09	0.01	87	0.10	0	0.02	82
50% Thiol	0.25	0.03	88	0.11	55	0.02	93
60% Thiol	0.35	0.04	89	0.15	59	0.02	94

The Ellman's assay confirms that a higher level of functionalization is achieved for both the thermally initiated "click" and Michael addition reactions across all three thiol concentrations. This could be attributed to the longer reaction times associated with these two methods compared with

the photoinitiated functionalization reaction or due to a lack of penetration of UV into the opaque polyHIPE.

The level of functionalization achieved using the photoinitiated "click" method on the 40% TMPTMP polyHIPE was much lower than expected (~0%). The concentration of residual, unreacted thiol on the surface of all three polyHIPE samples post-functionalization via the photoinitiated "click" reaction are comparable, suggesting that a percentage of the thiols of the surface of a thiol-acrylate polyHIPE are inaccessible on the timescale of the photoinitiated "click" reaction. The initial concentration of thiol is much lower in the 40% TMPTMP sample than the other polyHIPE samples prepared (0.09 mmol g^{-1}, compared with 0.25 mmol g^{-1} and 0.35 mmol g^{-1} for the 50% TMPTMP and 60% TMPTMP polyHIPE respectively), and is roughly the same as the concentration obtained post-functionalization. Therefore, it can be concluded that all of the thiol on the surface of the 40% TMPTMP polyHIPE cannot be accessed by further acrylate containing molecules during the short reaction time associated with the photoinitiated "click" reaction.

The morphology of the functionalized polyHIPEs was investigated using SEM. As with the unfunctionalized polyHIPEs described previously, the polymers display an open cell morphology with fully interconnected voids (Figure 3.7).

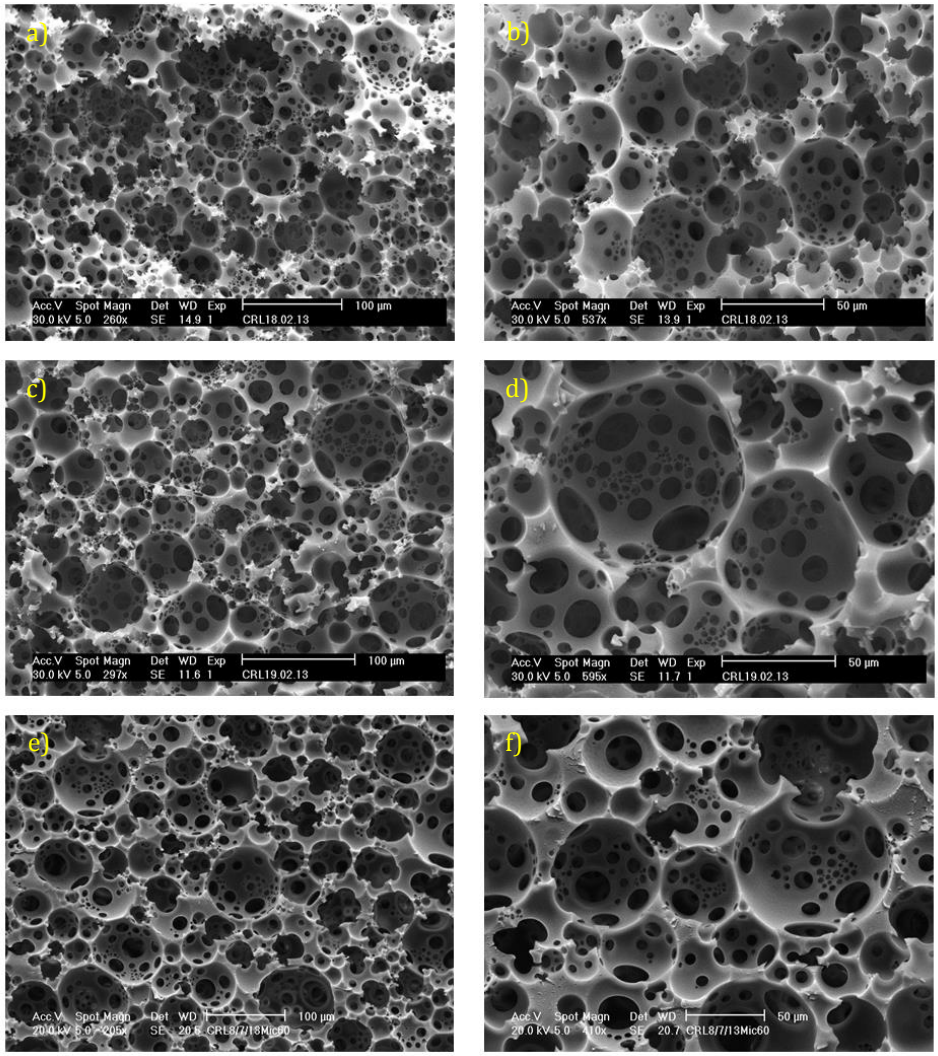

Figure 3.7 Morphology of TMPTMP/TMPTA polyHIPEs functionalized with HFIPA post-polymerization as obtained by SEM. a), b) SEM images of 60% TMPTMP polyHIPE after functionalization via a thermally initiated "click" reaction at two different magnifications. c), d) SEM images of 60% TMPTMP polyHIPE after functionalization via a UV initiated "click" reaction at two different magnifications. e), f) SEM images of 60% TMPTMP polyHIPE after functionalization via a Michael addition at two different magnifications.

The range of void diameters observed was measured and the results are summarized in Figure 3.8.

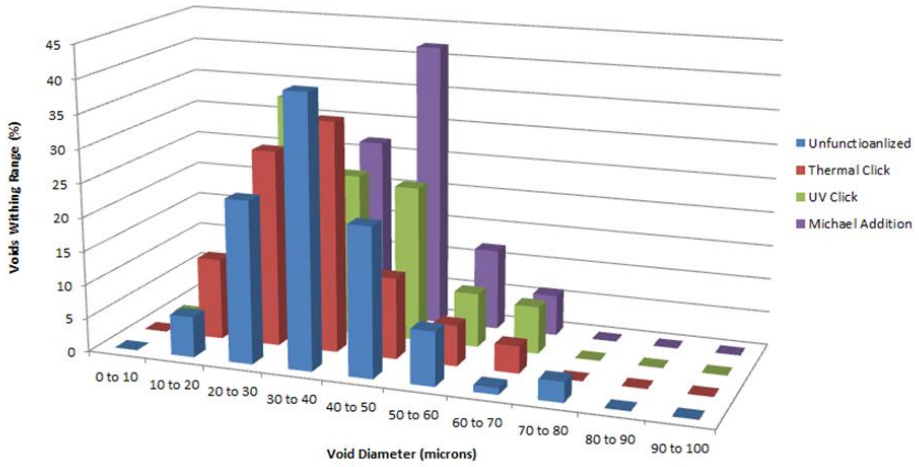

Figure 3.8 Void diameter range observed for (front to back) 40% TMTMP polyHIPE before functionalization, 40% TMPTMP polyHIPE after functionalization via a thermally initiated "click" reaction, 40% TMPTMP polyHIPE after functionalization via a photoinitiated "click" reaction, 40% TMPTMP polyHIPE after functionalization by a Michael addition.

The diameter of the observed voids falls within the same range as those in the unfunctionalized polyHIPEs and the surface of the polymer appears the same. Therefore, it can be deduced that surface functionalization of these thiol-acrylate polyHIPEs via "click" and Michael addition reactions does not alter the morphology of the polyHIPEs.

The fluorescent acrylate, fluorescein *O*-acrylate, was grafted to the surface in order to give a visual demonstration of the functionalization reaction (Figure 3.9). Prior to functionalization the polymer fluoresces blue under UV radiation. Upon grafting of fluorescein *O*-acrylate to the surface the polyHIPE then exhibits the yellow/green colour characteristic of the fluorescent acrylate. Extensive washing via Soxhlet extraction suggests that this colour change is due to fluorescein *O*-acrylate that is chemically bonded to the polyHIPE surface rather than trapped in the crosslinked polymer network.

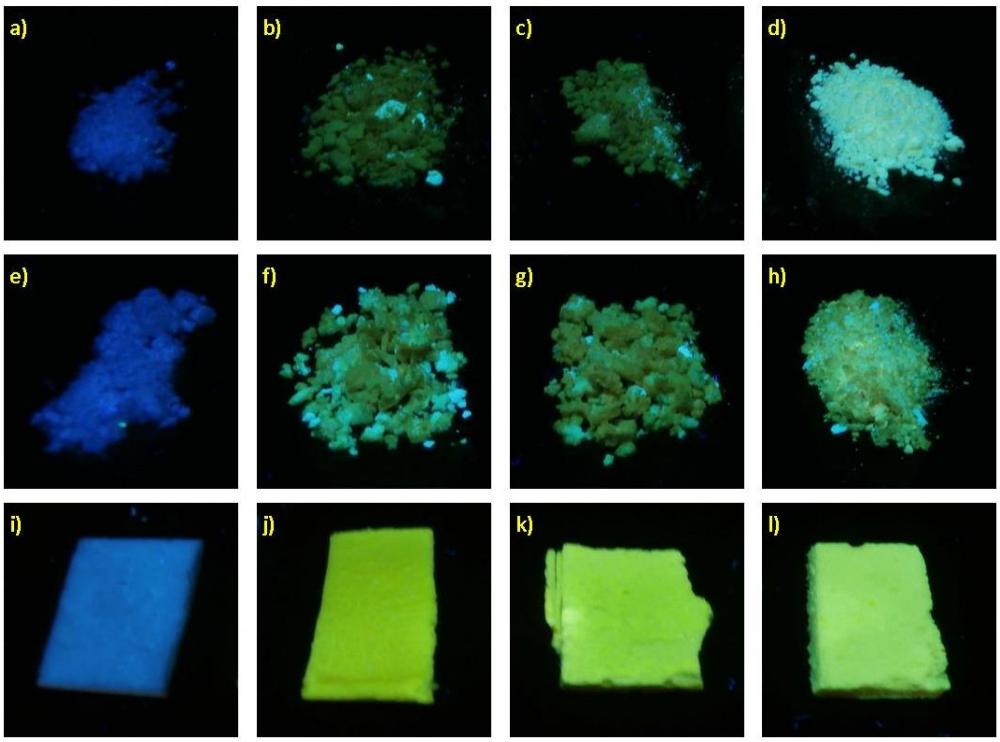

Figure 3.9 Thiol-acrylate polyHIPE functionalized with fluorescein *O*-acrylate under UV light. Functionalization carried out via a thermally initiated "click" reaction: a) unfunctionalized polyHIPE, b) 40% TMPTMP polyHIPE, c) 50% TMPTMP polyHIPE, d) 60% TMPTMP polyHIPE. Functionalization carried out via a photoinitiated "click" reaction: e) unfunctionalized polyHIPE, f) 40% TMPTMP polyHIPE, g) 50% TMPTMP polyHIPE, h) 60% TMPTMP polyHIPE. Functionalization carried out via a Michael addition: i) unfunctionalized polyHIPE, j) 40% TMPTMP polyHIPE, k) 50% TMPTMP polyHIPE, l) 60% TMPTMP polyHIPE.

It was hypothesized that surface functionalization via the thermally initiated "click" and Michael addition reactions should give sufficient levels of functionalization in order to change the surface properties of the polymer. In order to investigate this, a short chain PEG-methacrylate (PEGMA, Mn = 300 Da) was chosen and grafted to the surface. The presence of PEGMA within the polyHIPE network was then determined by solid state ^{13}C NMR spectroscopy (Figure 3.10). The peak at 71 ppm represents the carbon in the PEG chain and is not observed in the spectrum of an unfunctionalized sample.

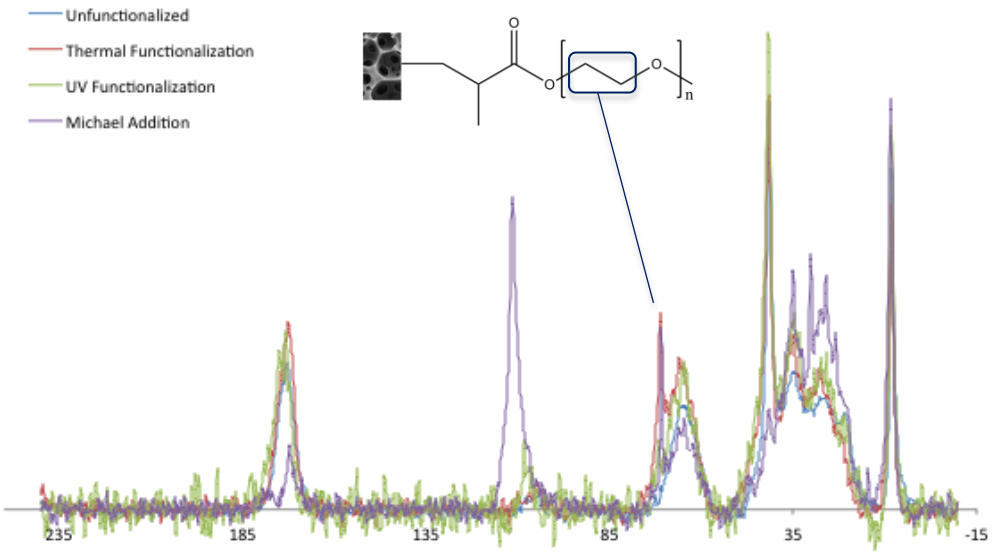

Figure 3.10 Solid state ^{13}C NMR spectrum of 50% TMPTMP thiol-acrylate polyHIPE functionalized post-polymerization with PEGMA.

The change in the hydrophobicity of the surface after the polyHIPEs were functionalized with PEGMA was tested as follows: water droplets coloured with blue food dye (a mixture of brilliant blue and carmoisine which should not affect the surface tension of water) were added to the surface of the polyHIPE and monitored in order to see if the droplets were absorbed into the polymer network (Figure 3.11). PolyHIPEs containing 60% TMPTMP functionalized by both the thermal "click" and Michael addition methods exhibited a changed in surface hydrophobicity and the water droplets were seen to soak into the polymer. The surface concentration of PEGMA was found to be too low to induce a change in the properties of the polymer surface in all samples containing lower TMPTMP concentrations as well as the 60% TMPTMP polyHIPE functionalized via the UV initiated "click" reaction.

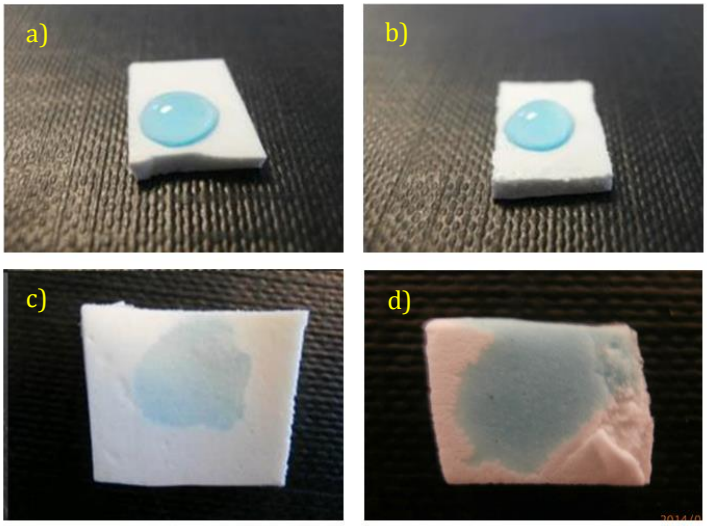

Figure 3.11 Water droplets added to the surface of 60% TMPTMP thiol-acrylate polyHIPEs. a) polyHIPE before addition of PEGMA to the surface, b) polyHIPE after the addition of PEGMA by a UV initiated "click" reaction, c) polyHIPE after the addition of PEGMA by a thermally initiated "click" reaction, d) polyHIPE after the addition of PEGMA by a Michael addition. Pink colouration observed in (d) is an artefact of the camera used to obtain the image.

3.1.3. Disulphide Bonds in Trithiol-Triacrylate PolyHIPEs

As well as thiol-ene "click" and Michael addition chemistries, thiol-containing molecules are also known to form disulphide bonds, and so it was hypothesized that the unreacted thiol in the thiol-acrylate polyHIPE network may form disulphide bonds with other thiol-containing molecules.

Disulphide bonds between the polymer surface and two different thiol containing molecules were formed via two reaction methods. The first of these methods is the base catalysed reaction of 5,5'-dithiobis-(2-nitrobenzoic acid) (Ellman's reagent) with the surface bound thiol groups, as shown in scheme 3.4. The disulphide bond in Ellman's reagent undergoes a disulphide exchange, releasing a chromogenic molecule, 5-sulphido-2-nitrobenzoate (TNB). TNB absorbs strongly at 412 nm, and a single molecule is released from each molecule of Ellman's reagent that reacts with a surface bound thiol group[224]. It is this quantitative release of a chromogenic molecule which is the basis of the colorimetric assay used to

determine the percentage of functionalization achieved using "click" and Michael addition chemistries.

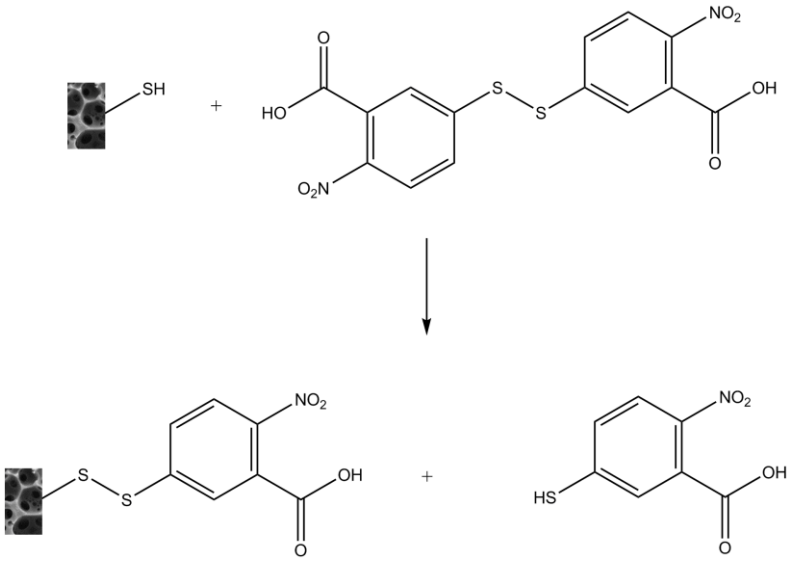

Scheme 3.4 Functionalization of thiol-acrylate polyHIPEs via a thiol-disulphide exchange with Ellman's reagent.

Due to its nitrogen content, the presence of Ellman's reagent on the surface of the polyHIPEs can be determined by both XPS, as shown in Figure 3.12, and elemental analysis.

a)

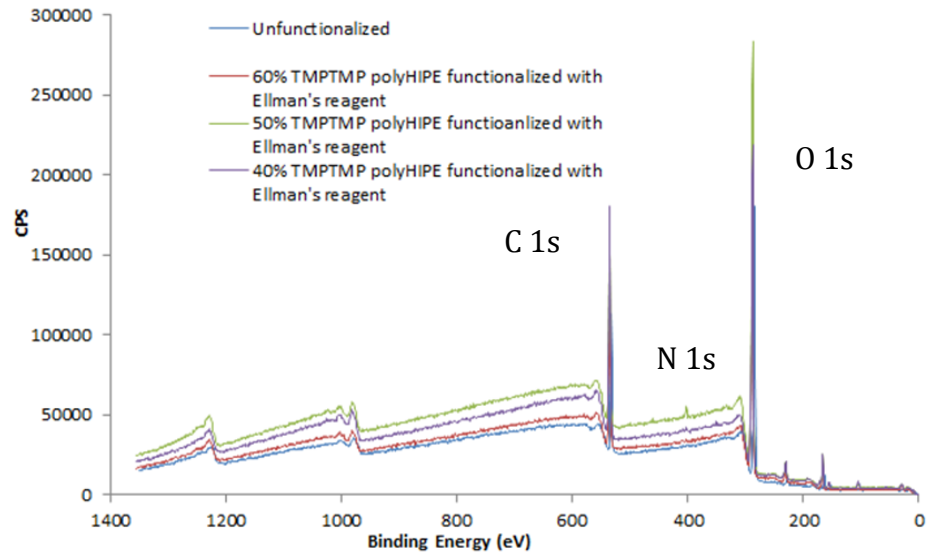

b)

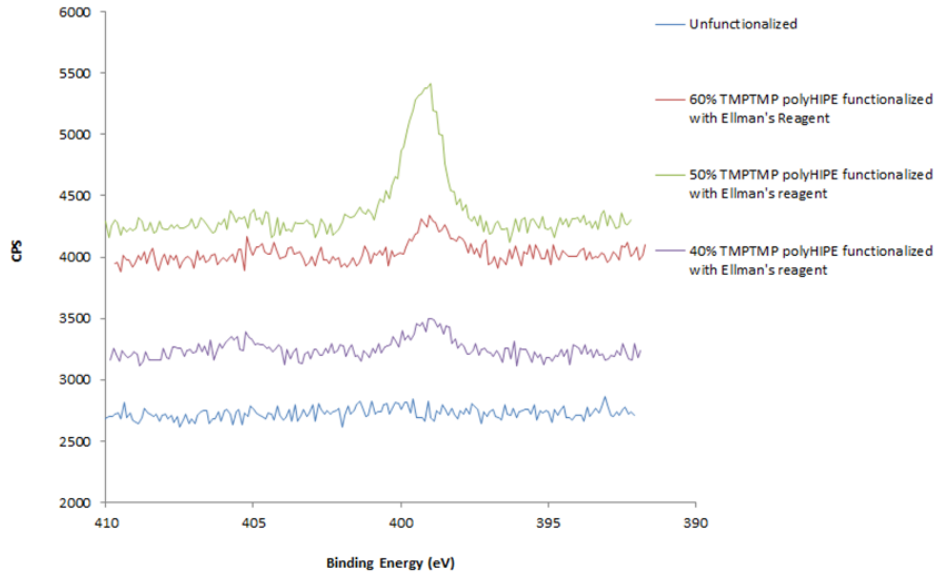

Figure 3.12 XPS of TMPTMP polyHIPEs surface functionalized with Ellman's reagent. a) Survey scan, b) high-resolution N 1s spectrum.

Both the survey scan and high resolution XPS spectra show a low intensity nitrogen peak at 399 eV, representing the nitrogen 1s electron, with peaks at 534 eV and 284 eV representing the 1s electrons in the carbon atoms of carbonyl groups and oxygen 1s electrons respectively . The low intensity of the nitrogen 1s peak indicates that the concentration of nitrogen at the polymer surface is low. The overall percentage functionalization achieved can be obtained by elemental analysis, the results of which are summarized in Table 3.2.

Table 3.2 Percentage functionalization of thiol-acrylate polyHIPEs functionalized with Ellman's reagent as determined by elemental analysis.

PolyHIPE	% Nitrogen (Theoretical)	% Nitrogen (Obtained)	% Functionalization
40% Thiol	0.64	0.64	100
50% Thiol	1.79	1.41	79
60% Thiol	2.50	<0.1	0

A high percentage functionalization was obtained for both the 40% TMPTMP and 50% TMPTMP samples, however, the percentage of nitrogen in the 60% TMPTMP sample was too low to be detected. The high-resolution N 1s XPS spectrum of the same sample indicates that there is a low concentration of nitrogen on the surface of the polymer. This nitrogen concentration may be too low to be detected by elemental analysis. In order to ascertain the reason for the conflicting elemental analysis and XPS results in the case of the 60% TMPTMP polyHIPE other analytical techniques must be explored. Using a wider range of thiol molecules would allow for a more thorough evaluation of this method using simple analytical techniques such as NMR and FT-IR spectroscopy. Longer reaction times may also result in a higher degree of functionalization, allowing for the detection of nitrogen using the elemental analysis technique. The high percentage of N observed by elemental analysis in the 40% TMPTMP sample may also be falsely high. This could be due to incorrect washing of the sample, resulting in Ellman's reagent being trapped in the polyHIPE network as opposed to bound to the polymer surface.

The morphology of the functionalized polyHIPEs was investigated using SEM (Figure 3.13).

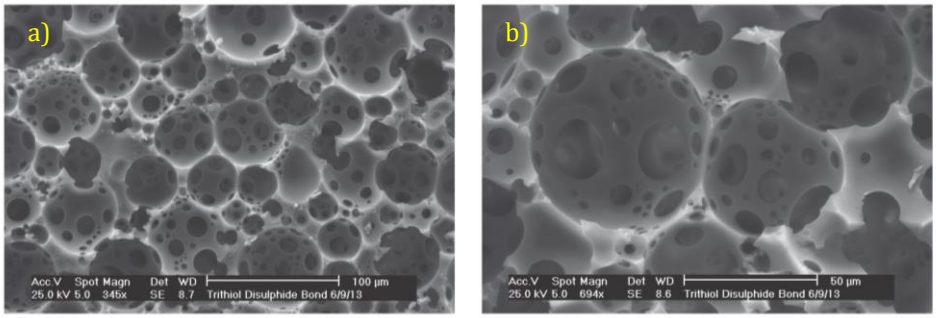

Figure 3.13 Morphology of TMPTMP/TMPTA polyHIPE after addition of Ellman's reagent to the polymer surface as obtained by SEM. a), b) SEM images of 40% TMPTMP polyHIPE at two different magnifications.

The polyHIPEs display open cell morphology with fully interconnected voids, suggesting the formation of disulphide bonds between the thiol groups in the polyHIPE network and the thiol group in Ellman's reagent has not resulted in any visible changes to the polymer surface. The void diameters were also measured, the results of which are shown in Figure 3.14

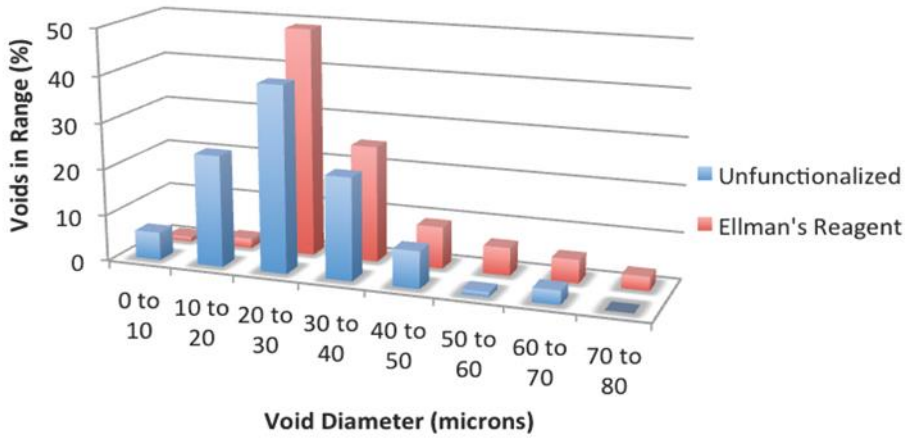

Figure 3.14 Void diameter range observed for 40% TMPTMP polyHIPE functionalized post-polymerization with Ellman's reagent.

The diameter of the obtained voids falls within the same range as those in the unfunctionalized polyHIPEs

The second method used in the formation of disulphide bonds between the surface of thiol-acrylate polyHIPEs and a thiol containing molecule uses sodium tetrathionate in order to form a reactive sulfenylthiosulphate intermediate. Another thiol group, in this case the thiol in 5-amino-1,3,4-thiadiazole-2-thiol (ATDT), can then be coupled to the reactive intermediate, displacing the thiolsulphate group, forming a disulphide bond, the mechanism for this is shown in Scheme 3.5. The thiol used, ATDT, was chosen due to its high nitrogen content, allowing for its detection by XPS and elemental analysis, and the presence of an amine group, which allows for the use of FT-IR spectroscopy.

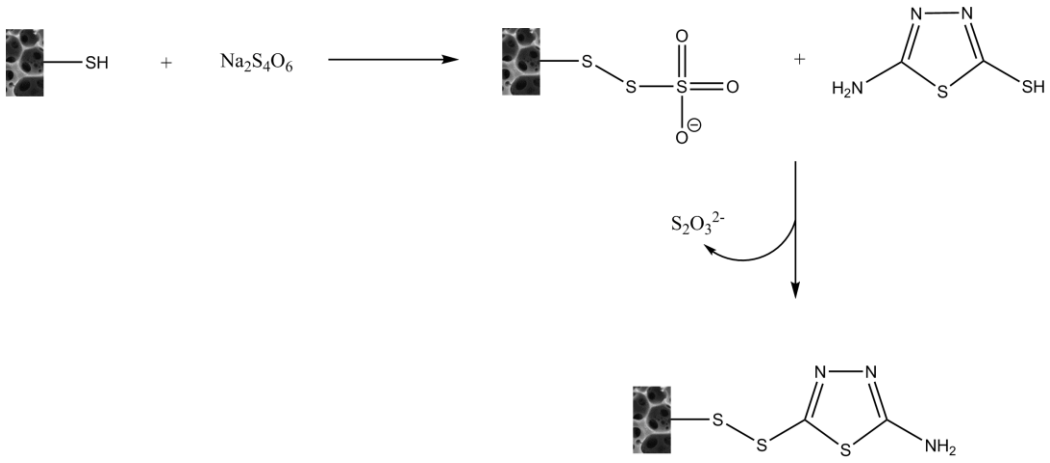

Scheme 3.5 Functionalization of thiol-acrylate polyHIPEs with ADTD via the formation of a reactive sulfenylthiosulphate intermediate.

Amines can be identified using FT-IR spectroscopy with two characteristic peaks: the first of these, the N-H stretch, occurs at 3400 – 3500 cm^{-1}; the second, the C-N stretch, at 1560 – 1640 cm^{-1}. The FT-IR spectrum obtained for a trithiol-triacrylate polyHIPE with ATDT grafted to the surface via a disulphide linkage is shown in Figure 3.15.

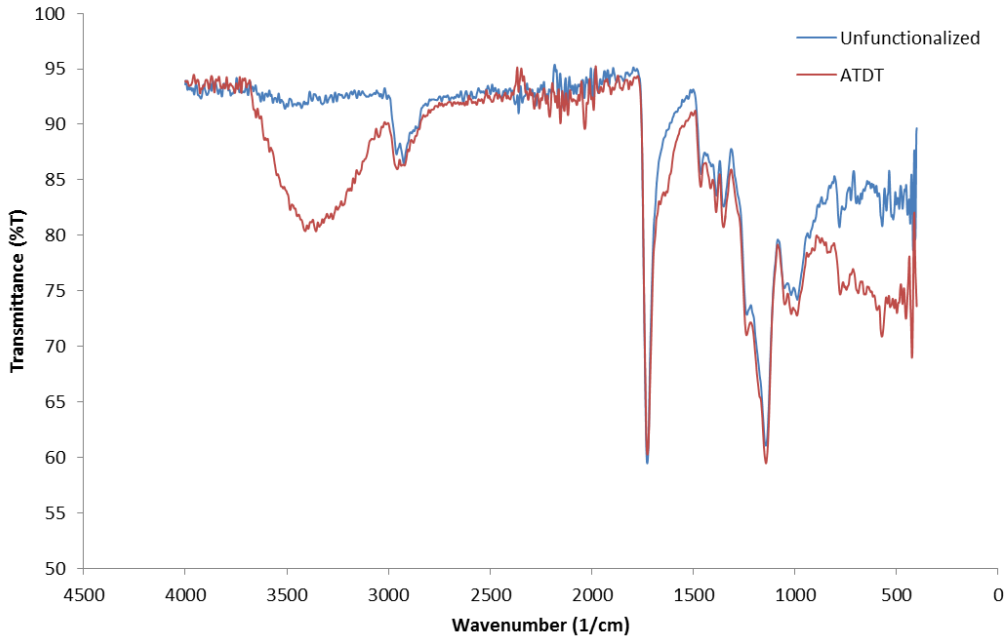

Figure 3.15 FT-IR spectrum of 60% TMPTMP polyHIPE functionalized post-polymerization with ATDT.

The broad peak at 3400 cm^{-1} and the smaller peak at 1640 cm^{-1} in the FT-IR spectrum of a 60% TMPTMP polyHIPE after undergoing surface functionalization with ATDT indicate the presence of an amine on the polymer surface. The nitrogen content of the functionalized polymer was also investigated by XPS, the results of which are shown in Figure 3.16.

a)

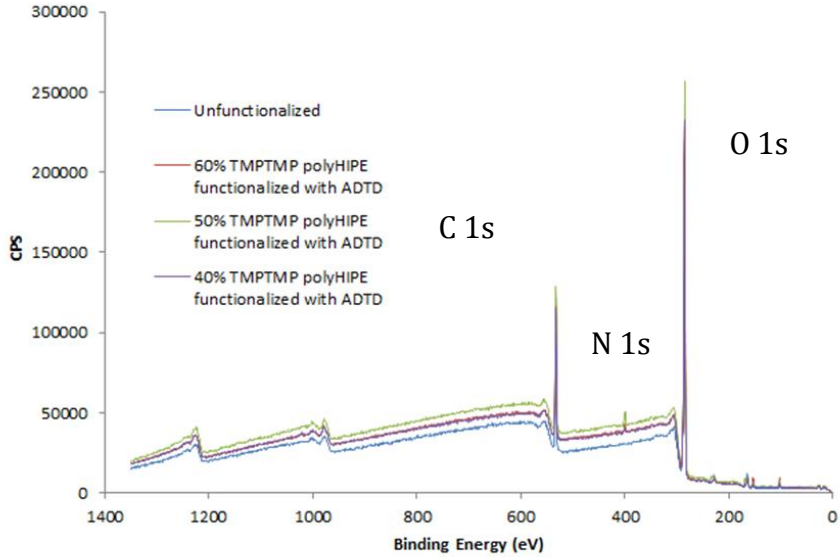

b)

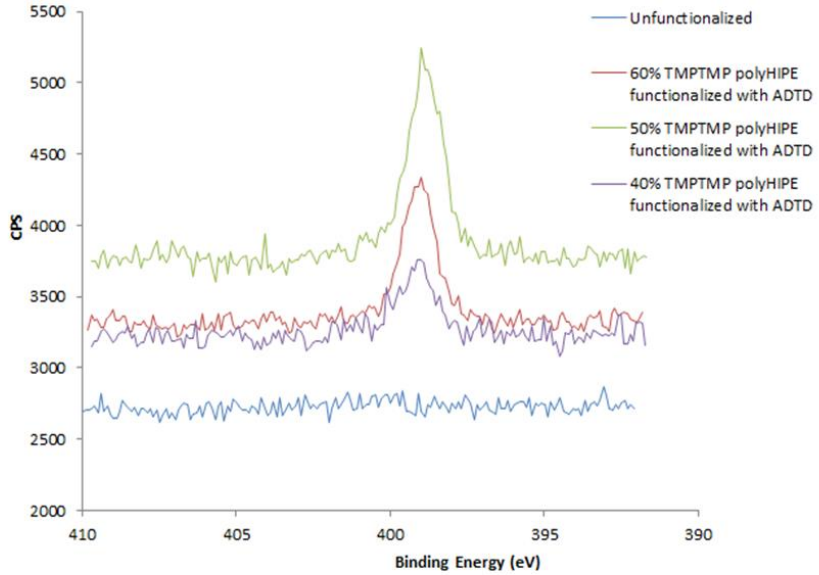

Figure 3.16 XPS of 50% TMPTMP polyHIPEs surface functionalized with ATDT. a) Survey scan, b) high-resolution N spectrum.

Both the survey scan and high resolution XPS spectra show a low intensity nitrogen peak at 399 eV, representing the nitrogen 1s electron, with peaks at 534 eV and 284 eV representing the 1s electrons in the carbon atoms of carbonyl groups and oxygen 1s electrons respectively . The low intensity of the nitrogen 1s peak indicates that the concentration of nitrogen at the polymer surface is low. The overall percentage functionalization achieved can be obtained by elemental analysis, the results of which are summarized in Table 3.3.

Table 3.3 Percentage functionalization of thiol-acrylate polyHIPEs functionalized with ATDT as determined by elemental analysis.

PolyHIPE	% Nitrogen (Theoretical)	% Nitrogen (Obtained)	% Functionalization
40% Thiol	1.90	0.52	27
50% Thiol	5.35	0.32	6
60% Thiol	7.49	<0.1	0

The level of functionalization obtained using sodium tetrathionate to initiate the formation of disulphide bonds between the polymer surface and ATDT is significantly lower than that obtained in the previous method. As with the previous method, a higher level of functionalization was achieved in the 40% TMPTMP sample, and the concentration of nitrogen in the 60% TMPTMP sample was too low to be detected. XPS and FT-IR analysis on the 60% TMPTMP polyHIPE sample indicate that there is nitrogen on the surface of the polymer. The concentration of nitrogen within the 60% TMPTMP polyHIPE may be too low to be detected by elemental analysis. The low level of functionalization obtained in all samples could be due to a number of factors, including inefficient displacement of the thiosulphate ion from the sulfenylthiosulphate intermediate. Repeating the reaction with an increased reaction time or with a larger excess of ATDT may lead to an increase in the level of functionalization observed. Using a wider range of thiol molecules would allow also for a more thorough evaluation of this method using simple analytical techniques such as NMR and FT-IR spectroscopy.

The morphology of the functionalized polyHIPEs was investigated using SEM (Figure 3.17).

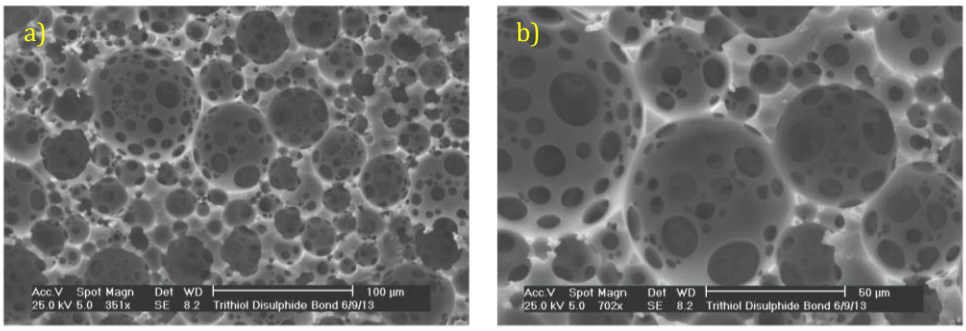

Figure 3.17 Morphology of TMPTMP/TMPTA polyHIPE as obtained by SEM. A), b) SEM images of 50% TMPTMP polyHIPE two different magnifications.

The polyHIPEs display the same open cell morphology as seen in the unfunctionalized samples. The diameter of the obtained voids was measured and the results are summarized in Figure 3.18.

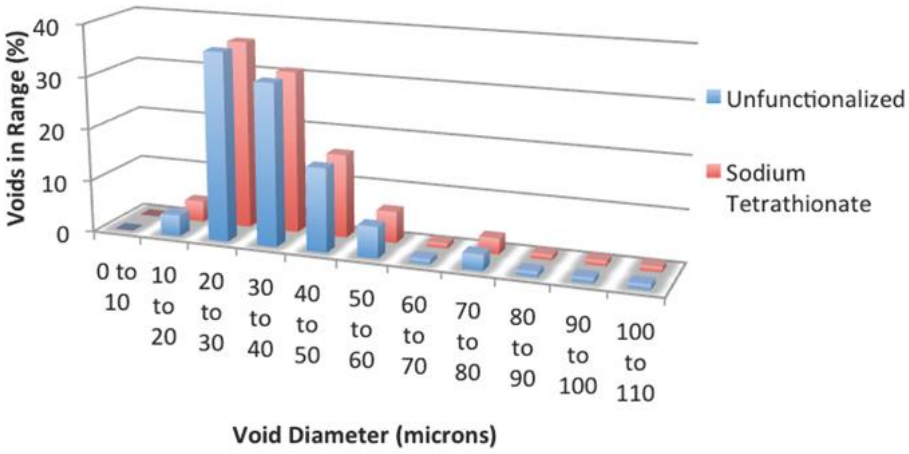

Figure 3.18 Void diameter range observed for 50% TMPTMP polyHIPE functionalized post-polymerization with ADTD.

The diameter of the voids fall within the same range as those in the unfunctionalized polyHIPEs, suggesting that surface functionalization of the polymer with the thiol ATDT has not resulted in any changes to the polyHIPE morphology.

3.2. Trithiol-Penta/HexaAcrylate PolyHIPEs

3.2.1. Trithiol-Penta/Hexa Acrylate polyHIPE Synthesis

The formation of polyHIPEs from dipentaerythritol penta-/hexa-acrylate (DPEHA) and TMPTMP has been described previously[99] (Scheme 3.6). Briefly: water was added dropwise to an oil phase consisting of TMPTMP, DPEHA, dichloroethane, surfactant and a photoinitiator. Once the emulsion was formed it was then poured into a mould and cured by passing under UV radiation. The solid polyHIPE was then washed in acetone to remove the aqueous droplet phase and dried under reduced pressure to yield the final polyHIPE polymer.

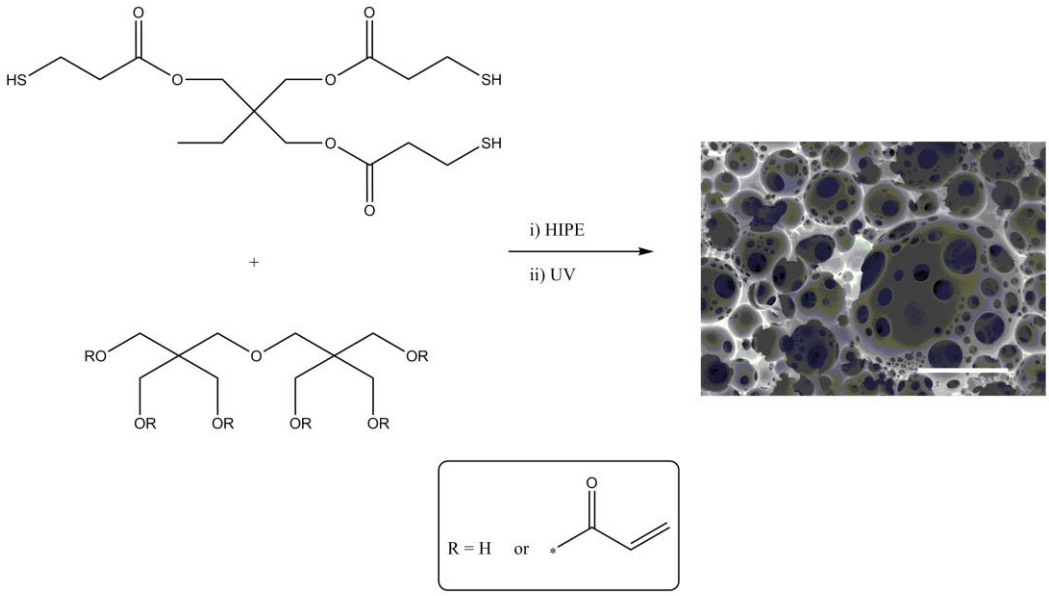

Scheme 3.6 Preparation of thiol-acrylate polyHIPEs from TMPTMP and DPEHA. Scale bar = 50 µm.

The morphology of these polyHIPEs was investigated via SEM (Figure 3.19).

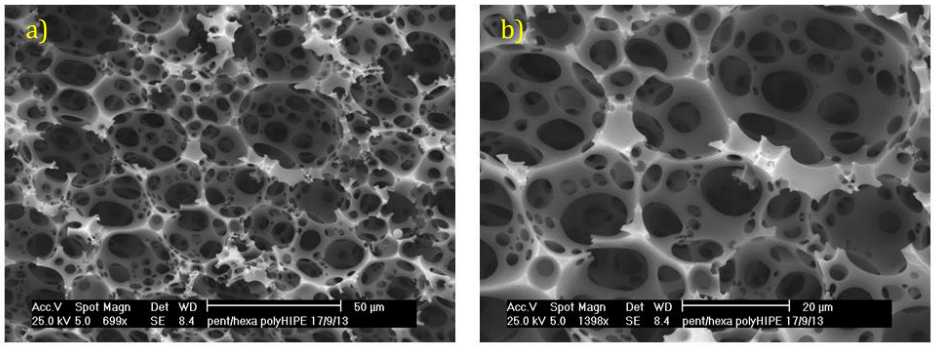

Figure 3.19 Morphology of TMPTMP/DPEHA polyHIPEs with 25% PFPA. a), b) SEM images at two different magnifications.

The morphology of the polyHIPEs was found to be the typical open cell structure seen in previous polyHIPEs, with a fully interconnected porous network. The observed void diameters were also measured, the results of which are summarized in Figure 3.20

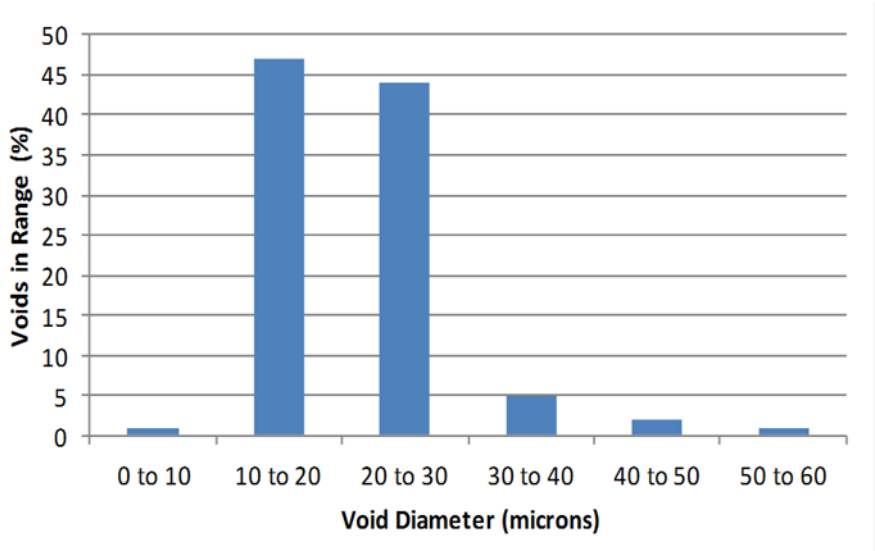

Figure 3.20 Void diameter range observed for DEPHA/TMPTMP polyHIPE.

The void diameters were calculated to be in the range of 0 to 60 µm. The use of a penta-/hexa-acrylate, such as DPEHA, results in a material with a higher crosslink density than those formed using TMPTA. This higher crosslink density results in a slight decrease in the void diameter, when compared to thiol-acrylate polyHIPEs formed using TMPTA, and an increase in the mechanical strength of the material[44]. This increase in crosslink density allows for non-crosslinking acrylates to be incorporated into a thiol-acrylate polyHIPE, resulting in a further route to the chemical functionalization of these materials.

3.2.2. Incorporation of Other Monomers into Trithiol-Penta/Hexa Acrylate polyHIPE

It has been shown previously that the addition of active esters, such as pentafluorophenyl acrylate (PFPA), into the continuous phase of an emulsion yields polyHIPEs that retain the functionality of the ester upon curing[99]. These groups can then be used to further functionalize the polyHIPE post-polymerization using simple organic reactions. Up to 50% of the acrylate monomer concentration can be replaced by a functional acrylate, such as PFPA, before the effect on the mechanical properties becomes too great. The incorporation and subsequent reactions of PFPA can be monitored via solid state NMR spectroscopy (figure 3.21).

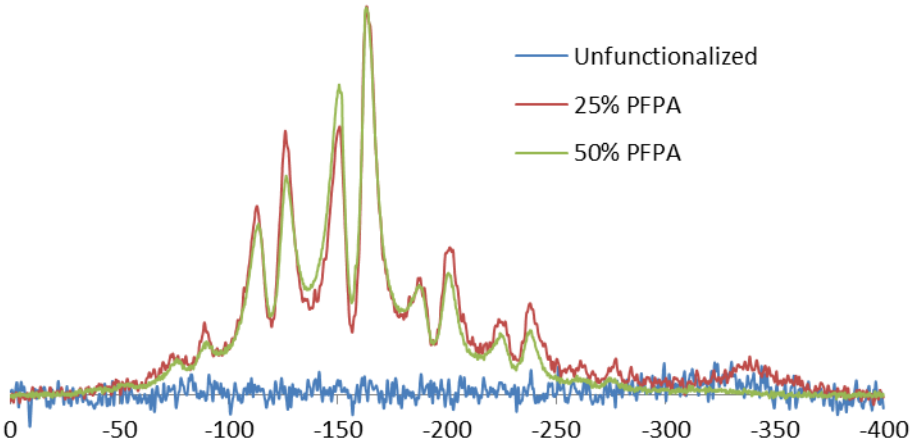

Figure 3.21 Solid state ^{19}F NMR spectrum of thiol-acrylate with and without PFPA.

The multiplet signal in the ^{19}F NMR spectra of the polyHIPEs indicates that PFPA has been successfully incorporated into the polymer matrix. Solid state ^{13}C NMR spectroscopy can also be used to determine the presence of PFPA within the polyHIPE (Figure 3.22)

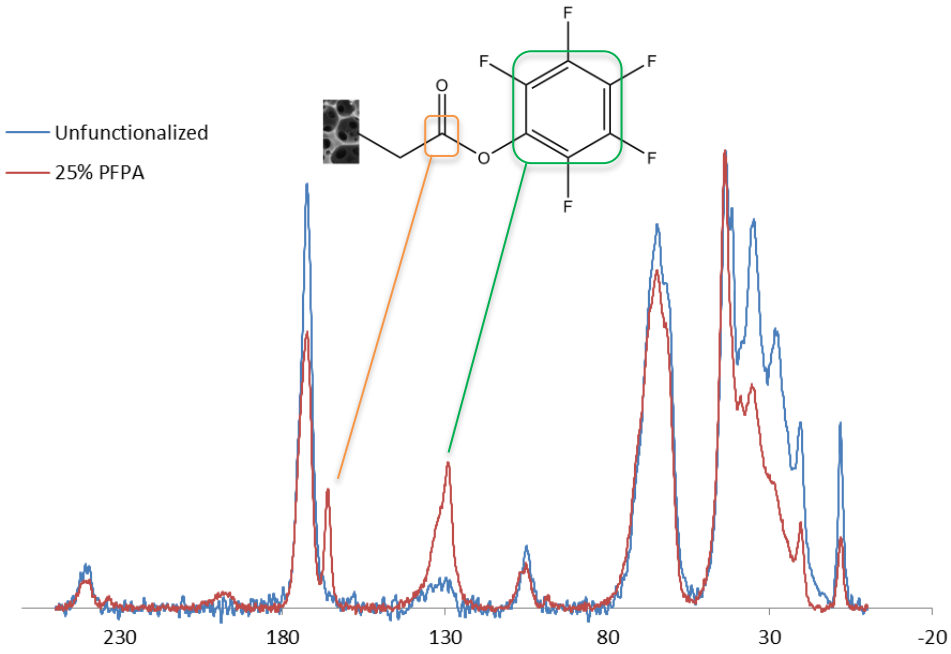

Figure 3.22 Solid state ^{13}C NMR spectrum of PFPA-polyHIPE.

The solid state ^{13}C NMR spectrum of the PFPA-polyHIPE shows two peaks representative of the PFPA molecule: the first of these, at 129 ppm, indicates the presence of the aromatic carbons; the second, at 166 ppm, indicates the presence of carbonyl carbon in an ester group. The two PFPA peaks are not present in the ^{13}C NMR spectrum of a PFPA free thiol-acrylate polyHIPE.

PFPA can be identified using FT-IR spectroscopy via three peaks: the C-O-C stretch of the ester group can be occurs at 1145 cm^{-1}; the carbonyl at 1727 cm^{-1}; and the aromatic carbon stretch at 1519 cm^{-1}. The FT-IR spectrum of the 25% PFPA-polyHIPE is shown in Figure 3.23

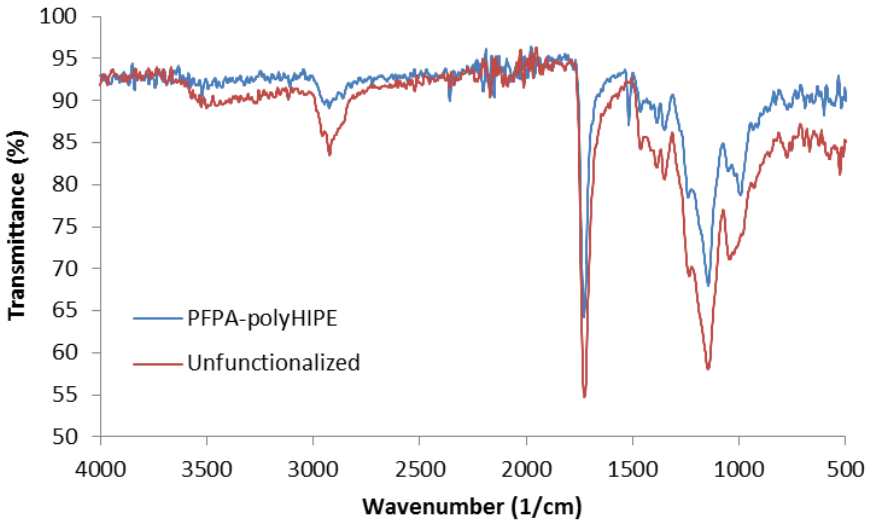

Figure 3.23 FT-IR spectrum of PFPA-polyHIPE

In the FT-IR spectrum of the PFPA-polyHIPE the PFPA can clearly be identified by the peak at 1519 cm^{-1}, which does not appear in the spectrum of a thiol-acrylate polyHIPE without PFPA. The carbonyl and C-O-C ester stretches indicative of PFPA are not clearly distinguishable as they appear in the same position as the carbonyl and C-O-C ester stretches of the DPEHA.

The morphology of the PFPA-polyHIPEs was investigated using SEM (Figure 3.24).

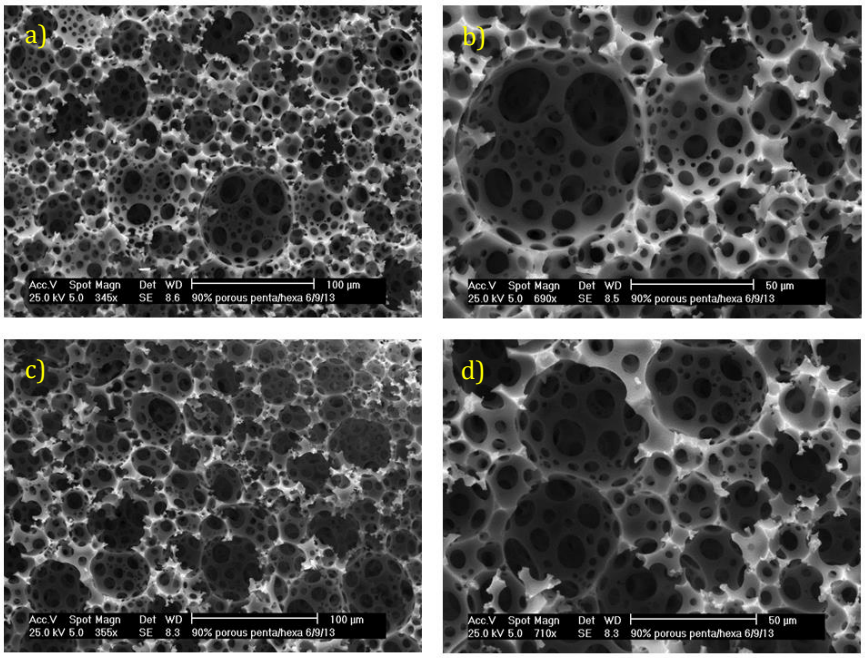

Figure 3.24 Morphology of TMPTMP/DPEHA/PFPA polyHIPEs. a), b) SEM of 25% PFPA-polyHIPE images at two different magnifications. c), d) SEM of 50% PFPA-polyHIPE at two different magnifications.

The morphology of the polyHIPEs was found to be the typical open cell structure seen in previous polyHIPEs, with a fully interconnected porous network. The void diameters obtained upon inclusion of PFPA into the emulsion were measured, as shown in Figure 3.25.

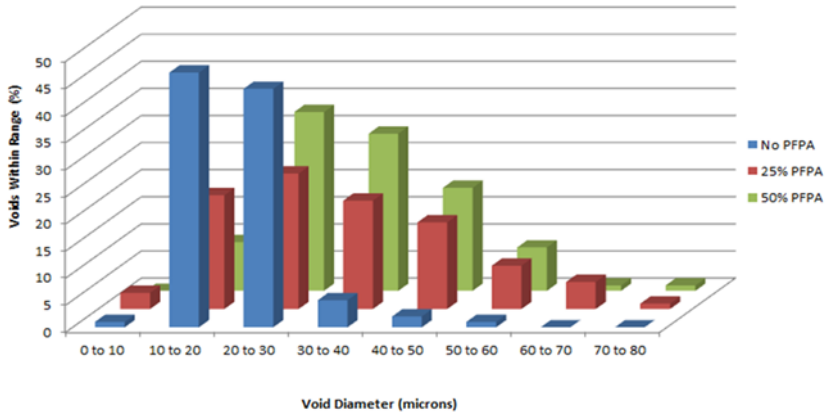

Figure 3.25 Void diameter range observed for (front to back) DPEHA/TMPTMP polyHIPE before functionalization, 25% PFPA-polyHIPE, 50% PFPA-polyHIPE.

The void diameters are calculated to be in the range of 0 to 80 μm. The increase in the obtained void diameter upon inclusion of PFPA is probably as a result of the slightly higher solubility of PFPA in the aqueous phase compared to DPEHA. The solubility of each monomer in the aqueous phase can be quantified by their partition coefficient (log P), which is obtained using Equation 3.2

$$\log P = \frac{[Solute]_{\text{octanol}}}{[Solute]_{\text{un-ionized water}}} \qquad (3.2)$$

where $[Solute]_{\text{octanol}}$ and $[Solute\}_{\text{un-ionized water}}$ represent the solubility of a given solute in octanol and un-ionized water, respectively. The partition coefficient (log P) values for PFPA, DPEHA and TMPTMP are shown in Table 3.4. The values of log P indiciate that the addition of PFPA to the continuous phase of a HIPE results in a slight increase in the hydrophilicity, and hence to a slight destabilization of the emulsion, allowing water droplets to aggregate. The aggregation of water droplets leads to the larger void diameters observed. This increase in void diameter will need to be accounted for when synthesizing polyHIPEs for specific applications where the void diameter is important.

Table 3.4 Partition coefficient (log P) values of monomers used in DPEHA/TMPTMP polyHIPE synthesis[225-227].

Monomer	log P
TMPTMP	3.01
DPEHA	2.65
PFPA	2.55

Incorporating non-crosslinking acrylates into the continuous phase of the HIPE can also be used to directly alter the chemical properties of the polyHIPE without the need for further reaction after curing. Monomers, such as PEGMA, can be included in the emulsion in order to change the

hydrophobicity of the surface. The incorporation of PEGMA into the polymer network, by replacing 25% DPEHA with PEGMA, can be monitored by solid state ^{13}C NMR spectroscopy, as shown in Figure 3.26.

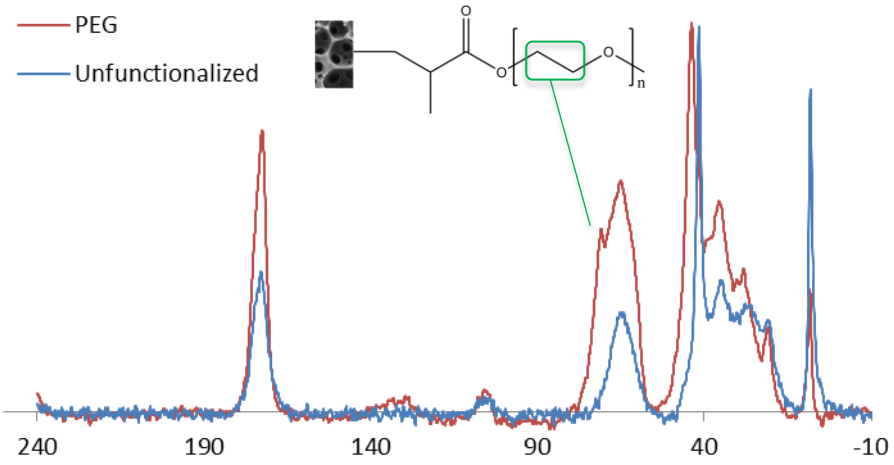

Figure 3.26 Solid State ^{13}C NMR spectrum of 25% PEGMA-polyHIPE.

The peak observed at 71 ppm represents the PEG chain and is not observed in the spectrum of the thiol-acrylate polyHIPE without PEGMA.

The morphology of the PEG-polyHIPE was investigated using SEM, the results of which are shown in Figure 3.27.

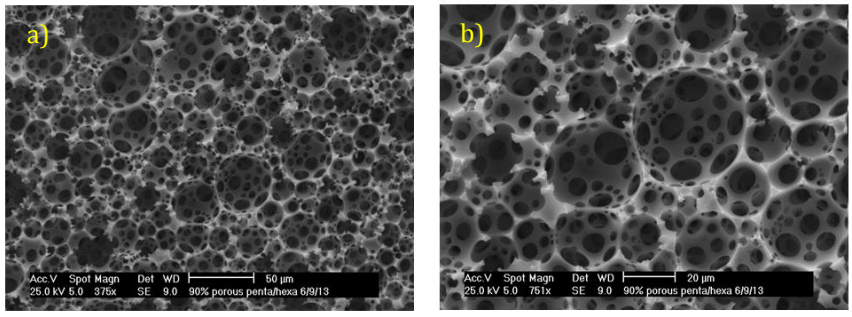

Figure 3.27 Morphology of PEGMA-polyHIPE. a), b) SEM images of PEG-polyHIPE at two different magnifications.

The PEGMA-polyHIPE displays the same open cell morphology and the voids are fully interconnected. The void diameters of the PEGMA-polyHIPE were measured, the results of which are summarized in Figure 3.28

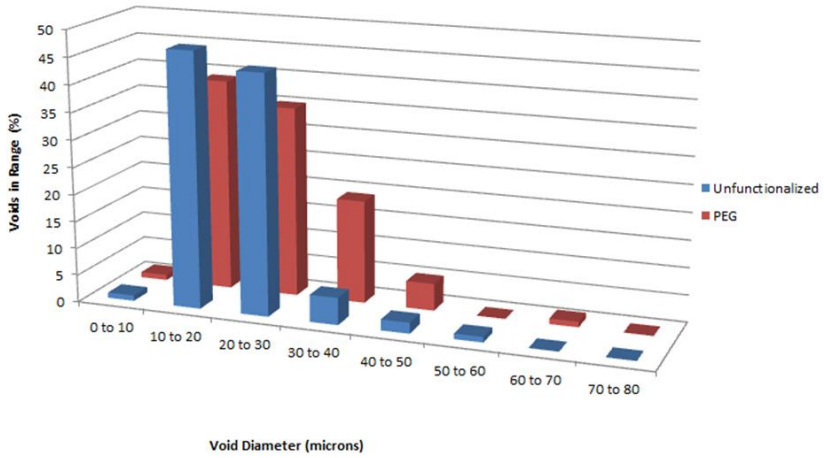

Figure 3.28 Void diameters observed for (front to back) DPEHA/TMPTMP polyHIPE and PEGMA-polyHIPE.

As seen with the PFPA-polyHIPEs, there is an increase in the observed void diameters. This increase also arises from the hydrophilic nature of the PEG chain in the PEGMA monomer.

The influence the addition of the PEGMA monomer has on the surface properties of the polymer was investigated in the same way as described previously. A water droplet is placed on the surface of the polyHIPE and is monitored to see if it soaks into the polyHIPE (Figure 3.29).

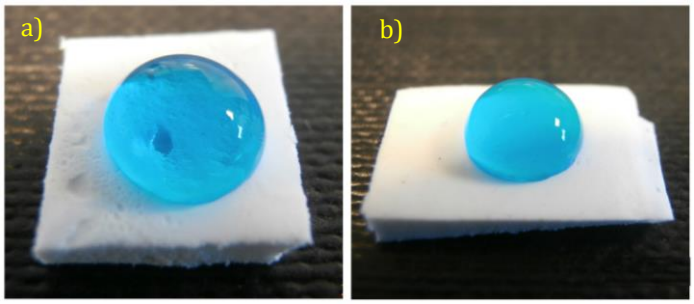

Figure 3.29 Water droplet added to the surface of trithiol-penta/hexa acrylate polyHIPEs. a) Before inclusion of PEGMA into the emulsion. b) PEGMA-polyHIPE.

Replacing 25% of the acrylate concentration of a trithiol-penta/hexa-acrylate polyHIPE with PEGMA does not result in a change in the surface properties of the final polymer. This method of functionalization leads to a

lower concentration of PEG at the polymer surface than the "click" and Michael addition functionalizations described previously. In this case the active monomer is included in the polymerization mixture and can be found throughout the bulk of the polymer in the porous network, as opposed to just on the polymer surface as occurs using the previous grafting techniques. This lower concentration of PEG at the surface means that the same change in surface properties is not observed. Including PEGMA in the monomer system may offer another advantage when developing polyHIPEs to be used as scaffolds for 3D cell culture and tissue engineering. PEG has been shown to inhibit non-specific protein adsorption to the surface of polymer scaffolds[228]. This may be an advantage when bioactive molecules such as sugars or small peptides are added to the polymer surface, as it may prevent the proteins found in serum and media used in cell culture from interfering with the way in which cultured cells interact with the surface bound molecules. Extensive cell culture work would be required in order to prove this hypothesis.

Since up to 50% of the acrylate monomer can be replaced by a functional acrylate, polyHIPEs containing both PFPA and PEG were synthesized. Both ^{19}F (Figure 3.30) and ^{13}C solid state can be used to confirm the presence of PEGMA and PFPA within the polymer network.

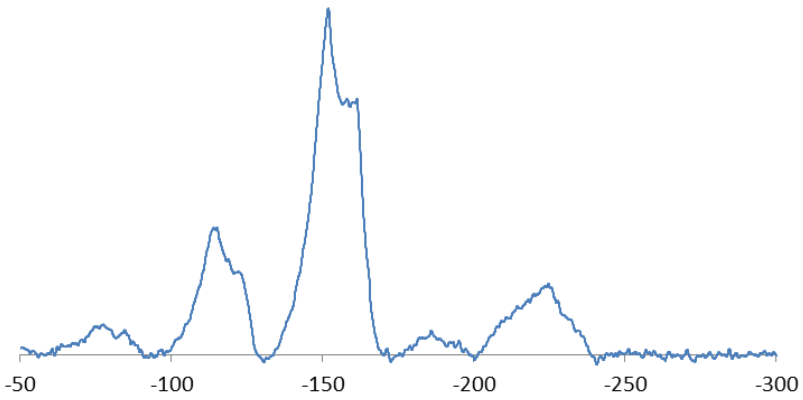

Figure 3.30 Solid state ^{19}F NMR spectrum of PFPA-PEGMA-polyHIPE.

The multiplet signal in the ^{19}F spectrum of the PFPA-PEGMA-polyHIPE occurs in the same region as the PFPA-polyHIPE and as the ^{19}F NMR spectrum of the PFPA monomer. The presence of PFPA within the PFPA-PEGMA-polyHIPE can also be determined by FT-IR spectroscopy (Figure 3.31).

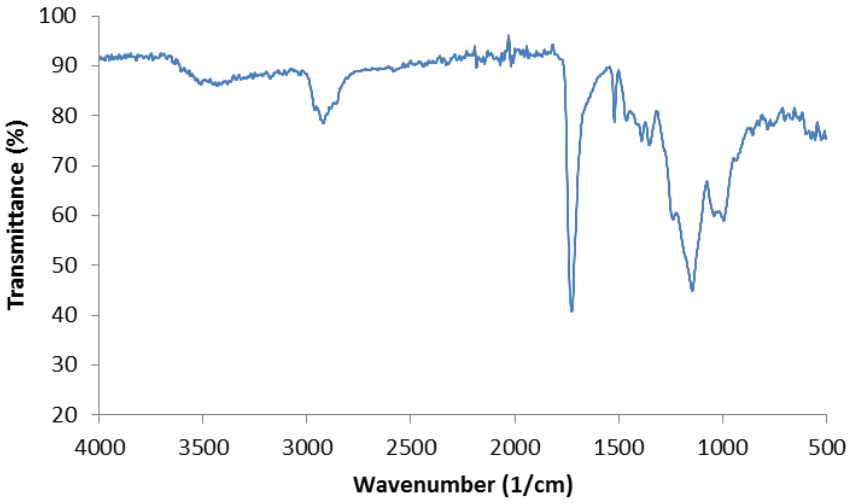

Figure 3.31 FT-IR spectrum of PFPA-PEGMA-polyHIPE.

The PFPA aromatic carbons can be seen in the PFPA-PEGMA-polyHIPE sample at 1519 cm^{-1}. The PFPA ester stretches are, once again, masked by the same ester stretches from the DPEHA monomer.

Solid state ^{13}C NMR spectroscopy was also carried out on the same PFPA-PEGMA-polyHIPE sample, the results of which are shown in Figure 3.32.

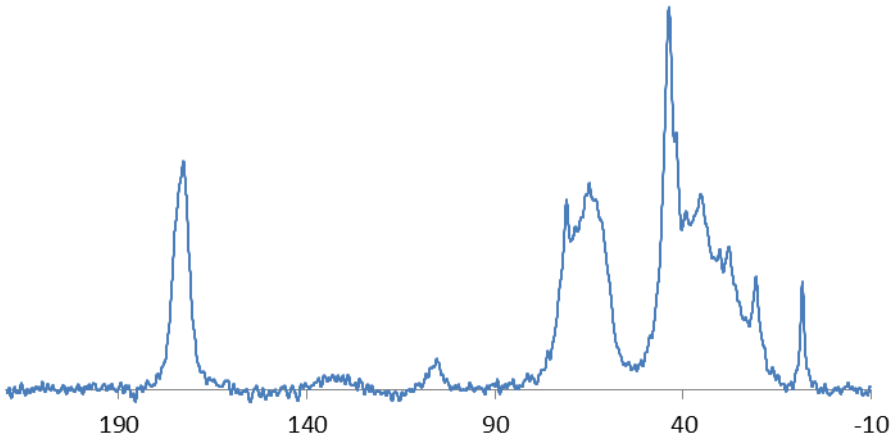

Figure 3.32 Solid State ^{13}C NMR spectrum of PFPA-PEGMA-polyHIPE.

The PEG chain can be observed at 71 ppm as seen with the previous PEGMA functionalized polyHIPE.

The morphology of the PFPA-PEGMA-polyHIPE was investigated using SEM, the results of which are shown in Figure 3.33.

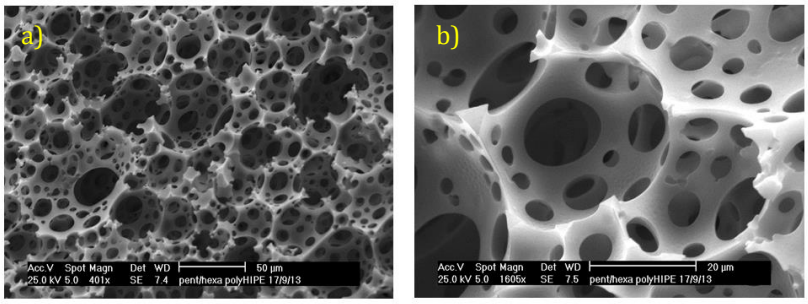

Figure 3.33 Morphology of PFPA-PEGMA-polyHIPE. a), b) SEM images of PFPA-PEGMA-polyHIPE at two different magnifications.

The morphology observed for the PFPA-PEGMA-polyHIPE is much the same as the morphology observed for both the PEGMA- and PFPA-polyHIPEs. The void diameters obtained for the PFPA-PEGMA-polyHIPE were measured, the results of which are summarized in Figure 3.34.

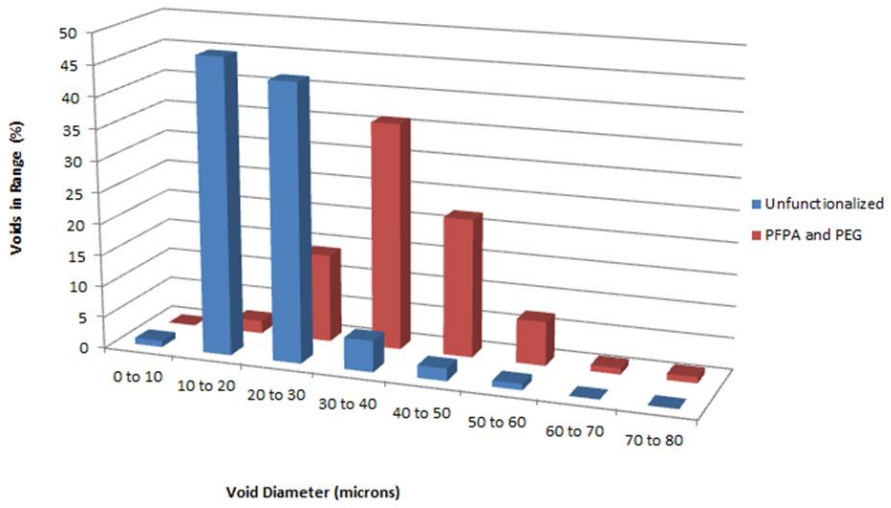

Figure 3.34 Void diameters observed for (front to back) DPEHA/TMPTMP polyHIPE and PFPA-PEGMA-polyHIPE.

As seen with both the PFPA-polyHIPE and the PEGMA-polyHIPE there is an increase in the average void diameter upon the inclusion of functional monomers in the HIPE.

3.2.3. Functionalization of PFPA-polyHIPE With Tris(2-Aminoethyl) Amine

Once incorporated into the polyHIPE polymer network, PFPA can undergo further reactions with nucleophiles, leading to functionalized polyHIPEs. The mechanism for this functionalization reaction is shown in Scheme 3.7. The first nucleophile chosen is tris(2-aminoethyl) amine (TAEA). This amine was chosen due to its high nitrogen content, allowing for its detection by elemental analysis. Solid state NMR and IR can also be used to monitor the reaction as the peaks relating to the PFPA molecule will disappear.

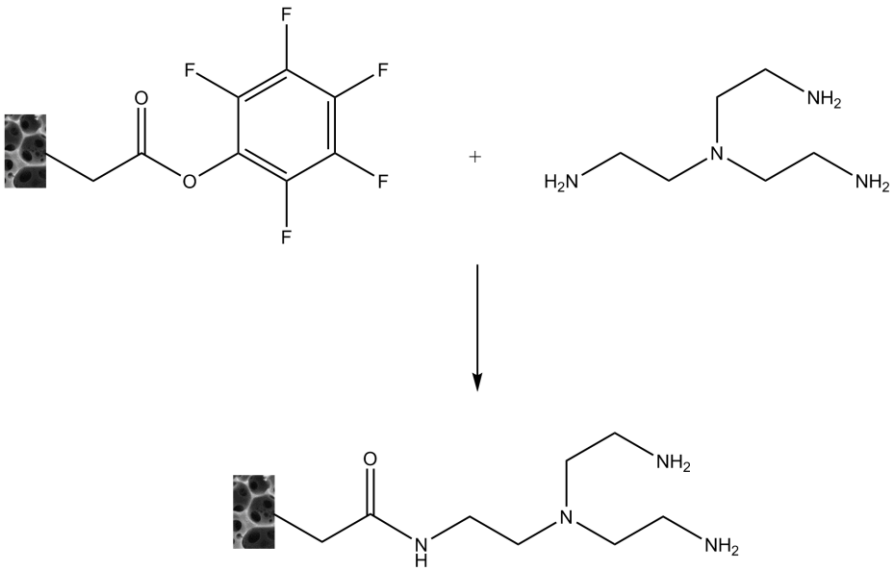

Scheme 3.7 Functionalization of PFPA-polyHIPE with TAEA.

The solid state ^{19}F NMR spectrum of both a PFPA-polyHIPE and a PFPA-PEGMA-polyHIPE functionalized with TAEA is shown in Figure 3.35.

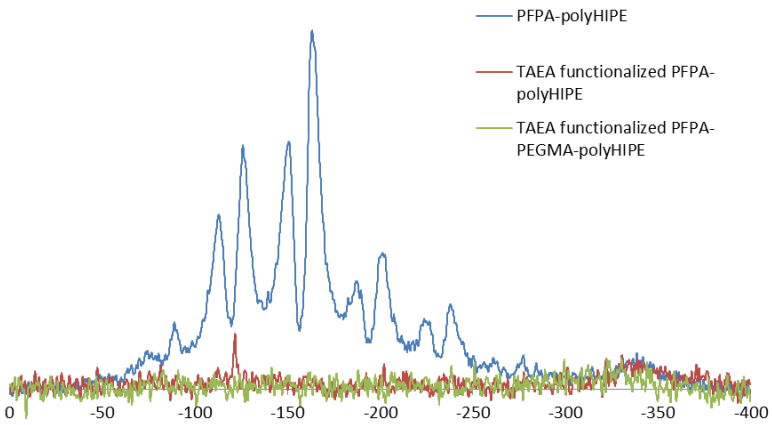

Figure 3.35 Solid state ^{19}F NMR spectra of PFPA-polyHIPE and PFPA-PEGMA-polyHIPE functionalized post-polymerization with TAEA.

No signal can be seen in the solid state ^{19}F NMR spectrum of the PFPA-polyHIPE or the PFPA-PEGMA-polyHIPE functionalized with TAEA, indicating that there is no PFPA left in the polyHIPEs after functionalization. The reaction of PFPA with TAEA can also be observed by FT-IR spectroscopy (Figure 3.36).

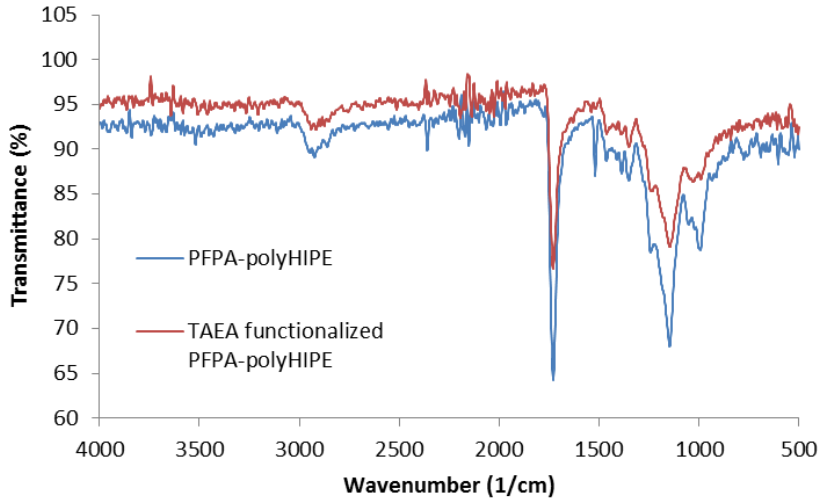

Figure 3.36 FT-IR spectra of TAEA functionalized PFPA-polyHIPE.

The disappearance of the aromatic carbon stretch of PFPA at 1519 cm^{-1} indicates that no PFPA remains in the polyHIPE sample after functionalization with the amine TAEA.

Solid state ^{13}C NMR spectroscopy was carried out on the PFPA-PEGMA-polyHIPE sample, the results of which are shown in Figure 3.37.

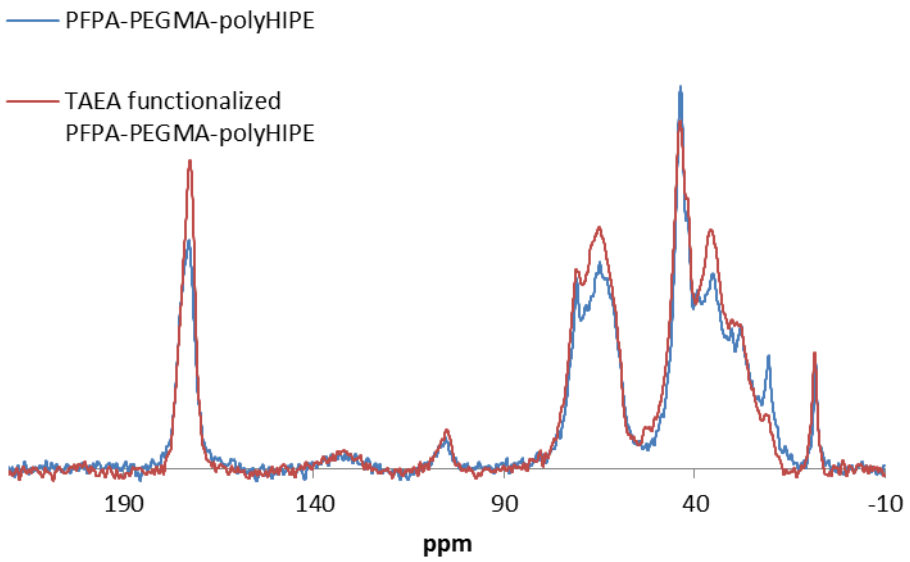

Figure 3.37 Solid state ^{13}C NMR spectrum of PFPA-PEGMA-polyHIPE functionalized post-polymerization with TAEA.

The PEG signal, at 71 ppm, remains unchanged in the PFPA-PEGMA-polyHIPE upon functionalization with TAEA. The results of both the solid

state ^{19}F NMR spectroscopy and solid state ^{13}C NMR spectroscopy indicate that the inclusion of PEGMA in to the polyHIPE network does not have a negative effect on the subsequent reactions of the PFPA monomer, and that the reactions of the PFPA within the polymer network does not affect the PEG chains in the polyHIPE polymer.

The percentage functionalization of PFPA can be obtained via elemental analysis (Table 3.5).

Table 3.5 Percentage functionalization of PFPA-polyHIPE and PFPA-PEGMA-polyHIPE after post-polymerization functionalization with TAEA as determined by elemental analysis.

PolyHIPE	% Nitrogen (Theoretical)	% Nitrogen (Obtained)	% Functionalization
PFPA-polyHIPE	0	<0.1	0
PFPA-PEG-polyHIPE	0	<0.1	0
TAEA functionalized PFPA-polyHIPE	0.86	0.61	71
TAEA functionalized PFPA-PEG-polyHIPE	0.86	0.86	100

A high level of functionalization is achieved for both the PFPA-polyHIPE and PFPA-PEGMA-polyHIPE samples. This high level of functionalization and the mild conditions at which they were achieved suggests that this post-polymerization functionalization method may be a suitable route to the incorporation of biomolecules into the polyHIPE polymer network.

The morphology of the TAEA functionalized polyHIPEs was investigated via SEM (Figure 3.38).

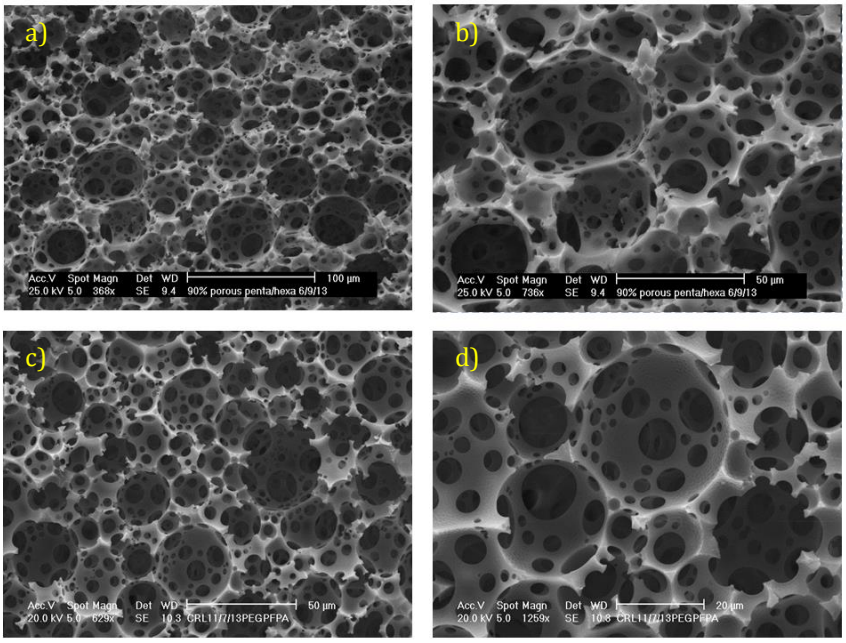

Figure 3.38 Morphology of PFPA-polyHIPE and PFPA-PEGMA-polyHIPE functionalized with TAEA post-polymerization. a), b) SEM images of TAEA functionalized PFPA-polyHIPE at two different magnifications. c), d) SEM images of TAEA functionalized PFPA-PEGMA-polyHIPE at two different magnifications.

The morphology observed for the TAEA functionalized polyHIPEs remains the same as the observed for the PFPA-polyHIPE and PFPA-PEGMA-polyHIPE. The range of obtained void diameters was measured and the results are summarized in Figure 3.39.

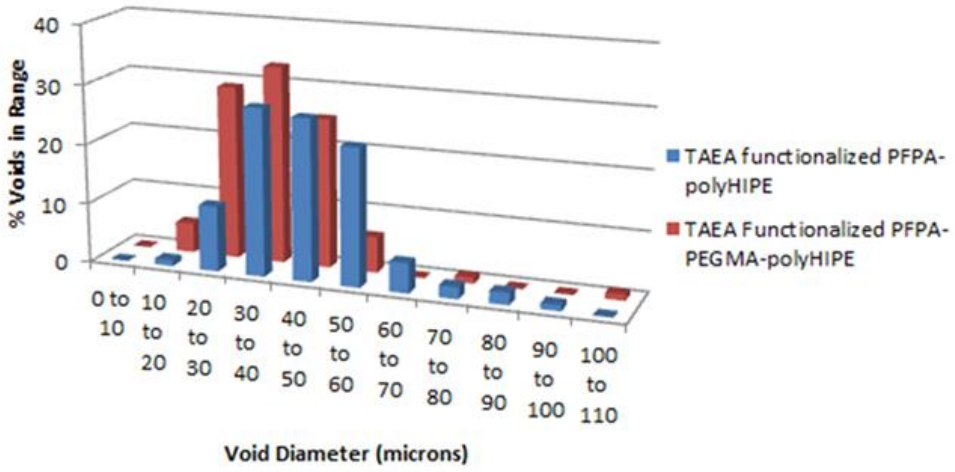

Figure 3.39 Void diameters observed for (front to back) TAEA functionalized PFPA-polyHIPE and TAEA functionalized PFPA-PEGMA-polyHIPE.

As would be expected from the previous post-polymerization functionalization methods, there is no change in the morphology or void diameter range observed upon functionalization.

3.2.4. Functionalization of PFPA With L-Alanine and RGD

PFPA within the polymer network will undergo reactions with a wide range of nucleophilic amines. Many molecules of biological importance, including amino acids and peptides, contain nucleophilic amines, and so can be incorporated into the polyHIPE network via the post-polymerization functionalization reaction described previously. The short chain peptide arginylglycylaspartic acid (RGD) was chosen due to its extensive use in biomaterials for cell culture[79, 229, 230]. The RGD sequence is associated with many extracellular matrix (ECM) proteins, including fibronectin and collagen I, and interacts with integrin receptors on the cell surface to facilitate focal point adhesion to the surface of the ECM[231]. RGD has been incorporated into biomaterials via conjugation to a wide range of polymers, and has been shown to promote cell proliferation and differentiation[229, 232, 233]. The advantage of incorporating the RGD peptide into a biomaterial, as opposed to a whole ECM protein, lies in the small size of the peptide. This small size allows for a higher packing density of the molecule within the biomaterial, giving a higher density of cell adhesion points.

In order to investigate the potential of incorporating peptides into a PFPA-polyHIPE, an amino acid, L-alanine, was first added to the polymer, followed by the RGD peptide (obtained from Sigma Aldrich). The progress of the reaction was monitored by solid state ^{19}F and ^{13}C spectroscopy, FT-IR spectroscopy and elemental analysis. SEM was also used in order to investigate the impact the functionalization process has on the polyHIPE polymer surface.

The solid state ^{19}F NMR spectrum of both the L-alanine and RGD functionalized PFPA-polyHIPEs are shown in Figure 3.40.

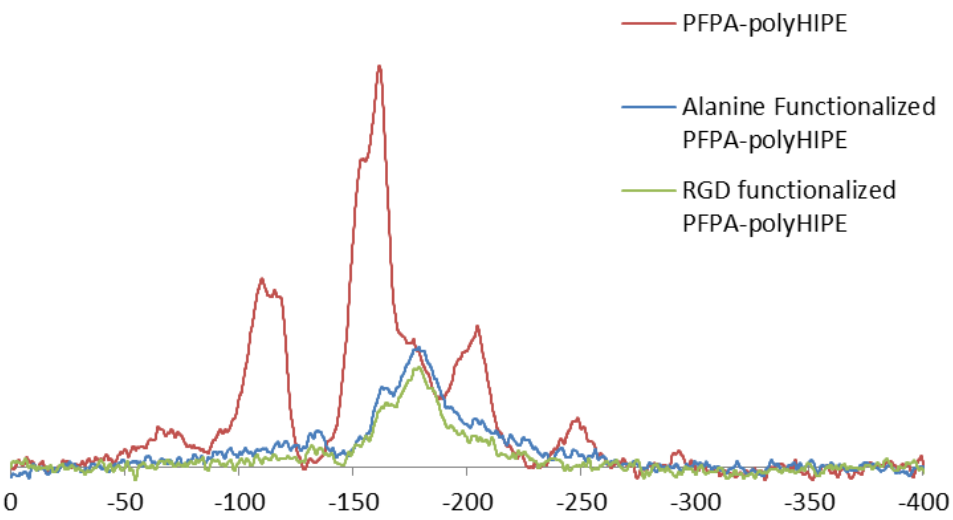

Figure 3.40 Solid state ^{19}F NMR spectra of PFPA-polyHIPE functionalized with alanine and RGD.

The signal is seen to be at a reduced intensity in the ^{19}F NMR spectrum of the L-alanine and RGD functionalized PFPA-polyHIPE, indicating that there is little PFPA left in the polyHIPE after functionalization.

The reaction of the polymer bound PFPA can also be observed by FT-IR spectroscopy (Figure 3.41).

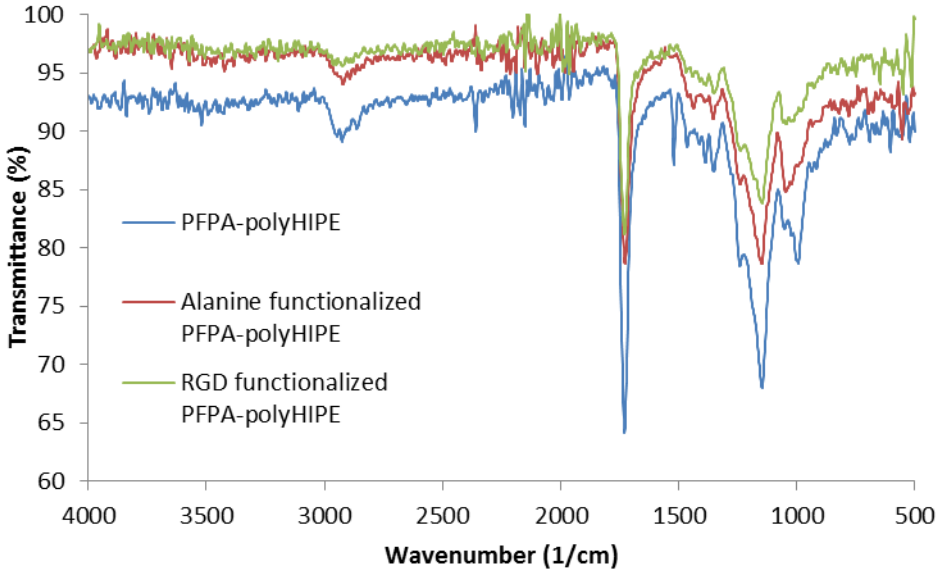

Figure 3.41 FT-IR spectra of PFPA-polyHIPE functionalized with alanine and RGD.

The aromatic carbons of the PFPA molecule can be clearly seen in the FT-IR spectrum of the PFPA-polyHIPE at 1519 cm^{-1}. Upon reaction with both L-alanine and RGD this peak can be seen to disappear, indicating that no PFPA remains in the sample upon completion of the functionalization reaction.

The presence of the biomolecules in the polyHIPE network can be shown by solid state ^{13}C NMR spectroscopy (Figure 3.42).

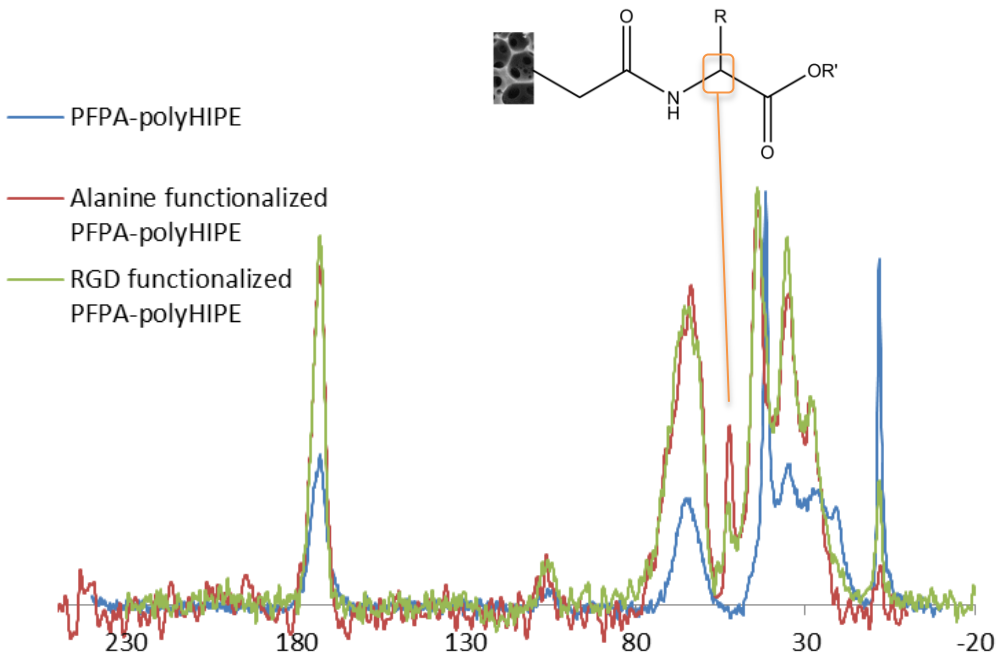

Figure 3.42 Solid state ^{13}C NMR spectra of PFPA-polyHIPE functionalized with L-alanine and RGD.

Upon incorporating the amino acid and peptide into the polymer network a signal at 52 ppm can be observed in the solid state ^{13}C NMR spectra. This signal is indicative of an amine and cannot be seen in the ^{13}C NMR spectrum of PFPA-polyHIPE, suggesting that the biomolecules have been successfully bonded to the polymer.

Elemental analysis can be used to determine the percentage conversion of PFPA to biomolecule, the results of which are summarized in Table 3.6.

Table 3.6 Percentage functionalization of PFPA-polyHIPE and PFPA-PEGMA-polyHIPE after post-polymerization functionalization with L-alanine and RGD as determined by elemental analysis.

PolyHIPE	% Nitrogen (Theoretical)	% Nitrogen (Obtained)	% Functionalization
L-Alanine functionalized PFPA-polyHIPE	0.22	0.54	245
L-Alanine functionalized PFPA-PEG-polyHIPE	0.22	0.56	254
RGD functionalized PFPA-polyHIPE	1.28	0.57	44

The high levels of functionalization observed for the functionalization of PFPA-polyHIPE could be explained in a number of ways. The first of these is that the L-alanine has adsorbed onto the polymer surface rather than undergoing a reaction with PFPA. In order to investigate this, the reaction was repeated on a PFPA-PEGMA-polyHIPE as PEG has been shown at have anti-biofouling properties. The similarly high concentration observed in the L-alanine functionalized PFPA-PEGMA-polyHIPE sample would suggest either the high percentage nitrogen is not as a result of adsorption onto the polymer surface, or that the anti-biofouling properties of PEG are not effective when biomolecules with a very low molecular weight are used. Other possible reasons for the high level of nitrogen observed compared with the theoretical level include: the previously measured percentage of

PFPA within PFPA-polyHIPE network is lower than the level in the sample used or; elemental analysis is not a reliable method for calculating the concentration of nitrogen within a polyHIPE.

The low level of functionalization achieved for the RGD functionalized PFPA-polyHIPE is due to the lower ratio of RGD to PFPA (1:1, where a ratio of 2:1 was used during the L-alanine functionalization) used for this reaction.

The morphology of the alanine and RGD functionalized polyHIPEs was investigated using SEM, the results of which are shown in Figure 3.43.

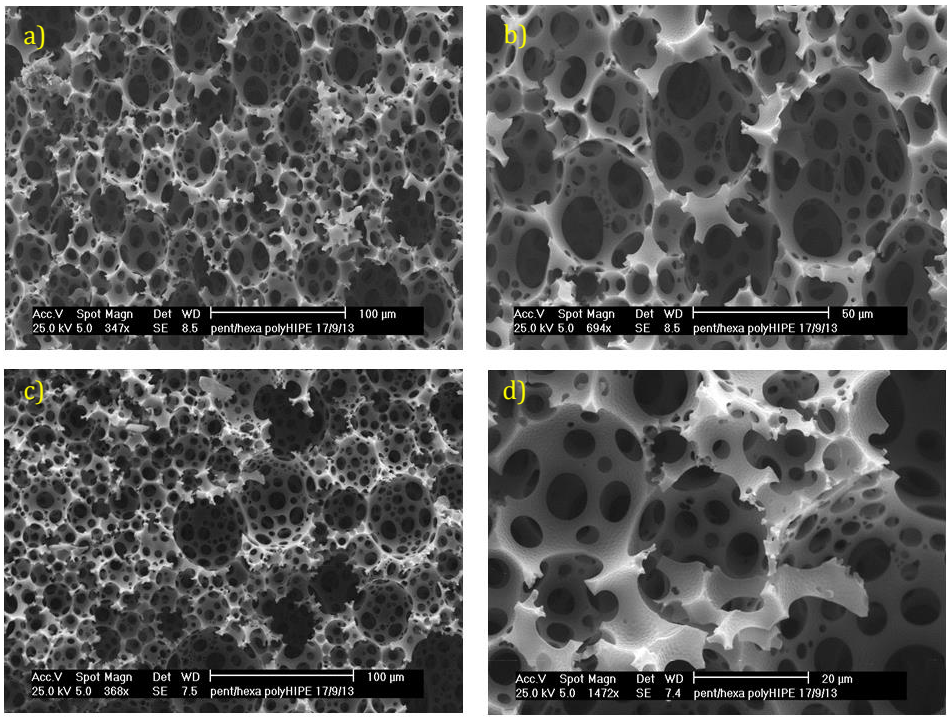

Figure 3.43 Morphology of PFPA-polyHIPE functionalized with alanine and RGD post-polymerization. a), b) SEM images of alanine functionalized PFPA-polyHIPE at two different magnifications. c), d) SEM images of RGD functionalized PFPA-polyHIPE at two different magnifications.

As can be seen from the SEM images in Figure 10.4, functionalization of PFPA-polyHIPE with alanine and RGD post-polymerization does not have any impact on the morphology of the polyHIPE. The diameters of the voids observed were measured and the results are summarized in Figure 3.44.

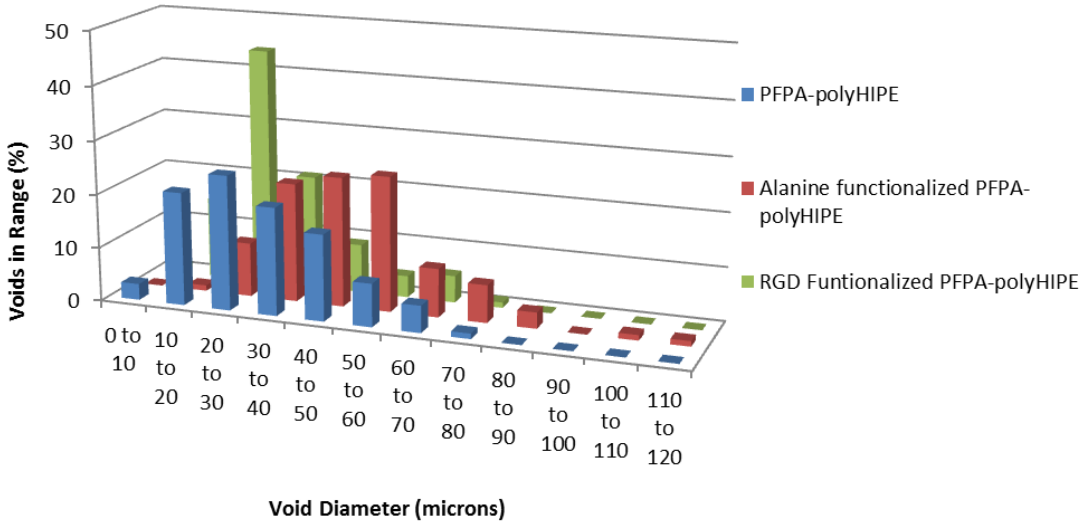

Figure 3.44 Void diameters observed for (front to back) PFPA-polyHIPE, alanine functionalized PFPA-polyHIPE and RGD functionalized PFPA-polyHIPE.

The void diameters in the alanine and RGD functionalized polyHIPEs fall within the expected range.

4. Conclusions

Thiol-ene chemistry has been used to produce four thiol-acrylate polyHIPEs via photopolymerization. These polyHIPEs have then been successfully functionalized post-polymerization via several methods, including "click" reactions and Michael additions, the formation of disulphide bonds, and the incorporation and subsequent reaction of reactive monomers in to the HIPE prior to curing. The effect the post-polymerization functionalizations have on the morphology of the polyHIPEs was monitored by scanning electron microscopy, and was found to remain constant.

Surface functionalization of trithiol-TMPTA polyHIPE polymers was achieved by both radical mediated "click" reactions and by Michael addition. Molecules including fluorinated and fluorescent acrylates, as well as PEGMA, were successfully grafted to the polymer surface under mild conditions, with high levels of functionalization observed. The addition of PEGMA to the polymer surface allowed for the preparation of hydrophilic polyHIPEs. The formation of disulphide bonds between the residual thiols at the polymer surface and thiol containing molecules has also been used to prepare surface functionalized polyHIPEs.

Non-crosslinking monomers, including the active ester PFPA, were added to trithiol-DPEHA polyHIPE, allowing for their functionalization post-polymerization. The reactivity of PFPA was tested using an amine with high nitrogen content before repeating the functionalization with bioactive molecules, including the amino acid alanine, and a short integrin binding peptide RGD. Conversions of up to 100% were achieved, with any unreacted PFPA being removed from the polyHIPE by hydrolysis.

Overall it has been shown that these thiol-acrylate polyHIPEs can undergo chemical functionalization via a wide variety of methods, retaining their highly porous and interconnected morphology.

5. Further Work – GGRGD Synthesis

This project has demonstrated the ease with which thiol-acrylate polyHIPEs can be chemically functionalized post-polymerization. Further work into how the addition of chemical functionality into the polymer network will enhance the range of applications available to these materials is required.

As previously discussed, polyHIPE polymers have found application in the field of tissue engineering and 3D cell culture, with the chemical functionalization of the polymers enhancing the viability of cells cultured in this environment. Thiol-acrylate polyHIPEs also have the added benefit of biodegradability, a feature which may make these materials suitable for implant. This project has demonstrated the ease with which a short chain integrin binding peptide (RGD) can be grafted to the surface of the polymer, under mild conditions. In order to ascertain if the inclusion of biomolecules such as RGD into the polymer network does create an environment more suited to cells, a detailed *in vitro* cell culture study must be carried out. In order for this study to be carried out one limiting factor must be addressed. This limiting factor is the cost of the RGD peptide. With tissue culture plastic being cheap to manufacture on large scales, any chemical or process which increases the cost of scaffold production will hinder any possibility of 3D cell culture becoming the norm.

PolyHIPE functionalization worked carried out in this project utilized RGD purchased from Sigma Aldrich. One way of reducing this cost is to synthesize the peptide in house using the solid phase peptide synthesis methodology. Preparing the peptide in house also allows for the inclusion of a short spacer (two extra glycine units), which should lift the integrin binding section of the peptide off the polymer surface, allowing cells better access[232]. Solid phase peptide synthesis should also allow for production of the peptide on the large scales often needed when working with polyHIPE polymers.

GGRGD was synthesized on rink amide resin, with a yield of 0.3 g being targeted. Once synthesized, the peptide was then analysed by MALDI mass spectroscopy, the results of which are shown in Figure 5.1

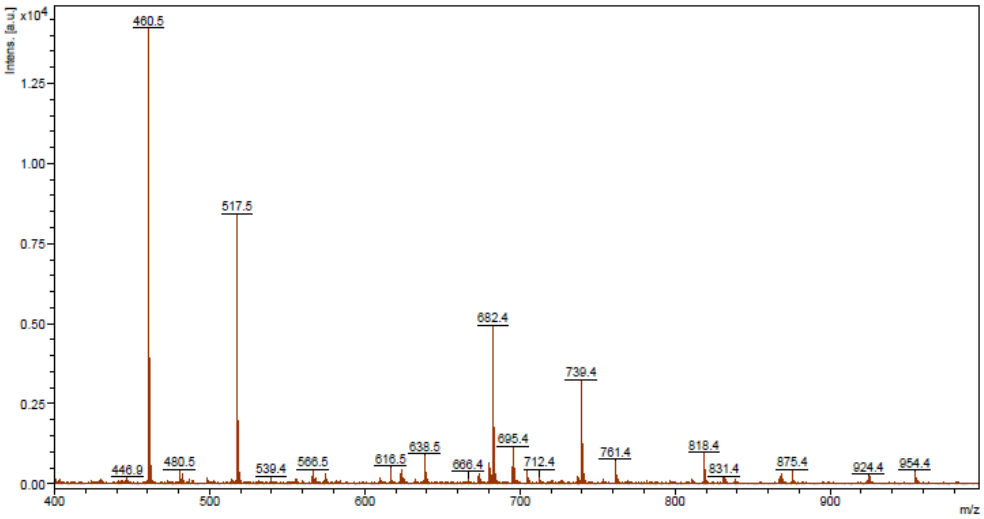

Figure 5.1 MALDI mass spectrum of GGRGD peptide.

The peak at 460.5 m/z represents the targeted GGRGD peptide. The other peaks at 517.5, 682.4 and 739.4 m/z represent the insertion of extra glycine and arginine residues into the chain. In order to obtained 0.3 g peptide, 1 g rink amide resin was used. It is possible that this mass of resin was too large for the peptide synthesis tube used, making it difficult to remove the reagents at the end of each synthesis step. Purification of the peptide was via HPLC; however, the peptide appeared to stick to the column.

The GGRGD integrin binding peptide can be synthesized, however the work must be carried out on a smaller scale and other methods to purify the peptide must be explored. Unfortunately, due to time constraints, it was not possible to further this work or carry out the cell culture experiments required in order to assess the impact surface bound peptides have on cells cultured on thiol-acrylate polyHIPE scaffolds.

6. References

1. C. E. Hoyle and C. N. Bowman, *Angewandte Chemie-International Edition*, 2010, **49**, 1540-1573.
2. A. B. Lowe, *Polymer Chemistry*, 2010, **1**, 17-36.
3. N. Hadjichristidis, H. Iatrou, M. Pitsikalis and J. Mays, *Progress in Polymer Science*, 2006, **31**, 1068-1132.
4. A. Hirao, M. Hayashi, S. Loykulnant and K. Sugiyama, *Progress in Polymer Science*, 2005, **30**, 111-182.
5. J. Chiefari, Y. K. Chong, F. Ercole, J. Krstina, J. Jeffery, T. P. T. Le, R. T. A. Mayadunne, G. F. Meijs, C. L. Moad, G. Moad, E. Rizzardo and S. H. Thang, *Macromolecules*, 1998, **31**, 5559-5562.
6. C. Barner-Kowollik and S. Perrier, *Journal of Polymer Science Part a-Polymer Chemistry*, 2008, **46**, 5715-5723.
7. C. J. Hawker, A. W. Bosman and E. Harth, *Chemical Reviews*, 2001, **101**, 3661-3688.
8. M. Ouchi, T. Terashima and M. Sawamoto, *Chemical Reviews*, 2009, **109**, 4963-5050.
9. F. di Lena and K. Matyjaszewski, *Progress in Polymer Science*, 2010, **35**, 959-1021.
10. H. C. Kolb, M. G. Finn and K. B. Sharpless, *Angewandte Chemie-International Edition*, 2001, **40**, 2004-2021.
11. L. Y. Liang and D. Astruc, *Coordination Chemistry Reviews*, 2011, **255**, 2933-2945.
12. M. A. Tasdelen and Y. Yagci, *Angewandte Chemie-International Edition*, 2013, **52**, 5930-5938.
13. H. Stockmann, A. A. Neves, S. Stairs, K. M. Brindle and F. J. Leeper, *Organic & Biomolecular Chemistry*, 2011, **9**, 7303-7305.
14. B. S. Sumerlin and A. P. Vogt, *Macromolecules*, 2010, **43**, 1-13.
15. A. B. Lowe, C. E. Hoyle and C. N. Bowman, *Journal of Materials Chemistry*, 2010, **20**, 4745-4750.
16. W. H. Binder and C. Kluger, *Current Organic Chemistry*, 2006, **10**, 1791-1815.
17. J. A. Johnson, M. G. Finn, J. T. Koberstein and N. J. Turro, *Macromolecular Rapid Communications*, 2008, **29**, 1052-1072.
18. P. Lundberg, C. J. Hawker, A. Hult and M. Malkoch, *Macromolecular Rapid Communications*, 2008, **29**, 998-1015.
19. W. H. Binder and R. Sachsenhofer, *Macromolecular Rapid Communications*, 2007, **28**, 15-54.
20. W. H. Binder and R. Sachsenhofer, *Macromolecular Rapid Communications*, 2008, **29**, 952-981.
21. R. A. Evans, *Australian Journal of Chemistry*, 2007, **60**, 384-395.
22. J. E. Moses and A. D. Moorhouse, *Chemical Society Reviews*, 2007, **36**, 1249-1262.
23. P. D. Topham, N. Sandon, E. S. Read, J. Madsen, A. J. Ryan and S. P. Armes, *Macromolecules*, 2008, **41**, 9542-9547.
24. J. A. Opsteen and J. C. M. van Hest, *Chem Commun (Camb)*, 2005, 57-59.

25. J. Yin, Z. Ge, H. Liu and S. Liu, *Journal of Polymer Science Part a-Polymer Chemistry*, 2009, **47**, 2608-2619.
26. A. J. de Graaf, E. Mastrobattista, C. F. van Nostrum, D. T. S. Rijkers, W. E. Hennink and T. Vermonden, *Chem Commun (Camb)*, 2011, **47**, 6972-6974.
27. T. Posner, *Berichte Der Deutschen Chemischen Gesellschaft*, 1905, **38**, 646-657.
28. N. B. Cramer, S. K. Reddy, A. K. O'Brien and C. N. Bowman, *Macromolecules*, 2003, **36**, 7964-7969.
29. C. E. Hoyle, T. Y. Lee and T. Roper, *Journal of Polymer Science Part a-Polymer Chemistry*, 2004, **42**, 5301-5338.
30. M. Uygun, M. A. Tasdelen and Y. Yagci, *Macromolecular Chemistry and Physics*, 2010, **211**, 103-110.
31. A. F. Senyurt, H. Wei, C. E. Hoyle, S. G. Piland and T. E. Gould, *Macromolecules*, 2007, **40**, 4901-4909.
32. T. Y. Lee, Z. Smith, S. K. Reddy, N. B. Cramer and C. N. Bowman, *Macromolecules*, 2007, **40**, 1466-1472.
33. H. Wei, A. F. Senyurt, S. Jonsson and C. E. Hoyle, *Journal of Polymer Science Part a-Polymer Chemistry*, 2007, **45**, 822-829.
34. C. O. Bounds, J. Upadhyay, N. Totaro, S. Thakuri, L. Garber, M. Vincent, Z. Y. Huang, M. Hupert and J. A. Pojman, *Acs Applied Materials & Interfaces*, 2013, **5**, 1643-1655.
35. O. Okay, S. K. Reddy and C. N. Bowman, *Macromolecules*, 2005, **38**, 4501-4511.
36. N. B. Cramer, J. P. Scott and C. N. Bowman, *Macromolecules*, 2002, **35**, 5361-5365.
37. T. Y. Lee, T. M. Roper, E. S. Jonsson, I. Kudyakov, K. Viswanathan, C. Nason, C. A. Guymon and C. E. Hoyle, *Polymer*, 2003, **44**, 2859-2865.
38. N. B. Cramer, S. K. Reddy, M. Cole, C. Hoyle and C. N. Bowman, *Journal of Polymer Science Part a-Polymer Chemistry*, 2004, **42**, 5817-5826.
39. L. V. Natarajan, D. P. Brown, J. M. Wofford, V. P. Tondiglia, R. L. Sutherland, P. F. Lloyd and T. J. Bunning, *Polymer*, 2006, **47**, 4411-4420.
40. A. F. Senyurt and C. E. Hoyle, *European Polymer Journal*, 2006, **42**, 3133-3139.
41. T. F. Scott, C. J. Kloxin, R. B. Draughon and C. N. Bowman, *Macromolecules*, 2008, **41**, 2987-2989.
42. B. D. Mather, K. Viswanathan, K. M. Miller and T. E. Long, *Progress in Polymer Science*, 2006, **31**, 487-531.
43. J. W. Chan, C. E. Hoyle and A. B. Lowe, *Journal of the American Chemical Society*, 2009, **131**, 5751-5753.
44. E. Lovelady, S. D. Kimmins, J. J. Wu and N. R. Cameron, *Polymer Chemistry*, 2011, **2**, 559-562.
45. C. N. Salinas and K. S. Anseth, *Macromolecules*, 2008, **41**, 6019-6026.
46. K. L. Killops, L. M. Campos and C. J. Hawker, *Journal of the American Chemical Society*, 2008, **130**, 5062-5064.
47. J. W. Chan, B. Yu, C. E. Hoyle and A. B. Lowe, *Chem Commun (Camb)*, 2008, 4959-4961.

48. J. Justynska and H. Schlaad, *Macromolecular Rapid Communications*, 2004, **25**, 1478-1481.
49. J. Justynska and H. Schlaad, *Macromolecular Rapid Communications*, 2004, **25**, 1478-1481.
50. J. Justynska, Z. Hordyjewicz and H. Schlaad, *Polymer*, 2005, **46**, 12057-12064.
51. A. Gress, A. Volkel and H. Schlaad, *Macromolecules*, 2007, **40**, 7928-7933.
52. N. ten Brummelhuis, C. Diehl and H. Schlaad, *Macromolecules*, 2008, **41**, 9946-9947.
53. C. Diehl and H. Schlaad, *Macromolecular Bioscience*, 2009, **9**, 157-161.
54. L. Lotti, S. Coiai, F. Ciardelli, M. Galimberti and E. Passaglia, *Macromolecular Chemistry and Physics*, 2009, **210**, 1471-1483.
55. C. Boyer, A. Granville, T. P. Davis and V. Bulmus, *Journal of Polymer Science Part a-Polymer Chemistry*, 2009, **47**, 3773-3794.
56. L. M. Campos, K. L. Killops, R. Sakai, J. M. J. Paulusse, D. Damiron, E. Drockenmuller, B. W. Messmore and C. J. Hawker, *Macromolecules*, 2008, **41**, 7063-7070.
57. M. Li, P. De, S. R. Gondi and B. S. Sumerlin, *Journal of Polymer Science Part a-Polymer Chemistry*, 2008, **46**, 5093-5100.
58. J. W. Chan, B. Yu, C. E. Hoyle and A. B. Lowe, *Chemical Communications*, 2008, 4959-4961.
59. P. Antoni, M. J. Robb, L. Campos, M. Montanez, A. Hult, E. Malmstrom, M. Malkoch and C. J. Hawker, *Macromolecules*, 2010, **43**, 6625-6631.
60. A. Dondoni, *Angewandte Chemie-International Edition*, 2008, **47**, 8995-8997.
61. L. M. Campos, I. Meinel, R. G. Guino, M. Schierhorn, N. Gupta, G. D. Stucky and C. J. Hawker, *Advanced Materials*, 2008, **20**, 3728-3733.
62. A. K. O'Brien, N. B. Cramer and C. N. Bowman, *Journal of Polymer Science Part a-Polymer Chemistry*, 2006, **44**, 2007-2014.
63. S. K. Reddy, O. Okay and C. N. Bowman, *Macromolecules*, 2006, **39**, 8832-8843.
64. O. Okay and C. N. Bowman, *Macromolecular Theory and Simulations*, 2005, **14**, 267-277.
65. C. E. Hoyle, T. Y. Lee and T. Roper, *Journal of Polymer Science Part a-Polymer Chemistry*, 2004, **42**, 5301-5338.
66. J. L. Drury and D. J. Mooney, *Biomaterials*, 2003, **24**, 4337-4351.
67. K. Y. Lee and D. J. Mooney, *Chemical Reviews*, 2001, **101**, 1869-1879.
68. J. Cabral and S. C. Moratti, *Future Medicinal Chemistry*, 2011, **3**, 1877-1888.
69. P. van de Wetering, A. T. Metters, R. G. Schoenmakers and J. A. Hubbell, *Journal of Controlled Release*, 2005, **102**, 619-627.
70. A. E. Rydholm, C. N. Bowman and K. S. Anseth, *Biomaterials*, 2005, **26**, 4495-4506.
71. B. D. Fairbanks, M. P. Schwartz, A. E. Halevi, C. R. Nuttelman, C. N. Bowman and K. S. Anseth, *Advanced Materials*, 2009, **21**, 5005-5010.
72. H. Shih and C. C. Lin, *Biomacromolecules*, 2012, **13**, 2003-2012.
73. D. L. Elbert, A. B. Pratt, M. P. Lutolf, S. Halstenberg and J. A. Hubbell, *Journal of Controlled Release*, 2001, **76**, 11-25.

74. A. E. Rydholm, S. K. Reddy, K. S. Anseth and C. N. Bowman, *Biomacromolecules*, 2006, **7**, 2827-2836.
75. C. S. Ki, H. Shih and C. C. Lin, *Polymer*, 2013, **54**, 2115-2122.
76. C.-C. Lin, A. Raza and H. Shih, *Biomaterials*, 2011, **32**, 9685-9695.
77. B. D. Fairbanks, S. P. Singh, C. N. Bowman and K. S. Anseth, *Macromolecules*, 2011, **44**, 2444-2450.
78. T. Yang, H. Long, M. Malkoch, E. Kristofer Gamstedt, L. Berglund and A. Hult, *Journal of Polymer Science Part A: Polymer Chemistry*, 2011, **49**, 4044-4054.
79. C. N. Salinas, B. B. Cole, A. M. Kasko and K. S. Anseth, *Tissue Engineering*, 2007, **13**, 1025-1034.
80. Y. T. Hao, H. Shih, Z. Munoz, A. Kemp and C. C. Lin, *Acta Biomaterialia*, 2014, **10**, 104-114.
81. K. D. Xu, Y. Fu, W. J. Chung, X. X. Zheng, Y. J. Cui, I. C. Hsu and W. J. Kao, *Acta Biomaterialia*, 2012, **8**, 2504-2516.
82. N. R. Cameron, *Polymer*, 2005, **46**, 1439-1449.
83. S. Caldwell, D. W. Johnson, M. P. Didsbury, B. A. Murray, J. J. Wu, S. A. Przyborski and N. R. Cameron, *Soft Matter*, 2012, **8**, 10344-10351.
84. Y. Q. Lv, Z. X. Lin and F. Svec, *Analyst*, 2012, **137**, 4114-4118.
85. B. Preinerstorfer, W. Bicker, W. Lindner and M. Lammerhofer, *Journal of Chromatography A*, 2004, **1044**, 187-199.
86. C. Triantafillidis, M. S. Elsaesser and N. Husing, *Chemical Society Reviews*, 2013, **42**, 3833-3846.
87. E. A. Jackson and M. A. Hillmyer, *Acs Nano*, 2010, **4**, 3548-3553.
88. Y. Liang, L. H. Zhang and Y. K. Zhang, *Analytical and Bioanalytical Chemistry*, 2013, **405**, 2095-2106.
89. E. Knight, B. Murray, R. Carnachan and S. Przyborski, in *3d Cell Culture: Methods and Protocols*, ed. J. W. Haycock, 2011, vol. 695, pp. 323-340.
90. S. D. Kimmins, P. Wyman and N. R. Cameron, *Polymer*, 2014, **55**, 416-425.
91. M. S. Silverstein, H. W. Tai, A. Sergienko, Y. L. Lumelsky and S. Pavlovsky, *Polymer*, 2005, **46**, 6682-6694.
92. C. D. Wood, B. Tan, A. Trewin, H. Niu, D. Bradshaw, M. J. Rosseinsky, Y. Z. Khimyak, N. L. Campbell, R. Kirk, E. Stöckel and A. I. Cooper, *Chemistry of Materials*, 2007, **19**, 2034-2048.
93. C. D. Wood, B. Tan, A. Trewin, F. Su, M. J. Rosseinsky, D. Bradshaw, Y. Sun, L. Zhou and A. I. Cooper, *Advanced Materials*, 2008, **20**, 1916-1921.
94. C. F. Martin, E. Stoeckel, R. Clowes, D. J. Adams, A. I. Cooper, J. J. Pis, F. Rubiera and C. Pevida, *Journal of Materials Chemistry*, 2011, **21**, 5475-5483.
95. C.-C. Chao, T.-C. Wang, R.-M. Ho, P. Georgopanos, A. Avgeropoulos and E. L. Thomas, *Acs Nano*, 2010, **4**, 2088-2094.
96. H. Deleuze, R. Faivre and V. Herroguez, *Chem Commun (Camb)*, 2002, 2822-2823.
97. M. A. Hillmyer, in *Block Copolymers Ii*, ed. V. Abetz, 2005, vol. 190, pp. 137-181.

98. D. Wu, F. Xu, B. Sun, R. Fu, H. He and K. Matyjaszewski, *Chemical Reviews*, 2012, **112**, 3959-4015.
99. L. Kircher, P. Theato and N. R. Cameron, *Polymer*, 2013, **54**, 1755-1761.
100. M. Guerrouache, S. Mahouche-Chergui, M. M. Chehimi and B. Carbonnier, *Chem Commun (Camb)*, 2012, **48**, 7486-7488.
101. M. Guerrouache, M. C. Millot and B. Carbonnier, *Macromolecular Rapid Communications*, 2009, **30**, 109-113.
102. P. M. Budd, E. S. Elabas, B. S. Ghanem, S. Makhseed, N. B. McKeown, K. J. Msayib, C. E. Tattershall and D. Wang, *Advanced Materials*, 2004, **16**, 456-459.
103. B. Li, X. Huang, L. Liang and B. Tan, *Journal of Materials Chemistry*, 2010, **20**, 7444-7450.
104. A. P. Cote, A. I. Benin, N. W. Ockwig, M. O'Keeffe, A. J. Matzger and O. M. Yaghi, *Science*, 2005, **310**, 1166-1170.
105. K. S. W. Sing, D. H. Everett, R. A. W. Haul, L. Moscou, R. A. Pierotti, J. Rouquerol and T. Siemieniewska, *Pure and Applied Chemistry*, 1985, **57**, 603-619.
106. W. Busby, N. R. Cameron and C. A. B. Jahoda, *Biomacromolecules*, 2001, **2**, 154-164.
107. R. J. Carnachan, M. Bokhari, S. A. Przyborski and N. R. Cameron, *Soft Matter*, 2006, **2**, 608-616.
108. R. Pons, I. Carrera, P. Erra, H. Kunieda and C. Solans, *Colloids and Surfaces a-Physicochemical and Engineering Aspects*, 1994, **91**, 259-266.
109. K. J. Lissant, *Journal of Colloid and Interface Science*, 1966, **22**, 462-468.
110. H. Bartl and W. Vonbonin, *Makromolekulare Chemie*, 1962, **57**, 74-95.
111. *Euorpean Patent*, EP0060138, 1986.
112. J. M. Williams, A. J. Gray and M. H. Wilkerson, *Langmuir*, 1990, **6**, 437-444.
113. J. M. Williams, *Langmuir*, 1991, **7**, 1370-1377.
114. J. M. Williams and D. A. Wrobleski, *Langmuir*, 1988, **4**, 656-662.
115. J. Jiao and D. J. Burgess, *Journal of Colloid and Interface Science*, 2003, **264**, 509-516.
116. M. G. Freire, A. M. A. Dias, M. A. Z. Coelho, J. A. P. Coutinho and I. M. Marrucho, *Journal of Colloid and Interface Science*, 2005, **286**, 224-232.
117. N. R. Cameron, D. C. Sherrington, L. Albiston and D. P. Gregory, *Colloid and Polymer Science*, 1996, **274**, 592-595.
118. P. Hainey, I. M. Huxham, B. Rowatt, D. C. Sherrington and L. Tetley, *Macromolecules*, 1991, **24**, 117-121.
119. U. Sevšek, J. Brus, K. Jeřabek and P. Krajnc, *Polymer*, 2014, **55**, 410-415.
120. N. R. Cameron and D. C. Sherrington, *Journal of Materials Chemistry*, 1997, **7**, 2209-2212.
121. Y. Tunc, N. Hasirci and K. Ulubayram, *Soft Materials*, 2012, **10**, 449-461.

122. N. R. Cameron, D. C. Sherrington, I. Ando and H. Kurosu, *Journal of Materials Chemistry*, 1996, **6**, 719-726.
123. M. Ottens, G. Leene, A. Beenackers, N. Cameron and D. C. Sherrington, *Industrial & Engineering Chemistry Research*, 2000, **39**, 259-266.
124. A. Barbetta, N. R. Cameron and S. J. Cooper, *Chem Commun (Camb)*, 2000, 221-222.
125. P. Krajnc, J. F. Brown and N. R. Cameron, *Organic Letters*, 2002, **4**, 2497-2500.
126. S. Kovacic and P. Krajnc, *Journal of Polymer Science Part a-Polymer Chemistry*, 2009, **47**, 6726-6734.
127. P. Krajnc, N. Leber, J. F. Brown and N. R. Cameron, *Reactive & Functional Polymers*, 2006, **66**, 81-91.
128. A. Mercier, H. Deleuze and O. Mondain-Monval, *Reactive & Functional Polymers*, 2000, **46**, 67-79.
129. A. Mercier, H. Deleuze and O. Mondain-Monval, *Macromolecular Chemistry and Physics*, 2001, **202**, 2672-2680.
130. L. Moine, H. Deleuze and B. Maillard, *Tetrahedron Letters*, 2003, **44**, 7813-7816.
131. D. Myers, *Surfactant Science and Technology*, 3rd edn., John Wiley and Sons, 2005.
132. A. Barbetta, M. Dentini, L. Leandri, G. Ferraris, A. Coletta and M. Bernabei, *Reactive & Functional Polymers*, 2009, **69**, 724-736.
133. P. Krajnc, N. Leber, D. Stefanec, S. Kontrec and A. Podgornik, *Journal of Chromatography A*, 2005, **1065**, 69-73.
134. C. Yao, L. Qi, H. Jia, P. Xin, G. Yang and Y. Chen, *Journal of Materials Chemistry*, 2009, **19**, 767-772.
135. M. A. Gauthier, M. I. Gibson and H.-A. Klok, *Angewandte Chemie-International Edition*, 2009, **48**, 48-58.
136. W. Busby, N. R. Cameron and A. B. C. Jahoda, *Polymer International*, 2002, **51**, 871-881.
137. S. Kovacic, P. Krajnc and C. Slugovc, *Chem Commun (Camb)*, 2010, **46**, 7504-7506.
138. O. Kulygin and M. S. Silverstein, *Soft Matter*, 2007, **3**, 1525-1529.
139. A. Barbetta, M. Dentini, E. M. Zannoni and M. E. De Stefano, *Langmuir*, 2005, **21**, 12333-12341.
140. C. Palocci, A. Barbetta, A. La Grotta and M. Dentini, *Langmuir*, 2007, **23**, 8243-8251.
141. S. Kovacic, D. Stefanec and P. Krajnc, *Macromolecules*, 2007, **40**, 8056-8060.
142. A. Barbetta, M. Dentini, M. S. De Vecchis, P. Filippini, G. Formisano and S. Caiazza, *Advanced Functional Materials*, 2005, **15**, 118-124.
143. A. Barbetta, M. Massimi, L. C. Devirgiliis and M. Dentini, *Biomacromolecules*, 2006, **7**, 3059-3068.
144. A. Barbetta, M. Massimi, B. Di Rosario, S. Nardecchia, M. De Colli, L. C. Devirgiliis and M. Dentini, *Biomacromolecules*, 2008, **9**, 2844-2856.
145. H. F. Zhang and A. I. Cooper, *Soft Matter*, 2005, **1**, 107-113.
146. R. Butler, C. M. Davies and A. I. Cooper, *Advanced Materials*, 2001, **13**, 1459-1463.
147. J. M. DeSimone, *Science*, 2002, **297**, 799-803.

148. R. Butler, I. Hopkinson and A. I. Cooper, *Journal of the American Chemical Society*, 2003, **125**, 14473-14481.
149. R. Butler, I. Hopkinson and A. I. Cooper, *Journal of the American Chemical Society*, 2003, **125**, 14473-14481.
150. B. Tan, J.-Y. Lee and A. I. Cooper, *Macromolecules*, 2007, **40**, 1945-1954.
151. C. Boyere, A. F. Leonard, B. Grignard, A. Favrelle, J.-P. Pirard, M. Paquot, C. Jerome and A. Debuigne, *Chem Commun (Camb)*, 2012, **48**, 8356-8358.
152. C. Boyere, A. Favrelle, A. F. Leonard, F. Boury, C. Jerome and A. Debuigne, *Journal of Materials Chemistry A*, 2013, **1**, 8479-8487.
153. S. J. Pierre, J. C. Thies, A. Dureault, N. R. Cameron, J. C. M. van Hest, N. Carette, T. Michon and R. Weberskirch, *Advanced Materials*, 2006, **18**, 1822-1826.
154. *European Patent*, EP0216622 1988.
155. *European Patent*, EP1218440A1, 2001.
156. D. Cummins, P. Wyman, C. J. Duxbury, J. Thies, C. E. Koning and A. Heise, *Chemistry of Materials*, 2007, **19**, 5285-5292.
157. M. T. Gokmen, W. Van Camp, P. J. Colver, S. A. F. Bon and F. E. Du Prez, *Macromolecules*, 2009, **42**, 9289-9294.
158. S. D. Kimmins, P. Wyman and N. R. Cameron, *Reactive & Functional Polymers*, 2012, **72**, 947-954.
159. D. W. Johnson, C. Sherborne, M. P. Didsbury, C. Pateman, N. R. Cameron and F. Claeyssens, *Advanced Materials*, 2013, **25**, 3178-3181.
160. F. Claeyssens, E. A. Hasan, A. Gaidukeviciute, D. S. Achilleos, A. Ranella, C. Reinhardt, A. Ovsianikov, S. Xiao, C. Fotakis, M. Vamvakaki, B. N. Chichkov and M. Farsari, *Langmuir*, 2009, **25**, 3219-3223.
161. V. Melissinaki, A. A. Gill, I. Ortega, M. Vamvakaki, A. Ranella, J. W. Haycock, C. Fotakis, M. Farsari and F. Claeyssens, *Biofabrication*, 2011, **3**, 12.
162. I. Ortega, P. Deshpande, A. A. Gill, S. MacNeil and F. Claeyssens, *Biofabrication*, 2013, **5**, 11.
163. B. Sergent, M. Birot and H. Deleuze, *Reactive & Functional Polymers*, 2012, **72**, 962-966.
164. M. Susec, S. C. Ligon, J. Stampfl, R. Liska and P. Krajnc, *Macromolecular Rapid Communications*, 2013, **34**, 938-943.
165. F. Su, C. L. Bray, B. Tan and A. I. Cooper, *Advanced Materials*, 2008, **20**, 2663-2666.
166. J. J. Parlow, R. V. Devraj and M. S. South, *Current Opinion in Chemical Biology*, 1999, **3**, 320-336.
167. Z. Bhumgara, *Filtration & Separation*, 1995, **32**, 245-251.
168. R. A. Sheldon, *Advanced Synthesis & Catalysis*, 2007, **349**, 1289-1307.
169. D. Ma and L.-M. Zhang, *Materials Science and Engineering: C*, 2013, **33**, 2632-2638.
170. N. Dizge, C. Aydiner, D. Y. Imer, M. Bayramoglu, A. Tanriseven and B. Keskinlera, *Bioresource Technology*, 2009, **100**, 1983-1991.
171. C. Zhao, E. Danish, N. R. Cameron and R. Kataky, *Journal of Materials Chemistry*, 2007, **17**, 2446-2453.

172. A. Ghanem, *Tetrahedron*, 2007, **63**, 1721-1754.
173. R. DiCosimo, J. McAuliffe, A. J. Poulose and G. Bohlmann, *Chemical Society Reviews*, 2013, **42**, 6437-6474.
174. B. H. Zhang, Y. Q. Weng, H. Xu and Z. P. Mao, *Applied Microbiology and Biotechnology*, 2012, **93**, 61-70.
175. R. Fernandez-Lafuente, P. Armisén, P. Sabuquillo, G. Fernández-Lorente and J. M. Guisán, *Chemistry and Physics of Lipids*, 1998, **93**, 185-197.
176. N. Dizge, C. Aydiner, D. Y. Imer, M. Bayramoglu, A. Tanriseven and B. Keskinler, *Bioresource Technology*, 2009, **100**, 1983-1991.
177. N. Dizge, B. Keskinler and A. Tanriseven, *Biochemical Engineering Journal*, 2009, **44**, 220-225.
178. N. Dizge, B. Keskinler and A. Tanriseven, *Colloids and Surfaces B-Biointerfaces*, 2008, **66**, 34-38.
179. F. Bordusa, *Chemical Reviews*, 2002, **102**, 4817-4867.
180. M. Capellas, G. Caminal, G. Gonzalez, J. LopezSantin and P. Clapes, *Biotechnology and Bioengineering*, 1997, **56**, 456-463.
181. D. J. Durbin and C. Malardier-Jugroot, *International Journal of Hydrogen Energy*, 2013, **38**, 14595-14617.
182. L. Schlapbach and A. Zuttel, *Nature*, 2001, **414**, 353-358.
183. U. Eberle, M. Felderhoff and F. Schüth, *Angewandte Chemie International Edition*, 2009, **48**, 6608-6630.
184. U. Sevsek, J. Brus, K. Jerabek and P. Krajnc, *Polymer*, 2014, **55**, 410-415.
185. N. L. Rosi, J. Eckert, M. Eddaoudi, D. T. Vodak, J. Kim, M. O'Keeffe and O. M. Yaghi, *Science*, 2003, **300**, 1127-1129.
186. J. H. Ahn, J. E. Jang, C. G. Oh, S. K. Ihm, J. Cortez and D. C. Sherrington, *Macromolecules*, 2006, **39**, 627-632.
187. *US Patent*, US3729457 A, 1973.
188. I. Pulko, J. Wall, P. Krajnc and N. R. Cameron, *Chemistry-a European Journal*, 2010, **16**, 2350-2354.
189. M. G. Schwab, I. Senkovska, M. Rose, N. Klein, M. Koch, J. Pahnke, G. Jonschker, B. Schmitz, M. Hirscher and S. Kaskel, *Soft Matter*, 2009, **5**, 1055-1059.
190. K. L. Lim, H. Kazemian, Z. Yaakob and W. R. W. Daud, *Chemical Engineering & Technology*, 2010, **33**, 213-226.
191. T. A. Strobel, C. A. Koh and E. D. Sloan, *Fluid Phase Equilibria*, 2007, **261**, 382-389.
192. H. Lee, J. W. Lee, D. Y. Kim, J. Park, Y. T. Seo, H. Zeng, I. L. Moudrakovski, C. I. Ratcliffe and J. A. Ripmeester, *Nature*, 2005, **434**, 743-746.
193. Y. P. Zhou, Y. X. Wang, H. H. Chen and L. Zhou, *Carbon*, 2005, **43**, 2007-2012.
194. L. J. Florusse, C. J. Peters, J. Schoonman, K. C. Hester, C. A. Koh, S. F. Dec, K. N. Marsh and E. D. Sloan, *Science*, 2004, **306**, 469-471.
195. R. H. Harrison, J.-P. St-Pierre and M. M. Stevens, *Tissue Engineering Part B-Reviews*, 2014, **20**, 1-16.

196. A. Schober, U. Fernekorn, S. Singh, G. Schlingloff, M. Gebinoga, J. Hampl and A. Williamson, *Engineering in Life Sciences*, 2013, **13**, 352-367.
197. S. J. Hollister, *Nature Materials*, 2005, **4**, 518-524.
198. R. Langer and J. P. Vacanti, *Science*, 1993, **260**, 920-926.
199. M. D. Duncan and D. S. Wilkes, *Proceedings of the American Thoracic Society*, 2005, **2**, 449-455.
200. R. R. Betz, *Orthopedics*, 2002, **25**, S561-S570.
201. Y. Takeuchi and R. A. Weiss, *Current Opinion in Immunology*, 2000, **12**, 504-507.
202. G. Chen, Q. Y. Sun, X. M. Wang, S. Q. Shen, H. Guo, H. Wang, Y. Wu, W. Y. Wang, Y. L. Xiong and S. Chen, *Xenotransplantation*, 2004, **11**, 123-132.
203. E. van Rongen, in *Xenotransplantation: Scientific Frontiers and Public Policy*, eds. J. Fishman, D. Sachs and R. Shaikh, New York Acad Sciences, New York, 1998, vol. 862, pp. 177-183.
204. K. Chatterjee, S. Lin-Gibson, W. E. Wallace, S. H. Parekh, Y. J. Lee, M. T. Cicerone, M. F. Young and C. G. Simon, Jr., *Biomaterials*, 2010, **31**, 5051-5062.
205. J. Zhu, *Biomaterials*, 2010, **31**, 4639-4656.
206. Y. F. Goh, I. Shakir and R. Hussain, *Journal of Materials Science*, 2013, **48**, 3027-3054.
207. B. Kundu, N. E. Kurland, S. Bano, C. Patra, F. B. Engel, V. K. Yadavalli and S. C. Kundu, *Progress in Polymer Science*, 2014, **39**, 251-267.
208. M. Okamoto and B. John, *Progress in Polymer Science*, 2013, **38**, 1487-1503.
209. M. W. Hayman, K. H. Smith, N. R. Cameron and S. A. Przyborski, *Biochemical and Biophysical Research Communications*, 2004, **314**, 483-488.
210. G. Akay, M. A. Birch and M. A. Bokhari, *Biomaterials*, 2004, **25**, 3991-4000.
211. A. S. Hayward, A. M. Eissa, D. J. Maltman, N. Sano, S. A. Przyborski and N. R. Cameron, *Biomacromolecules*, 2013, **14**, 4271-4277.
212. M. W. Hayman, K. H. Smith, N. R. Cameron and S. A. Przyborski, *Journal of Biochemical and Biophysical Methods*, 2005, **62**, 231-240.
213. M. Bokhari, R. J. Carnachan, N. R. Cameron and S. A. Przyborski, *Biochemical and Biophysical Research Communications*, 2007, **354**, 1095-1100.
214. M. Bokhari, R. J. Carnachan, N. R. Cameron and S. A. Przyborski, *Journal of Anatomy*, 2007, **211**, 567-576.
215. B. J. Kane, M. J. Zinner, M. L. Yarmush and M. Toner, *Analytical Chemistry*, 2006, **78**, 4291-4298.
216. Cancer Research UK, *Methotrexate (Maxtrex)*, http://www.cancerresearchuk.org/cancer-help/about-cancer/treatment/cancer-drugs/methotrexate, Accessed 27/3, 2014.
217. A. S. Hayward, N. Sano, S. A. Przyborski and N. R. Cameron, *Macromolecular Rapid Communications*, 2013, **34**, 1844-1849.
218. G. Ashwell and A. G. Morell, *Advances in Enzymology and Related Areas of Molecular Biology*, 1974, **41**, 99-128.

219. C. S. Cho, S. J. Seo, I. K. Park, S. H. Kim, T. H. Kim, T. Hoshiba, I. Harada and T. Akaike, *Biomaterials*, 2006, **27**, 576-585.
220. C. Rey, C. Combes, C. Drouet and M. J. Glimcher, *Osteoporosis International*, 2009, **20**, 2155-2155.
221. K. Kuroda and M. Okido, *Bioinorganic Chemistry and Applications*, 2012, 7.
222. W. Busby, N. R. Cameron and C. A. B. Jahoda, *Biomacromolecules*, 2001, **2**, 154-164.
223. M. T. Gokmen, J. Brassinne, R. A. Prasath and F. E. Du Prez, *Chem Commun (Camb)*, 2011, **47**, 4652-4654.
224. J. P. Badyal, A. M. Cameron, N. R. Cameron, D. M. Coe, R. Cox, B. G. Davis, L. J. Oates, G. Oye and P. G. Steel, *Tetrahedron Letters*, 2001, **42**, 8531-8533.
225. Royal Society of Chemistry, *Pentafluorophenyl Acrylate*, http://www.chemspider.com/Chemical-Structure.2056299.html, Accessed 27/3, 2014.
226. Royal Society of Chemistry, *3-(Acryloyloxy)-2-{[3-(acryloyloxy)-2-[(acryloyloxy)methyl]-2-(hydroxymethyl)propoxy]methyl}-2-[(acryloyloxy)methyl]propyl acrylate* http://www.chemspider.com/Chemical-Structure.97982.html, Accessed 27/3, 2014.
227. Royal Society of Chemistry, *Trimethylolpropane Tris(3-mercaptopropionate)*, http://www.chemspider.com/Chemical-Structure.105802.html, Accessed 27/3, 2014.
228. S. I. Jeon, J. H. Lee, J. D. Andrade and P. G. Degennes, *Journal of Colloid and Interface Science*, 1991, **142**, 149-158.
229. A. Hansson, N. Hashom, F. Falson, P. Rousselle, O. Jordan and G. Borchard, *Carbohydrate Polymers*, 2012, **90**, 1494-1500.
230. A. Meyer, J. Auemheimer, A. Modlinger and H. Kessler, *Current Pharmaceutical Design*, 2006, **12**, 2723-2747.
231. A. Huttenlocher and A. R. Horwitz, *Cold Spring Harbor Perspectives in Biology*, 2011, **3**, 16.
232. N. Ardjomandi, C. Klein, K. Kohler, A. Maurer, H. Kalbacher, J. Niederlander, S. Reinert and D. Alexander, *Journal of Biomedical Materials Research Part A*, 2012, **100A**, 2034-2044.
233. H. Lee, B. G. Choi, H. J. Moon, J. Choi, K. Park, B. Jeong and D. K. Han, *Macromolecular Research*, 2012, **20**, 106-111.